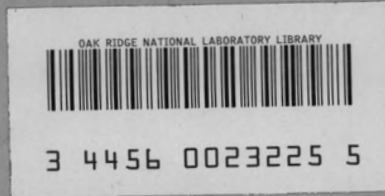




**OAK RIDGE NATIONAL LABORATORY**  
operated by  
**UNION CARBIDE CORPORATION**  
NUCLEAR DIVISION  
for the  
**U.S. ATOMIC ENERGY COMMISSION**



ORNL - TM - 3012



AUGER SPECTROSCOPY OF SIMPLE GASEOUS MOLECULES

(Thesis)

William Ervin Moddeman

OAK RIDGE NATIONAL LABORATORY  
CENTRAL RESEARCH LIBRARY  
DOCUMENT COLLECTION  
**LIBRARY LOAN COPY**  
DO NOT TRANSFER TO ANOTHER PERSON  
If you wish someone else to see this  
document, send in name with document  
and the library will arrange a loan.  
UCN-7969  
(3 3-67)

Submitted as a Dissertation to the Graduate School of the University of Tennessee in Partial Fulfillment of the Requirements for the Degree of Doctor of Philosophy.

LEGAL NOTICE

This report was prepared as an account of Government sponsored work. Neither the United States, nor the Commission, nor any person acting on behalf of the Commission:

- A. Makes any warranty or representation, expressed or implied, with respect to the accuracy, completeness, or usefulness of the information contained in this report, or that the use of any information, apparatus, method, or process disclosed in this report may not infringe privately owned rights; or
- B. Assumes any liabilities with respect to the use of, or for damages resulting from the use of any information, apparatus, method, or process disclosed in this report.

As used in the above, "person acting on behalf of the Commission" includes any employee or contractor of the Commission, or employee of such contractor, to the extent that such employee or contractor of the Commission, or employee of such contractor prepares, disseminates, or provides access to, any information pursuant to his employment or contract with the Commission, or his employment with such contractor.

ORNL-TM-3012

Contract No. W-7405-eng-26

PHYSICS DIVISION

AUGER SPECTROSCOPY OF SIMPLE GASEOUS MOLECULES

William Ervin Moddeman

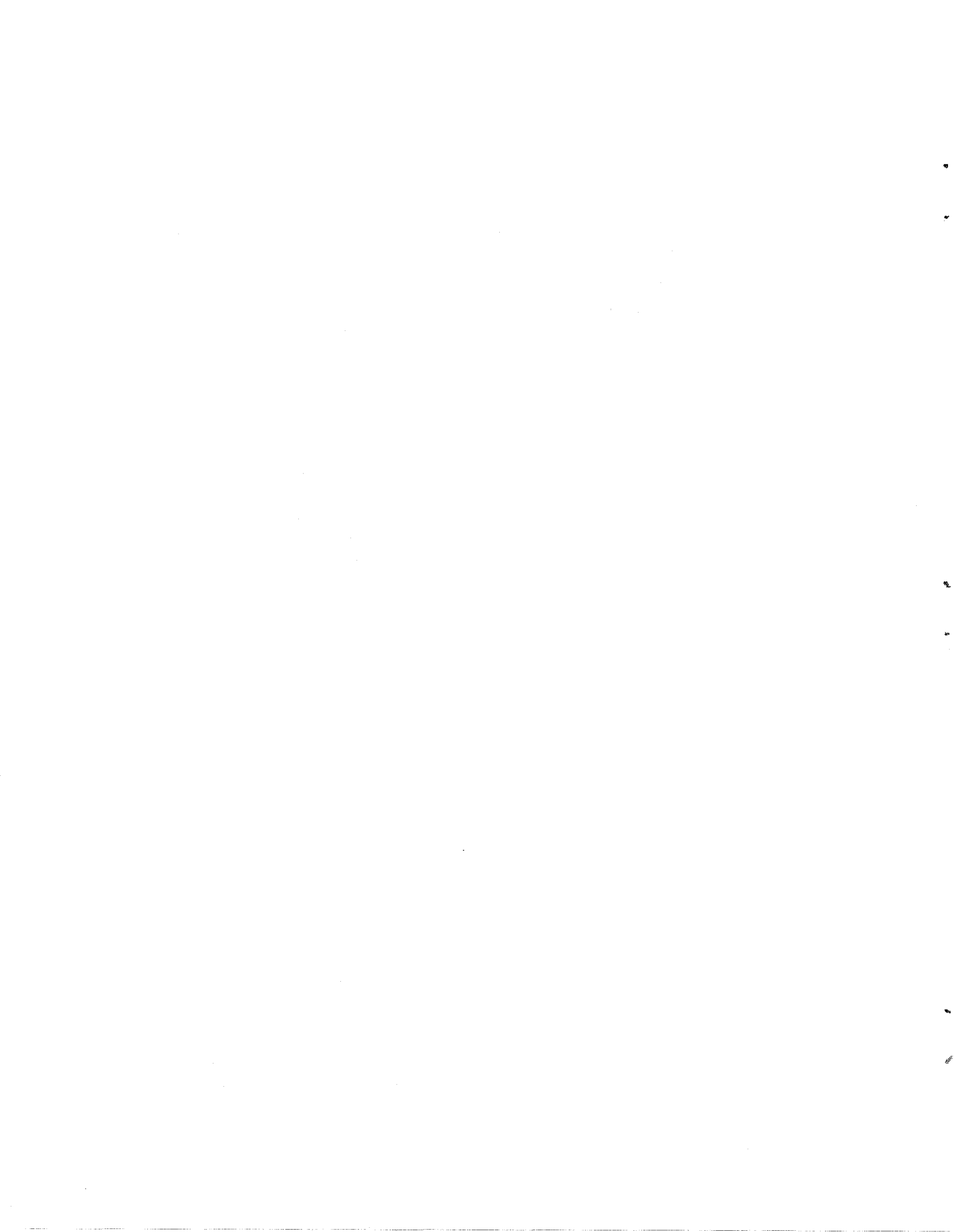
Submitted as a Dissertation to the Graduate School  
of the University of Tennessee in Partial  
Fulfillment of the Requirements for the  
Degree of Doctor of Philosophy

SEPTEMBER 1970

OAK RIDGE NATIONAL LABORATORY  
Oak Ridge, Tennessee  
operated by  
UNION CARBIDE CORPORATION  
for the  
U.S. ATOMIC ENERGY COMMISSION



3 4456 0023225 5



## ACKNOWLEDGEMENTS

The author wishes to express his gratitude and appreciation to Drs. G. K. Schweitzer and W. E. Bull for their guidance, encouragement and patience during the course of the graduate study. He also wishes to acknowledge the invaluable experience obtained under the direction of Dr. T. A. Carlson, whose advice and prior endeavors made the context of this research possible. The assistance of, and consultation with, Dr. M. O. Krause is also greatly appreciated.

The author wishes to thank Dr. B. P. Pullen for the many long hours he spent on design and construction in the initial stages of experimentation.

The author also is grateful to V. A. Miracle for his designing, to F. H. Ward for his instrument making, to M. F. Phillips for his aid in obtaining equipment and chemicals and to B. S. Dunlap for the figure drawings.

As a guest assignee to the Physics Division of the Oak Ridge National Laboratory<sup>\*</sup>, the author wishes to thank Dr. G. K. Schweitzer again for making available a research grant, NASA NGL 43-001-021, Supplement No. 3, to supplement this work.

Also, thanks go to Linda Knauer for reading this manuscript, to Ruby Burrell for typing the first draft, to Joan Cotter and Althea Tate for typing the Tables and especially to Harriett Steinke for typing the main body of the dissertation.

---

<sup>\*</sup>Operated by Union Carbide Nuclear Corporation for the U. S. Atomic Energy Commission.

## ABSTRACT

An inner-shell electron vacancy in atomic or molecular systems can be filled by one of two modes: characteristic x-ray emission or Auger electron emission. The Auger electron results from an Auger transition which can be described as an electron-electron coulombic interaction between two electrons of lower binding energy than the inner-shell vacancy. Usually the initial state, an inner-shell vacancy, is created without additional excitation. If this vacancy is filled with an Auger transition, the process is referred to as normal. An Auger readjustment to an initial state with additional excitation other than a hole in the K-level results in satellite processes. The normal processes result ordinarily in the most intense lines and their characterization is the main interest to the Auger spectroscopist.

If the K- and L-shell electrons are involved in the Auger transition, the interaction is referred to as a K-LL Auger process. The high resolution K-LL Auger spectra of some simple gaseous molecules were recorded and analyzed. The molecules that were studied are:  $N_2$ ,  $O_2$ , CO, NO,  $H_2O$ ,  $CO_2$ ,  $CH_4$ ,  $CH_3F$ ,  $CH_2F_2$ ,  $CHF_3$ ,  $CF_4$ ,  $SiH_4$  and  $SiF_4$ . Each spectrum was excited by electron impact. In addition to electron excitation, some portions of each spectrum were induced by x-ray irradiation. Also, the ls-photoelectron spectra in a few cases were recorded.

In the analysis of an Auger spectrum that was excited by electrons four different energy regions were located. The division of a spectrum in four regions was accomplished by using a very simple shell model. By incorporating auxiliary experiments, i.e., the ls-photoelectron and Auger

spectra that were excited by photons, the normal and some of the satellite Auger processes in each spectrum could be distinguished. The satellite processes that were considered in the analysis are (1) Auger electrons that resulted from the decay of (a) autoionization and (b) monopole excited and ionized states and (2) Auger lines that appear from ionizations and excitations by the normal Auger electrons.

From the identification of the normal lines in the Auger spectra, energy values were calculated for: (1) the minimum energy required for double electron removal for the ground state of a neutral molecule and (2) the second ionization energy for a given molecular orbital.

## TABLE OF CONTENTS

CHAPTER	PAGE
I. INTRODUCTION . . . . .	1
History of Auger Phenomenon - The Auger Effect . . . . .	3
Different Types of Auger Processes . . . . .	6
Nomenclature for the Auger Electron . . . . .	7
Energy of the Auger Electron for a Normal Auger Process . . . . .	9
Selection Rules - Transition Rates . . . . .	11
Instruments Used and Compounds Studied by Auger Spectroscopy . . . . .	12
Proposed Problem . . . . .	12
II. INSTRUMENTATION AND TECHNIQUES . . . . .	15
Electron Spectrometer . . . . .	15
Excitation Sources . . . . .	20
Operating Pressure of Sample Gas . . . . .	26
Energy Calibration of Spectrum . . . . .	26
Chemical Materials . . . . .	34
III. ANALYSES OF A K-LL AUGER SPECTRA INVOLVING THE VALENCE ELECTRONS . . . . .	36
Diatomic Molecules . . . . .	36
Triatomic Molecules . . . . .	104
Polyatomic Molecules . . . . .	114
Tabulation of Results . . . . .	145
IV. SUMMARY . . . . .	154
BIBLIOGRAPHY . . . . .	155

LIST OF TABLES

TABLE	PAGE
I. Auger Electron Symbols, Energies and Intensities for Different Transitions in a Free Atom . . . . .	10
II. Molecules Whose K-LL Auger Spectra Have Been Studied by High Resolution Electron Spectroscopy . . . . .	13
III. Slit Systems Used for Different Spectrometer Resolutions . . . . .	19
IV. K-LL Auger Electron Energies of Neon . . . . .	29
V. L-MM Auger Electron Energies of Argon . . . . .	30
VI. Gaseous Materials Studied and Their Percentage Purities . . . . .	35
VII. Electron Peak Energies in K-LL Auger Spectrum of Molecular Nitrogen . . . . .	43
VIII. Electron Peak Energies in K-LL Auger Spectrum of Molecular Oxygen . . . . .	44
IX. Electron Peak Energies in Carbon K-LL Auger Spectrum of Carbon Monoxide . . . . .	45
X. Electron Peak Energies in Oxygen K-LL Auger Spectrum of Carbon Monoxide . . . . .	46
XI. Electron Peak Energies in Nitrogen K-LL Auger Spectrum of Nitric Oxide . . . . .	47
XII. Electron Peak Energies in Oxygen K-LL Auger Spectrum of Nitric Oxide . . . . .	48

TABLE	PAGE
XIII. Assignments of the Peaks Appearing in the High Energy Satellite Region of the K-LL Auger Spectrum of Molecular Nitrogen . . . . .	55
XIV. Relative Energies and Intensities of the Observed Peaks in the 1s-Photoelectron Spectrum of Molecular Nitrogen . . . . .	60
XV. Relative Energies and Intensities of the Inelastic Scattered Electrons from Neutral Nitrogen at Approximately 5 Microns Pressure . . . . .	62
XVI. Assignments of the Peaks Appearing in the High Energy Satellite Region of the K-LL Auger Spectrum of Molecular Oxygen . . . . .	66
XVII. Relative Energies and Intensities of the Observed Peaks in the 1s-Photoelectron Spectrum of Molecular Oxygen .	68
XVIII. Assignments of the Peaks Appearing in High Energy Satellite Region of the K-LL Auger Spectra of Carbon Monoxide . . . . .	72
XIX. Relative Energies and Intensities of the Observed Peaks in the Carbon 1s-Photoelectron Spectrum of Carbon Monoxide . . . . .	77
XX. Relative Energies and Intensities of the Observed Peaks in the Oxygen 1s-Photoelectron Spectrum of Carbon Monoxide . . . . .	78
XXI. Assignments of the Peaks Appearing in High Energy Satellite Region of the K-LL Auger Spectra of Nitric Oxide . . . . .	81

TABLE	PAGE
XXII. Assignments of the Peaks in the Diagram Line Region of the Molecular Nitrogen K-LL Auger Spectrum . . . . .	85
XXIII. Comparison of Differences in Auger Electron Energies Between Regions B and C and Between D and D for Neon . . . . .	89
XXIV. Location of Regions C and D Relative to Region B in the K-LL Auger Spectra of N <sub>2</sub> , O <sub>2</sub> , CO and NO . . . . .	91
XXV. Assignments of the Peaks in the Diagram Line Region of the Molecular Oxygen K-LL Auger Spectrum . . . . .	94
XXVI. Energies of the Final Electronic States for the Doubly Charged Carbon Monoxide Molecular Ion . . . . .	99
XXVII. Energies of the Final Electronic States for the Doubly Charged Nitric Oxide Molecular Ion . . . . .	102
XXVIII. Assignments and Electron Peak Energies in Water K-LL Auger Spectrum . . . . .	108
XXIX. Electron Peak Energies in the Carbon and Oxygen K-LL Auger Spectra of Carbon Dioxide . . . . .	112
XXX. Assignments and Energies of the Final Electronic States for the Doubly Charged Carbon Dioxide Molecular Ion . . . . .	115
XXXI. Electron Peak Energies in the K-LL Auger Spectrum of Methane . . . . .	125
XXXII. Electron Peak Energies in the Carbon K-LL Auger Spectrum of Methyl Fluoride . . . . .	126
XXXIII. Electron Peak Energies in the Fluorine K-LL Auger Spectrum of Methyl Fluoride . . . . .	127
XXXIV. Electron Peak Energies in the Carbon K-LL Auger Spectrum of Difluoromethane . . . . .	128

TABLE	PAGE
XXXV. Electron Peak Energies in the Fluorine K-LL Auger Spectrum of Difluoromethane . . . . .	129
XXXVI. Electron Peak Energies in the Carbon K-LL Auger Spectrum of Trifluoromethane . . . . .	130
XXXVII. Electron Peak Energies in the Fluorine K-LL Auger Spectrum of Trifluoromethane . . . . .	131
XXXVIII. Electron Peak Energies in the Carbon K-LL Auger Spectrum of Tetrafluoromethane . . . . .	132
XXXIX. Electron Peak Energies in the Fluorine K-LL Auger Spectrum of Tetrafluoromethane . . . . .	133
XL. Summary of the Results Obtained from the K-LL Auger Spectra of Methane and the Fluoromethanes . . . . .	138
XLI. Electron Peak Energies in the Silicon L-MM Auger Spectrum of Silane . . . . .	143
XLII. Electron Peak Energies in the Silicon L-MM Auger Spectrum of Tetrafluorosilane . . . . .	144
XLIII. Electron Peak Energies in the Silicon K-LL Auger Spectrum of Silane . . . . .	148
XLIV. Electron Peak Energies in the Silicon K-LL Auger Spectrum of Tetrafluorosilane . . . . .	149
XLV. Electron Peak Energies in the Fluorine K-LL Auger Spectrum of Tetrafluorosilane . . . . .	151
XLVI. Minimum Energy Required for Double Electron Removal for a Number of Simple Molecules as Measured by Auger Spectroscopy . . . . .	152

TABLE

PAGE

XIVII. Second Ionization Energy of a Molecular Orbital for Some Simple Gaseous Molecules as Measured by Auger Spectroscopy . . . . .	153
--	-----

## LIST OF FIGURES

FIGURE	PAGE
1. Spectroscopic Techniques Used in Chemical Analysis and Used to Explore the Nature of the Chemical Bond . . . . .	2
2a. Inner-Shell Excitation of a Neon Atom by a Photon . . . . .	5
2b. De-excitation Modes of Ne <sup>K+</sup> . . . . .	5
3. High Resolution Electrostatic Electron Spectrometer Installed at Oak Ridge National Laboratory . . . . .	16
4. Heart of Electron Spectrometer . . . . .	17
5. Schematic Diagram of Electron Spectrometer and Associated Equipment . . . . .	18
6. Block Diagram of Experimental Apparatus Used for Measuring the Kinetic Energy of Photo- or Auger Electrons . . . . .	21
7. Electron Gun - Tektronix Cathode Ray Tube . . . . .	22
8. X-ray Tube . . . . .	25
9. Neon K-LL Auger Electron Spectrum on a 68 eV Sweep . . . . .	27
10. Argon L-MM Auger Electron Spectrum on a 30 eV Sweep . . . . .	28
11a. 68 eV Sweep Calibration Using a Neon K-LL Auger Electron Spectrum . . . . .	31
11b. 30 eV Sweep Calibration Using Argon L-MM Auger Electron Spectrum . . . . .	31
12. Calibration of Molecular Oxygen K-LL Auger Electron Peaks Using Neon, Argon and Oxygen Mixture . . . . .	33
13. Molecular Nitrogen K-LL Auger Electron Spectrum Excited by Electron Impact . . . . .	37

FIGURE	PAGE
14. Molecular Oxygen K-LL Auger Electron Spectrum Excited by Electron Impact . . . . .	38
15. Carbon K-LL Auger Electron Spectrum of Carbon Monoxide Excited by Electron Impact . . . . .	39
16. Oxygen K-LL Auger Electron Spectrum of Carbon Monoxide Excited by Electron Impact . . . . .	40
17. Nitrogen K-LL Auger Electron Spectrum of Nitric Oxide Excited by Electron Impact . . . . .	41
18. Oxygen K-LL Auger Electron Spectrum of Nitric Oxide Excited by Electron Impact . . . . .	42
19. Molecular Orbital Diagram for Nitrogen . . . . .	51
20a. Formation of $N_2^{K*}$ by Absorption of a $1s(K)$ Electron into the Empty $2p_g$ Level . . . . .	52
20b. Decay of $N_2^{K*}$ . . . . .	52
21. High Energy Portion of the K-LL Auger Electron Spectrum of Molecular Nitrogen Excited by Electrons and Aluminum $K_{\alpha}$ Photons . . . . .	54
22. Decay Modes of $N_2^{K+*}$ . . . . .	57
23. The $1s$ Photoelectron Spectrum of Nitrogen . . . . .	58
24. 1070 eV Electrons Elastically and Inelastically Scattered from Neutral Nitrogen Molecules at 5 Microns Gas Pressure . . . . .	59
25. Molecular Orbital Diagram for Oxygen . . . . .	63
26. High Energy Portion of the K-LL Auger Electron Spectrum of Molecular Oxygen Excited by Electrons and Aluminum $K_{\alpha}$ Photons . . . . .	64

FIGURE	PAGE
27. The 1s Photoelectron Spectrum of Oxygen . . . . .	67
28. Molecular Orbital Diagram for Carbon Monoxide . . . . .	70
29. High Energy Portion of the Carbon and Oxygen K-LL Auger Spectra of Carbon Monoxide Excited by Electrons and Aluminum $K_{\alpha}$ Photons . . . . .	71
30. The Carbon 1s-Photoelectron Spectrum of Carbon Monoxide . .	75
31. The Oxygen 1s-Photoelectron Spectrum of Carbon Monoxide . .	76
32. Molecular Orbital Diagram for Nitric Oxide . . . . .	79
33. High Energy Portions of the Auger Electron Spectra of Nitric Oxide Excited by Electrons and Aluminum $K_{\alpha}$ Photons . . . . .	80
34a. Normal Auger Processes Resulting in Diagram Lines from the Decay of $N_2^{K+}$ . . . . .	84
34b. Satellite Auger Processes Resulting in Low Energy Satellite Lines from the Decay of $N_2^{KL++}$ States . . . . .	84
35. Diagram Line Regions of the Carbon and Oxygen K-LL Auger Electron Spectra of Carbon Monoxide Excited by Electron Impact . . . . .	97
36. Diagram Line Regions of the Nitrogen and Oxygen K-LL Auger Electron Spectra of Nitric Oxide Excited by Electron Impact . . . . .	101
37. Molecular Orbital Diagram for Water . . . . .	105
38. K-LL Auger Electron Spectra of Water Excited by Electron Impact . . . . .	106
39. Molecular Orbital Diagram for Carbon Dioxide . . . . .	109

FIGURE	PAGE
40. Carbon K-LL Auger Electron Spectrum of Carbon Dioxide Excited by Electron Impact . . . . .	110
41. Oxygen K-LL Auger Electron Spectrum of Carbon Dioxide Excited by Electron Impact . . . . .	111
42. Diagram Line Regions of the Carbon and Oxygen K-LL Auger Electron Spectra of Carbon Dioxide Excited by Electron Impact . . . . .	113
43. K-LL Auger Electron Spectrum of Methane Excited by Electron Impact . . . . .	116
44. Carbon K-LL Auger Electron Spectrum of Methyl Fluoride Excited by Electron Impact . . . . .	117
45. Fluorine K-LL Auger Electron Spectrum of Methyl Fluoride Excited by Electron Impact . . . . .	118
46. Carbon K-LL Auger Electron Spectrum of Difluoromethane Excited by Electron Impact . . . . .	119
47. Fluorine K-LL Auger Electron Spectrum of Difluoromethane Excited by Electron Impact . . . . .	120
48. Carbon K-LL Auger Electron Spectrum of Trifluoromethane Excited by Electron Impact . . . . .	121
49. Fluorine K-LL Auger Electron Spectrum of Trifluoromethane Excited by Electron Impact . . . . .	122
50. Carbon K-LL Auger Electron Spectrum of Tetrafluoromethane Excited by Electron Impact . . . . .	123
51. Fluorine K-LL Auger Electron Spectrum of Tetrafluoromethane Excited by Electron Impact . . . . .	124

FIGURE	PAGE
52. Orbital Energies of $\text{CH}_4$ , $\text{CH}_3\text{F}$ , $\text{CH}_2\text{F}_2$ , $\text{CHF}_3$ and $\text{CF}_4$ . . . . .	134
53. Composite of the Carbon K-LL Auger Electron Spectra for the Fluoromethane Series . . . . .	135
54. Composite of the Fluorine K-LL Auger Electron Spectra for the Fluoromethane Series . . . . .	140
55. Silicon L-MM Auger Electron Spectrum of Silane Excited by Electron Impact . . . . .	141
56. Silicon L-MM Auger Electron Spectrum of Tetrafluorosilane Excited by Electron Impact . . . . .	142
57. Silicon K-LL Auger Electron Spectrum of Silane Excited by Electron Impact . . . . .	146
58. Silicon K-LL Auger Electron Spectrum of Tetrafluorosilane Excited by Electron Impact . . . . .	147
59. Fluorine K-LL Auger Electron Spectrum of Tetrafluorosilane Excited by Electron Impact . . . . .	150

## CHAPTER I

### INTRODUCTION

In the past century qualitative and quantitative chemical analysis and the nature of the chemical bond have been increasingly explored by many spectroscopic techniques (see Figure 1). One of these techniques, which in the last few years has proven to be a powerful and exciting instrumental tool with great potentialities, is high resolution electron spectroscopy. This technique measures the kinetic energy of electrons. The four main divisions of electron spectroscopy stem from the manner in which excitation is induced: electron impact spectroscopy (EIS) - scattered electrons from monoenergetic electron impact with the target gas; penning ionization spectroscopy (PIS) - electrons resulting from a process of the form  $A^* + M \rightarrow A + M^+ + e^-$  in which the target gas M interacts with  $A^*$ , an excited atom and often a metastable species; photoelectron spectroscopy (PES) - photoelectrons from the photoelectric effect; and Auger spectroscopy (AS) - secondary electrons from the Auger effect. EIS is useful for studying normally empty electronic levels and particularly for studying "forbidden" transitions of optical spectroscopy. The results of PIS studies yield information concerning filled valence levels of a molecule and the intermediate states of the  $A^* + M$  interaction. When applied to molecules, PES can be subdivided into measurements depending on whether the ejected electrons originated from the "inner" or "valence" shell of the atom. Since inner shell electrons are highly localized on a particular atom of a molecule, inner-shell binding energy measurements give

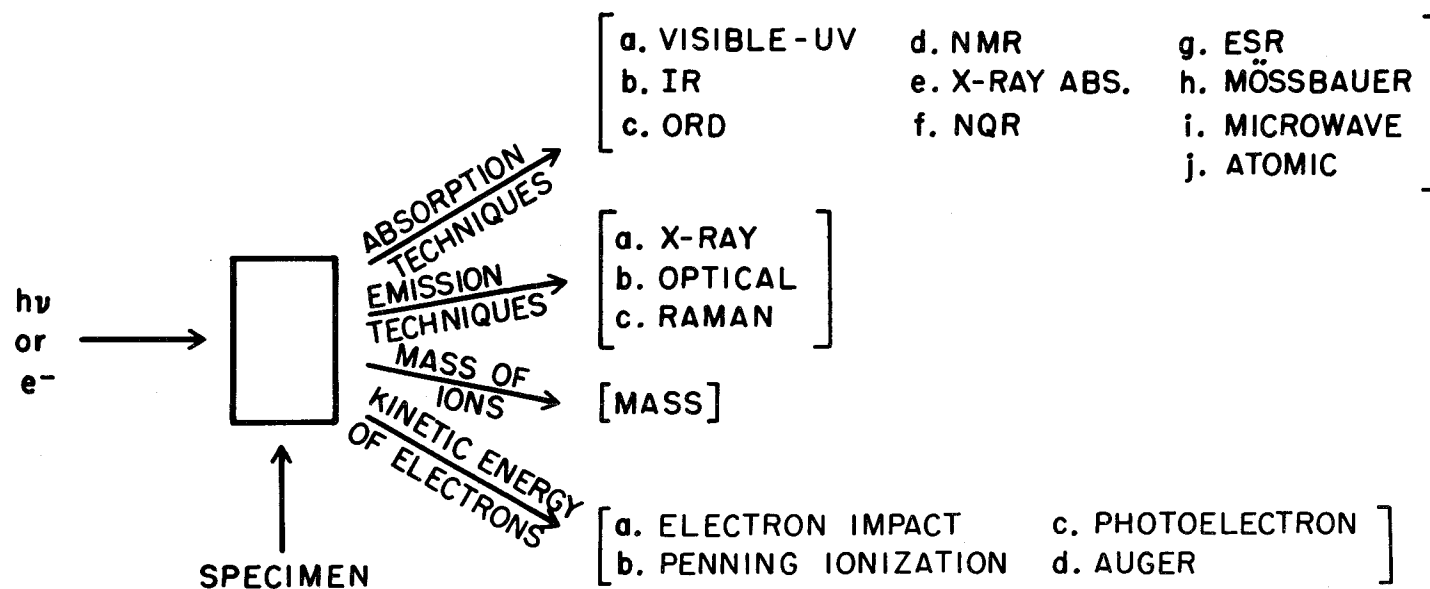


Figure 1. Spectroscopic techniques used in chemical analysis and used to explore the nature of the chemical bond.

information for each atom in a molecule. Changes in the chemical environment about an atom, such as a change in the oxidation state, are reflected in these inner-shell measurements. Valence shell binding energy measurements are descriptive of the electrons involved in chemical bonds, and these measurements have been related to theory, optical data, stability of the resulting singly positive ion, and also to the strength of the chemical bond. For further discussions on EIS, PIS and PES the reader is referred to references 1, 2, to 2, 3, and to 2, 4, 5, 6, respectively.

The last main division of electron spectroscopy, Auger spectroscopy, has been used for surface studies on solids, such as surface composition and contamination, particularly for the identification of low atomic number elements.<sup>7</sup> Also the Auger technique has been used to study gaseous molecules where the Auger data can be related to the final electronic states of the resulting positive ions.<sup>8-11</sup> This division of electron spectroscopy will now be discussed in detail.

#### A. History of Auger Phenomenon - The Auger Effect

In 1925 while studying the photoradiation of inert gases, Auger<sup>12</sup> reported paired tracks as seen in a Wilson expansion chamber. The two observed tracks were the result of ionization caused by the inner-shell photoelectron and the secondary Auger electron. The longer of the tracks was ascribed to the photoelectron which depended on the magnitude of  $h\nu$  and satisfied equation (1-1).  $E_{e^-}$  is the energy of the photoelectron

$$E_{e^-} = h\nu - b \quad (1-1)$$

which is directly proportional to the amount of ionization that occurs in

the cloud chamber and, therefore, to the length of the fog track;  $h\nu$  is the energy of the impinging monochromatic photon; and  $b$  is the binding energy of the electron being ejected. The shorter track was assigned to the Auger electron whose path length was independent of the energy of the  $h\nu$  beam. Auger supposed correctly that the shorter track electrons were associated with the decay of an excited atom following the ejection of the photoelectron from an inner shell.

An inner-shell vacancy can be created in an atom by photons, as in the case of Auger's experiments, or by charged particles, such as electrons. Within  $\sim 10^{-14}$  second this vacancy will be filled by one of two modes: characteristic x-ray emission or Auger electron emission. The Auger electron results from the Auger process which can be described as an electron-electron coulombic interaction between two electrons of lower binding energy than the initial inner photoelectron. This interaction is regarded as a perturbation under the action of which a transition takes place where one of the electrons fills the inner-shell vacancy and the other is raised into the continuum outside the atom. Consequently, the Auger process can simply be described as a non-radiative readjustment to an inner-shell vacancy. Figure 2a represents the interaction of a monochromatic photon with a K-electron of a Ne atom. The results of this interaction are (1) a K-photoelectron and (2) the formation of a singly positive ion,  $\text{Ne}^{\text{K}+}$ . Figure 2b shows the two modes of de-excitation of  $\text{Ne}^{\text{K}+}$ .

The number of transitions resulting from a non-radiative readjustment to an inner-shell vacancy can be expressed in terms of a matrix element,  $M$ , where  $M$  is described by equation (1-2).<sup>13</sup>

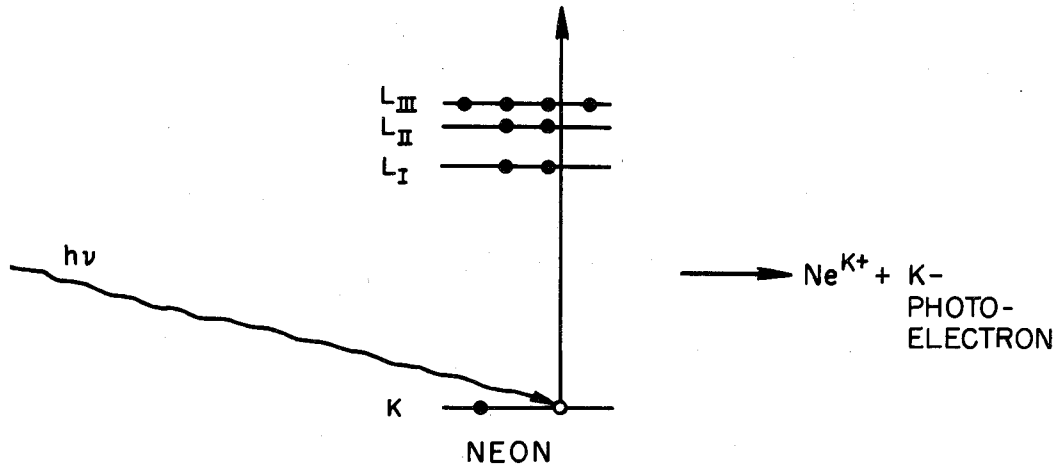


Figure 2a. Inner-shell excitation of a neon atom by a photon.

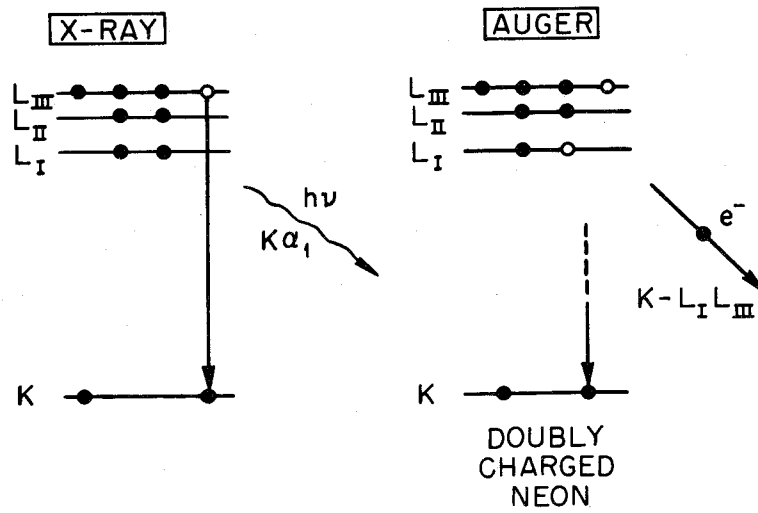


Figure 2b. De-excitation modes of  $\text{Ne}^{K+}$ .

$$M = \frac{1}{2} \sum_{\alpha, \beta, \dots} \left( \Pi_f(r_\alpha r_\beta \dots r_\gamma) \frac{1}{|r_\alpha - r_\beta|} \Pi_i(r_\alpha r_\beta \dots r_\gamma) \right) \quad (1-2)$$

$\Pi_f$  describes the raw eigenfunction of the final electronic state derived from a given coupling scheme (L-S, j-j), and  $\Pi_i$  describes the eigenfunctions of the initial vacancy plus the Auger electron, again coupled.

$r(r_\alpha, r_\beta \dots)$  is the radial coordinate for an electron ( $\alpha, \beta, \dots$ ) which incorporates the Auger transition.  $\frac{1}{|r_\alpha - r_\beta|}$  is a coulombic operator related to the coordinates of the initial and final states.

### B. Different Types of Auger Processes

Usually the more intense lines that appear in an Auger spectrum are the result of "normal" Auger processes and are referred to as "normal" lines. Frequently, the less intense peaks are due to the "satellite" Auger processes forming "satellite" Auger electrons. Ordinarily an initial inner-shell vacancy is created without additional excitation. If this vacancy is filled with an Auger transition, the process is referred to as normal. However, there is a high probability, for neon at least 20 percent<sup>14,15</sup> and probably higher for molecules, for the occurrence of initial excitation via promotion of one or more less tightly bound electrons either into the continuum causing multiple ionization or into discrete levels. Initial ionization or excitation is caused by monopole transitions resulting from a sudden change in the shielding as the inner-shell electron is being ejected. Initial monopole ionization has been referred to as the "shake-off" process,<sup>16,17</sup> and a non-radiative readjustment to a state formed by the shake-off process results in the formation of low energy satellite Auger electrons. Initial monopole excitation has been

referred to somewhat awkwardly as the "shake-up" process,<sup>4</sup> and readjustments to shake-up states usually result in high energy satellite lines.

Additional high energy satellite processes can occur as the result of an autoionization process. An autoionization state is formed by the resonance absorption of an inner-shell electron into an unoccupied molecular orbital. With electron excitation the inner-shell resonance absorption evolves from the inelastic collisions of the incident electron beam with the molecule during which the high energy electrons impart to the molecule only the necessary energy needed to excite the inner-shell electron into the vacant excited level. Decay of an autoionization state by a non-radiative transition results in high energy Auger satellite electrons.

Additional low energy satellite electrons can occur from sudden monopole excitations and ionizations ("double-Auger" processes)<sup>18</sup> when the Auger electron is ejected. These satellite lines do not in general cause confusion in identifying the normal line, as will be seen later in the analysis section, Chapter III, page 87.

Also characteristic of each of the different processes is the charge on the resulting ion following the Auger transition: normal processes,  $a + 2$ ; high energy satellite processes,  $a + 1$  from autoionization and  $a + 2$  from monopole excitation; low energy satellite processes,  $a + 3$  or greater from monopole ionization and  $a + 3$  from the double Auger process.

### C. Nomenclature for the Auger Electron

For atoms, normal Auger processes that result in the formation of doubly charged ions are labeled K-LL, K-IM, L-MM, etc. The first letter indicates the main energy level where the initial hole was made in the

atom, and the last two letters refer to the original levels of the two loosely bound electrons that are involved in the Auger process. Roman numeral subscripts are provided to denote the sublevels involved in the transition, i.e.,  $K-L_I L_I$  or  $L_{III}-M_I M_I$ . The Auger electron shown in Figure 2b, page 5, has been labeled  $K-L_I L_{III}$ , signifying one electron each from the  $L_I$  and  $L_{III}$  sublevels were involved in the Auger transition. Also included with each Auger electron, if known, will be the final electronic state of the charged ion.

The nomenclature for high and low energy satellite Auger electrons is similar. A  $KL-LLL$  satellite electron would indicate an initial  $KL$  ionization, formed by a shake-off process, followed by a transition promoted by the coulombic interaction of three  $L$ -shell electrons. A  $KM^{+1}-ML$  autoionization electron means initial  $K$  to  $M$  excitation followed by  $M,L$  electron-electron interaction.

The nomenclature for Auger processes in molecules to be used in this dissertation follows the general scheme used for atoms. The normal Auger processes involving only weakly bonding electrons,  $w$ , will be labeled  $ls-ww$  (like  $K-L_{II,III} L_{II,III}$  for neon). Those processes involving one weakly and one strongly bonding electron,  $s$ , will be labeled  $ls-ws$ ; processes involving two tightly bound electrons will be labeled  $ls-ss$ . An autoionization process, for example one which involves an electron in the excited orbital,  $e$ , and a weakly bonding electron, will be labeled  $lse^{+1}-ew$ . Satellite processes that result from the decay of multiply charged ions, such as  $X_2^{KL++}$ , will be labeled  $lsw-ww$ .

In this dissertation atoms in molecules with atomic number of less than 11 are studied (except for the two silicon-containing molecules which

will be given special attention later, page 139); therefore, Auger processes involving only the K and L shells are of interest. From an atomic point of view,  $L_{II}$  and  $L_{III}$  levels for these elements can be considered degenerate. Table I lists the six possible normal K-LL Auger lines that can result from a neon atom. The final electronic states of the doubly charged ion are also given in the table. These states arise by using the proper L-S coupling scheme for the doubly positive ion. A similar coupling scheme can be applied to diatomic molecules to derive the different possible final electronic states. These final states will be given in the discussion of the spectra of individual molecules.

#### D. Energy of the Auger Electron for a Normal Auger Process

The kinetic energy of the electrons resulting from K-LL Auger processes are approximately directly proportional to  $Z^2$ , and the normal processes for atoms are given by equation (1-3).<sup>19</sup>  $E_A$  is the Auger electron

$$E_A = E_K - E_L - E_{L'} \quad (1-3)$$

energy,  $E_K$  and  $E_L$  are the binding energies of the K and L shells, respectively, and  $E_{L'}$  is the binding energy of an L-shell electron appropriate to an element singly ionized. Since  $E_L$  and  $E_{L'}$  are small compared to  $E_K$ ,  $E_A$  is the same order of magnitude as  $E_K$ . Table I lists the calculated Auger electron energies that result from a free atom of each element from carbon through neon as taken from Appendix 4 of reference 4. These Auger electron energies were obtained as a difference between separate calculations on the total energy of an atom with a hole in the K-shell and the total energy of the final doubly charged ion. For these calculations relativistic, self-consistent wave functions were used.

TABLE I

AUGER ELECTRON SYMBOLS, ENERGIES AND INTENSITIES  
FOR DIFFERENT TRANSITIONS IN A FREE ATOM

Possible Normal Auger Electrons	Final Electronic State of the Doubly Charged Ion <sup>a</sup>	General "SP" Formalism	Auger Energies from Free Atom Calculations (eV) <sup>b</sup>					Experimentally Determined Intensities from Neon
			C	N	O	F	Ne	
K-L <sub>I</sub> L <sub>I</sub>	<sup>1</sup> S <sub>0</sub>	1s-2s2s	243	356	474	610	761	1.00 <sup>c</sup>
K-L <sub>I</sub> L <sub>II-III</sub>	<sup>1</sup> P <sub>1</sub>	1s-2s2p	252	362	486	627	781	2.87 ± 0.05 <sup>c</sup>
K-L <sub>I</sub> L <sub>II-III</sub>	<sup>3</sup> P <sub>0,1,2</sub>	1s-2s2p	258	369	495	638	794	1.06 ± 0.05 <sup>c</sup>
K-L <sub>II-III</sub> L <sub>II-III</sub>	<sup>1</sup> S <sub>0</sub>	1s-2p2p	265	373	504	650	808	1.5 ± 0.1 <sup>c</sup>
K-L <sub>II-III</sub> L <sub>II-III</sub>	<sup>1</sup> D <sub>2</sub>	1s-2p2p	266	375	507	654	813	10.00 ± 0.18 <sup>c</sup>
K-L <sub>II-III</sub> L <sub>II-III</sub>	<sup>3</sup> P <sub>0,1,2</sub>	1s-2p2p	267	377	509	657	816	< 0.02% <sup>d</sup>

<sup>a</sup>These states are derived from L-S coupling assuming the L<sub>II</sub> and L<sub>III</sub> levels to be degenerate.

<sup>b</sup>Values were taken from reference 4.

<sup>c</sup>Values were taken from reference 15. The intensities are related to the K-L<sub>I</sub>L<sub>I</sub>(<sup>1</sup>S<sub>0</sub>) line which is set equal to unity.

<sup>d</sup>Values were taken from reference 20.

Auger energies,  $E_A$ , for normal Auger lines in molecules can be described as the difference in the binding energy of the 1s shell,  $E_{1s}$ , and the total energy of an electronic state of the doubly charged ion relative to the ground electronic state of the neutral molecule,  $E_{X+2}$  (equation 1-4).

$$E_A = E_{1s} - E_{X+2} \quad (1-4)$$

However,  $E_{X+2}$  values are generally unknown and have been calculated only in a limited number of cases;<sup>21,22</sup> therefore, to estimate the Auger transition energies for different elements in molecules, equation (1-3) and/or Table I are often used.

#### E. Selection Rules - Transition Rates

Intensities of peaks or bands obtainable in spectroscopy are generally governed by selection rules. Mehlhorn has listed the rules for Auger processes for atoms<sup>23</sup> and for molecules.<sup>8</sup> For atoms: (1)  $J_i = J_f$ , (2)  $S_i = S_f$  and (3)  $L_i = L_f$ , where S, L and J are quantum numbers defining the initial, i, and final, f, states involved in the Auger process. For molecules: (1)  $J_i = J_f$ , (2) no change in the symmetry properties of the initial and final states, i.e.,  $+ \rightarrow +$  allowed, but  $+ \rightarrow -$  not allowed, (3) in the case of homonuclear molecules  $\mu \rightarrow \mu$  and  $g \rightarrow g$  are the only transitions allowed, (4)  $S_i = S_f$  and (5)  $\Lambda_i = \Lambda_f$ ,  $\Lambda_i \pm 1$  where  $\Lambda$  refers to total angular momentum of an initial or final state. In using these selection rules, the final states, f, are derived from electronic states of the doubly charged ion, and the initial state, i, evolves from the  $\Lambda$ -S coupling between the inner-shell vacancy and the emitted Auger electron.

The relative Auger intensities have been calculated for K-LL processes for a large number of atoms. Generally good agreement is found between

the calculated and experimental transition rates except for light elements.<sup>24</sup> The addition of configuration interaction into the theoretical calculation by Asaad<sup>25</sup> seems to lead to better agreement with the experimental values, but the situation is still far from satisfactory.<sup>26</sup> A rough intensity distribution can be obtained from the statistical occupation of the different orbitals involved in the Auger transition, e.g., 1s-2p2p processes are more probable than a 1s-2s2s process. Table I, page 10, gives the experimental relative intensities for the normal K-LI Auger process in neon.<sup>15</sup>

#### F. Instruments Used and Compounds Studied by Auger Spectroscopy

Basically, the instruments available for studying the Auger spectrum of atoms or molecules can be divided into two groups: low resolution instruments suitable for elemental identification of solid surfaces, and high resolution machines usable for detail analysis of gases and solids. Three companies, Varian, Veeco and Physical Electronics, make low resolution instruments for surface analysis of solids. Two companies, Varian and Picker, have on the market high resolution dispersion type spectrometers which in principal are capable of achieving detail Auger structure. Thus far all the high resolution spectra have been taken on non-commercial dispersion spectrometers. Table II lists some of the gas and solid samples that have been studied by Auger spectroscopy using these deflection type instruments.

#### G. Proposed Problem

In addition to assisting in the calibration of a high resolution electron spectrometer used at Oak Ridge National Laboratory (ORNL) and in

TABLE II

MOLECULES WHOSE K-LL AUGER SPECTRA HAVE BEEN STUDIED  
BY HIGH RESOLUTION ELECTRON SPECTROSCOPY

Sample	Phase	Reference	Sample	Phase	Reference
Ne	Gas	4, 15, 20, 23	Mg	Solid	29
Ar	Gas	11, 27	K	Solid	30
O <sub>2</sub>	Gas	11, 28	Cu	Solid	31, 32, 33
N <sub>2</sub>	Gas	8, 11	Cu <sub>2</sub> O	Solid	33
CO	Gas	11	CuO	Solid	33
CH <sub>4</sub>	Gas	4, 11	Ge	Solid	31
CF <sub>4</sub>	Gas	11	KCl	Solid	34
C <sub>6</sub> H <sub>6</sub>	Gas	11	K <sub>2</sub> SO <sub>4</sub>	Solid	34
C <sub>2</sub> H <sub>6</sub>	Gas	11	Na <sub>2</sub> S <sub>2</sub> O <sub>3</sub>	Solid	35
			NaCl	Solid	4
			NaF	Solid	36
			MgF <sub>2</sub>	Solid	36
			LiF	Solid	36
			TiO <sub>2</sub>	Solid	4

the design and construction of its excitation sources, this author became interested in Auger spectroscopy largely through the prior endeavors of Drs. Thomas A. Carlson and Manfred O. Krause at ORNL. Under the direction of Drs. G. K. Schweitzer and W. E. Bull at the University of Tennessee and Drs. Carlson and Krause, the study of the Auger spectrum excited by electron impact of each element in different molecules was proposed. The molecules were  $N_2$ ,  $O_2$ ,  $CO$ ,  $NO$ ,  $CO_2$ ,  $H_2O$ ,  $CH_4$ ,  $CH_3F$ ,  $CH_2F_2$ ,  $CHF_3$ ,  $CF_4$ ,  $SiH_4$  and  $SiF_4$ . The first four were chosen because they are simple homonuclear and heteronuclear diatomic molecules. The additional spectra of  $CO_2$  and  $H_2O$  allowed for the study of the Auger spectra of triatomic molecules and, in addition, permitted the comparison of the oxygen K-LL Auger spectrum in different chemical environments. The recording of the spectra in the fluoromethane series allowed one to observe the overall change in the spectrum of a given element in a homologous series. In order to elucidate some of the initial states available for Auger processes, the photoelectron and the Auger spectra excited by  $AlK_{\alpha}$  x-rays of a few of the above listed compounds were recorded.

## CHAPTER II

### INSTRUMENTATION AND TECHNIQUES

#### A. Electron Spectrometer

Figure 3 displays the electron spectrometer that was installed at ORNL. The heart of the spectrometer is exhibited in Figure 4 and is illustrated by a schematic diagram in Figure 5. The latter two figures show: (1) the target chamber, where the x-ray or electron beam from the excitation source interacts with the sample; (2) the two spherical sector plates (contained in an aluminum housing) where electrons are analyzed according to their kinetic energies; and (3) the detector. In brief, the Auger electrons produced in the target chamber are separated according to their kinetic energies by the electrical fields applied to the plates and then counted by the detector.

The region where interaction of the electron beam and the sample gas occurs is shown as an insert of Figure 5. Also shown in the same figure are the entrance slits used to define the resolution of the spectrometer. The slits are adjustable and Table III gives the spectrometer resolution for the various slit sizes.

The ejected Auger electrons produced in the target chamber enter the region of the two aluminum electrostatic plates. Predetermined voltages of opposite polarity are applied to the electrostatic plates. Two sawtooth voltages, also of opposite polarity, are superimposed on the electrostatic plates, and the sweep of the sawtooth is kept in synchronization with the channel advance of a RIDL 400 channel analyzer. Thus, for a given

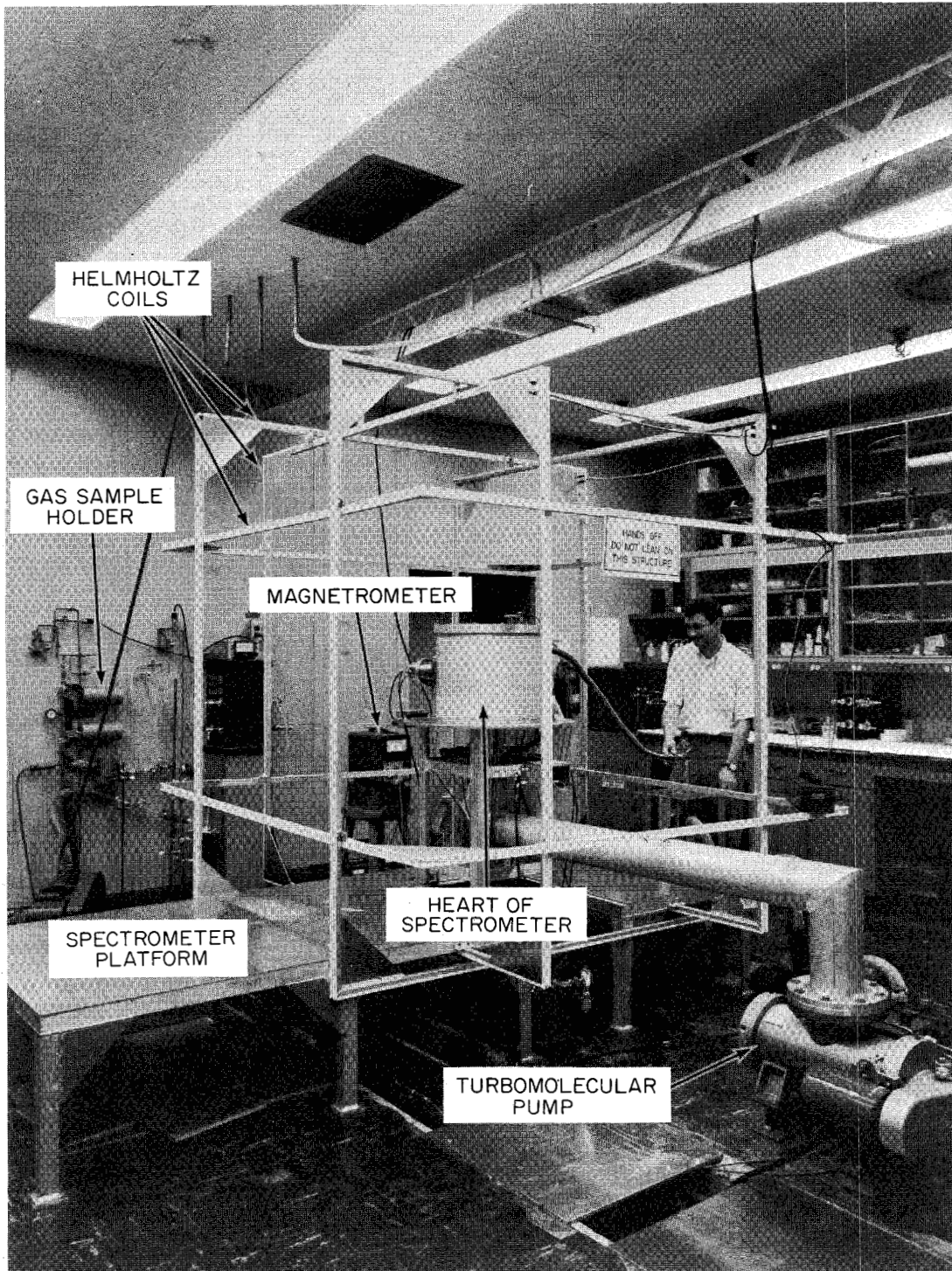


Figure 3. High resolution electrostatic electron spectrometer installed at Oak Ridge National Laboratory.

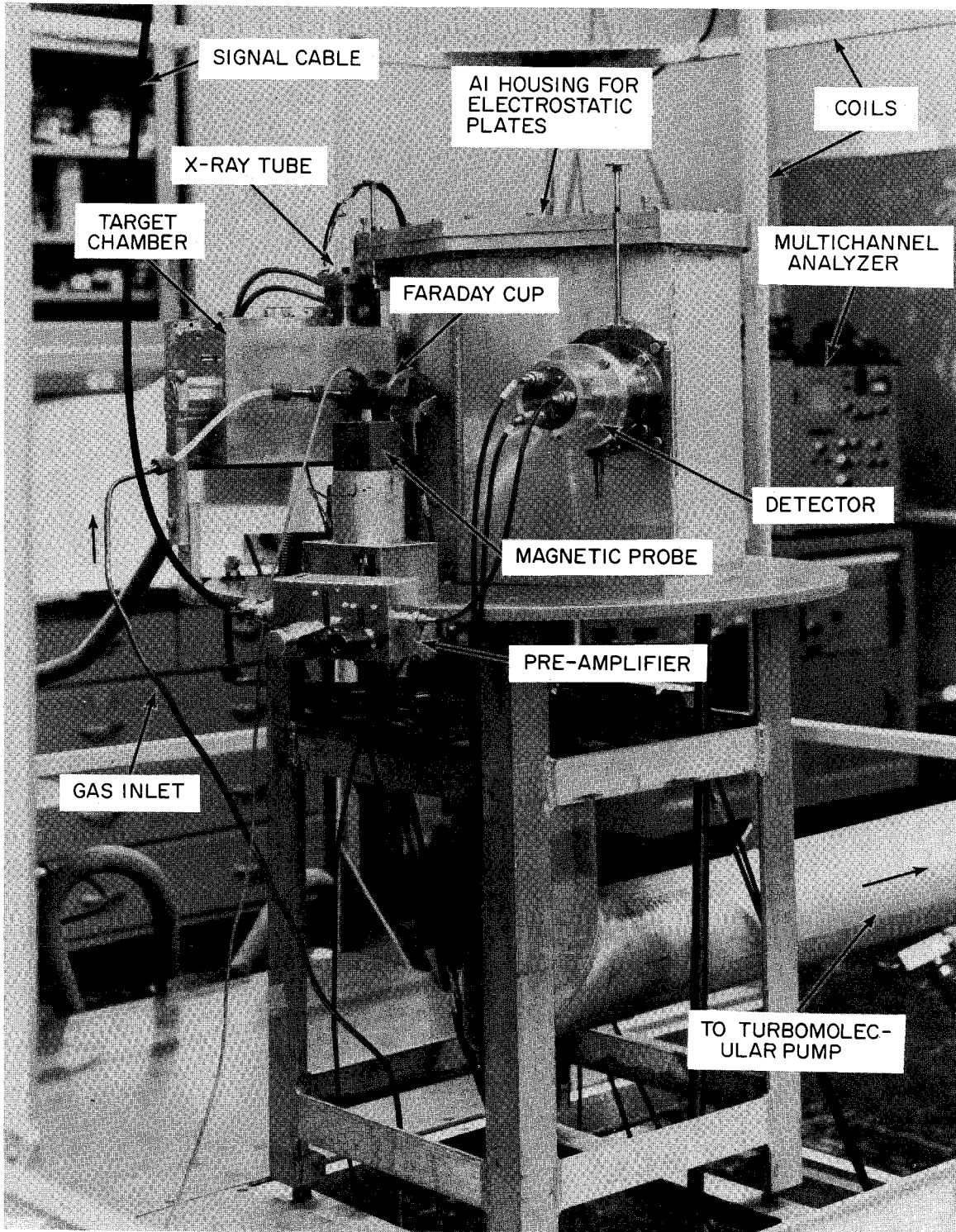


Figure 4. Heart of electron spectrometer.

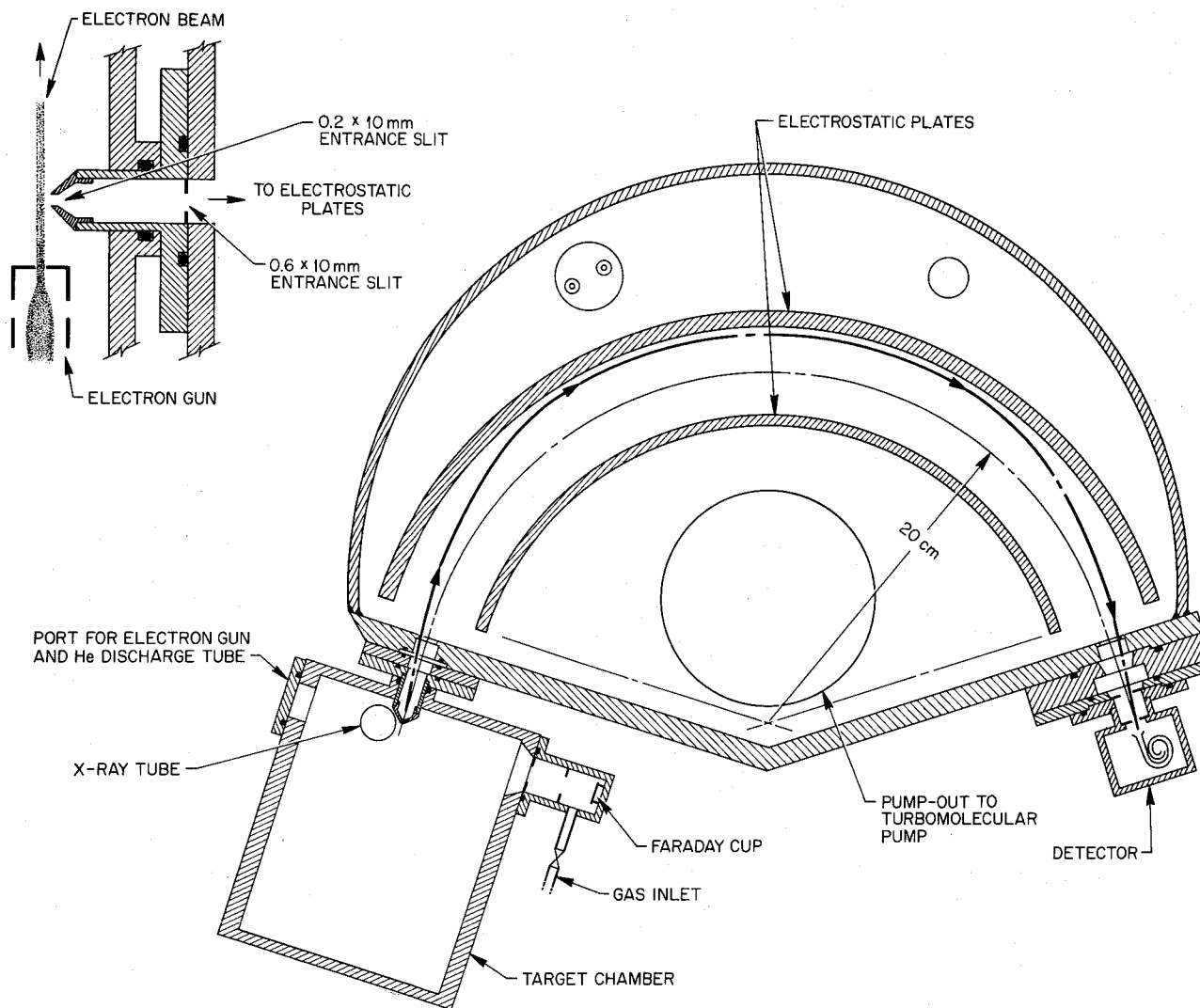


Figure 5. Schematic diagram of electron spectrometer and associated equipment.

TABLE III  
 SLIT SYSTEMS USED FOR DIFFERENT  
 SPECTROMETER RESOLUTIONS

Dimensions of Slit		Observed Percentage Energy Resolution <sup>b</sup>
Defining Slit (mm)	Baffle (mm)	
1.0 x 10	1.5 x 15	0.39
0.5 x 10	1 x 15	0.17
0.2 x 10	0.6 x 10	0.09
0.1 x 10 <sup>a</sup>	0.5 x 10	0.06

<sup>a</sup>The defining slit that was used to obtain 0.06 percent resolution was curved to a 20 cm radius.

<sup>b</sup>The percentage resolution was obtained by measuring the full width at half maximum (FWHM) of the most intense line (<sup>1</sup>D<sub>2</sub> line at 804.15 eV) in the neon K-LL Auger spectrum. Loss of resolution was noted at higher target chamber pressures and higher intensities of the excitation beam.

voltage on the plates, only electrons of specific kinetic energy are allowed to fall on the Millard Model No. B419BL electron multiplier. The signal is amplified prior to reaching the multichannel analyzer. A block diagram of the experimental apparatus is shown in Figure 6.

While traveling in the region between the electrostatic plates, the electrons move through a magnetic field free space ( $< \pm 2 \times 10^{-4}$  gauss). To obtain this field free space the earth's and stray magnetic fields were cancelled with three pairs of Helmholtz coils. The reader is referred to reference 37 for more detailed information on the spectrometer, such as the type of voltage supplies used and the dimensions of the aluminum electrostatic plates.

## B. Excitation Sources

Two excitation sources were used to excite Auger processes: (1) an electron gun and (2) an x-ray tube. The electron gun produced approximately fifty times the activity in a peak as the x-ray tube but with four times the background compared to peak intensity.

### 1. Electron Gun

The electron gun is shown in Figure 7. The main structure of the gun consists of a Tektronix cathode-ray tube which is mounted to flange A via glass stand-offs. The cathode-ray tube consists of four metal electrodes labeled (1), (2), (3) and (4). A tungsten filament taken from a General Electric No. 1630 light bulb sits inside electrode (1). When the electron gun is in operation these four electrodes are at negative, ground, negative and ground potentials, respectively. For example, to excite 3 keV

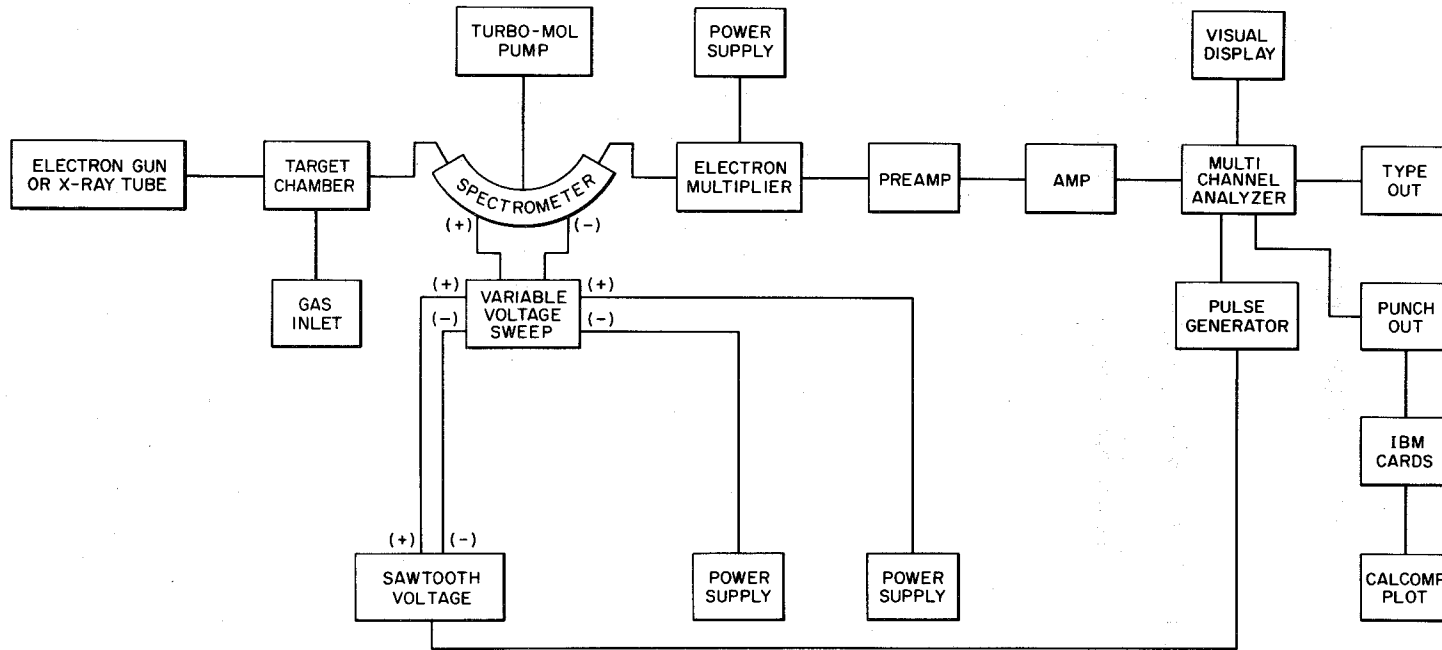


Figure 6. Block diagram of experimental apparatus used for measuring the kinetic energy of photo- or Auger electrons.

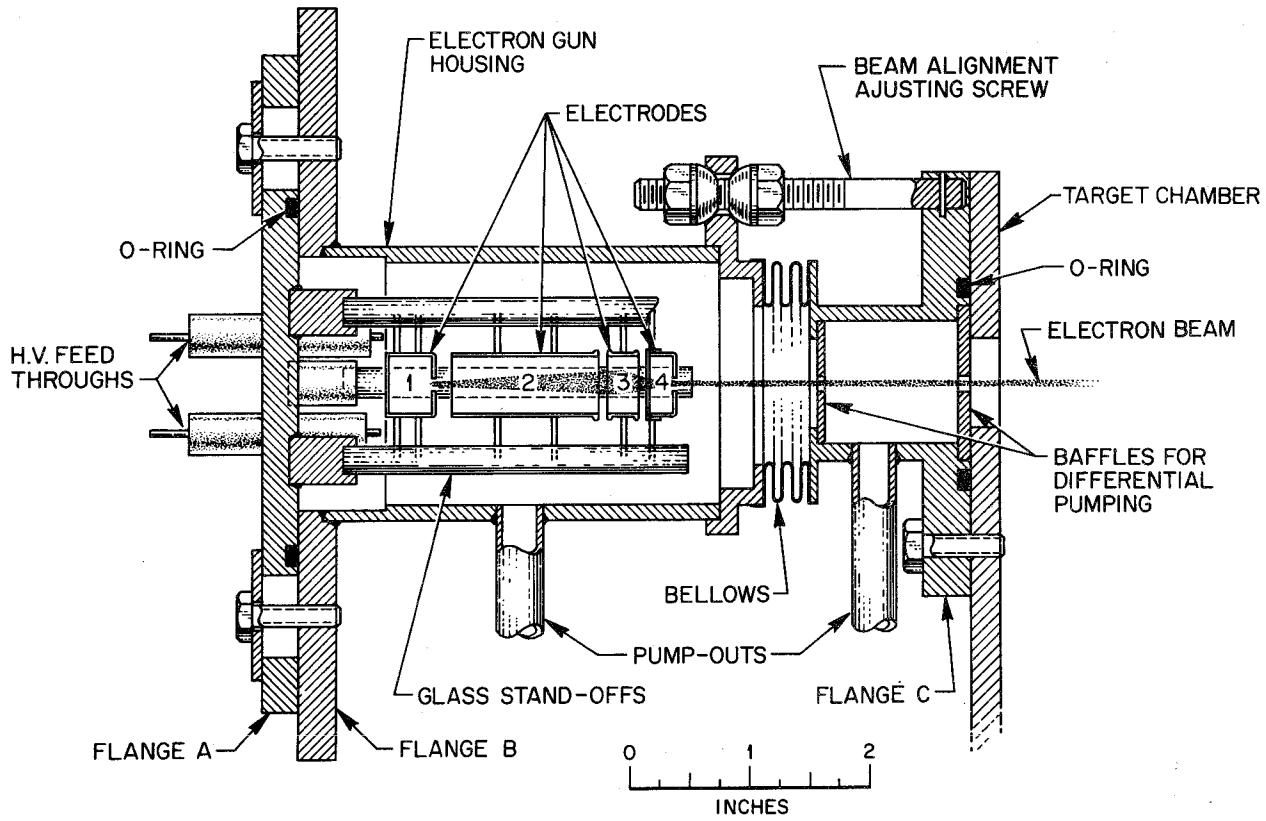
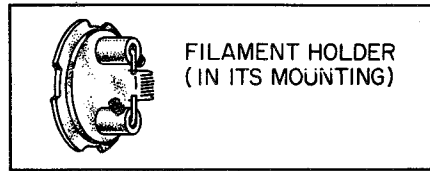


Figure 7. Electron gun - Tektronix cathode ray tube.

electrons a negative 3 kV would be applied to the filament and electrode (1). Electrons are emitted by passing either alternating or direct current through the filament wire. The electrons leaving the negative filament are accelerated through a one-eighth inch hole in electrode (1) to ground potential of electrode (2). Then they pass into electrode (3) where they are de-accelerated and focused into a beam source. Electrode (3) is operated at 2.4 kV (approximately 80 percent of the filament voltage). The focused beam is again accelerated by the ground potential of electrode (4). The resultant electron beam is one-eighth inch in diameter and 1 to 100 microamperes in intensity. The maximum kinetic energy of the electron beam obtainable from the gun was 5 keV.

The inner structure of the electron gun attached to flange A can be inserted into its housing via flange B. The housing contains baffles and portholes for differential pumping, three adjustment screws, and bellows for electron beam alignment. The differential pumping allows for minimal pressure in the electron gun, which in turn increases the life of the filament and increases the maximum operating voltage. The adjustment screws allow for alignment of the electron beam with the entrance slit of target chamber in order to obtain maximum detectable Auger processes. The electron gun assembly is mounted to the target chamber of the spectrometer via flange C.

For some of the later experiments a BTI (Brad Thompson Industries) model 780 electron gun was installed. The Pierce<sup>38</sup> geometry is used in the cathode-anode design. By employing this geometry no external focusing of the electrons into a beam source is required. The gun was operated at 5 to 6 kV and 30 to 100 microamperes emission, although it is capable

of obtaining 9.6 kV and 800 microamperes. Compared to the electron gun described previously, where two stages of differential pumping were used, the BTI gun employs one additional stage to aid in obtaining higher operating voltages.

## 2. X-ray Tube

An x-ray tube consists of a cathode electron source whose electrons bombard an anode to produce x-irradiation. The x-ray tube used in this study is shown in Figure 8. The cathode end of the tube consists of a tungsten filament (General Electric No. 1630), a vanadium window shield, leads for filament heating, high voltage pyrex glass stand-offs, and a water jacket for cooling. An aluminum anode, that was hollowed, beveled and insulated from ground, was used. The copper cylindrical housing of the x-ray tube has a window to allow for the x-ray beam passage into the target chamber.

Under normal operating conditions the cathode and anode are at a negative and positive voltage, respectively. Two amperes current are applied to the tungsten filament resulting in 20 milliamperes emission. The electron beam strikes the aluminum anode and x-radiation is produced. The aluminum  $K_{\alpha}$  radiation is allowed to pass through a 0.07 mm aluminum window. The thin aluminum window removes low energy Brehmsstrahlung from the x-ray beam and allows for a minimal amount of high energy Brehmsstrahlung. The aluminum  $K_{\alpha}$  line appears as an unresolved doublet ( $K_{\alpha_1} = 1.48670$  keV,  $K_{\alpha_2} = 1.48627$  keV)<sup>39</sup> with a FWHM of 0.9 eV.<sup>11</sup> Other detectable lines are  $K_{\beta}$  of 1.5574 keV<sup>39</sup> and  $K_{\alpha'}\alpha_{3,4}$  satellite of 1.4960 keV<sup>40</sup> at 6.5 and 13.0 percent abundance,<sup>40</sup> respectively, of the main  $K_{\alpha}$  line. The vanadium window

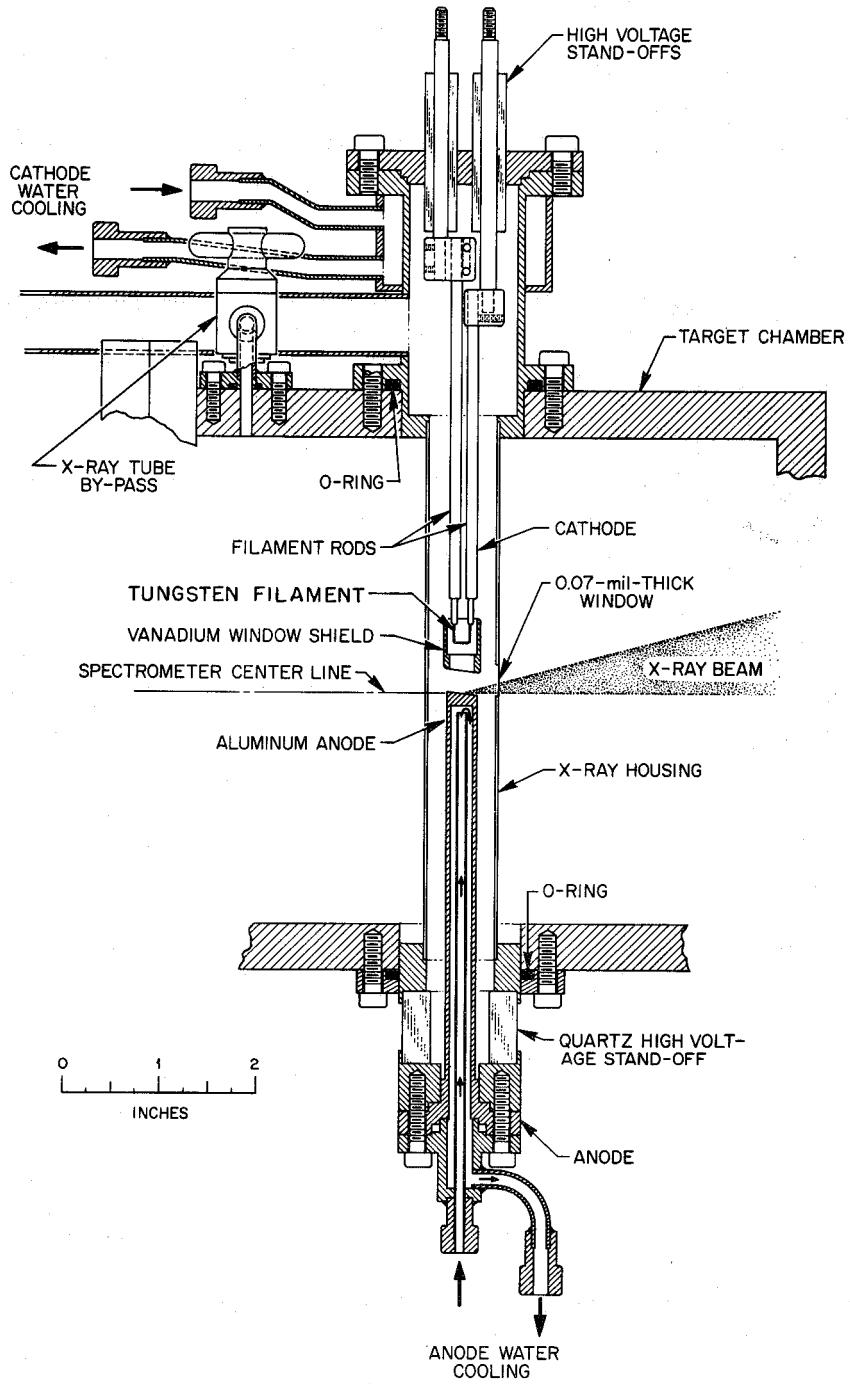


Figure 8. X-ray tube.

shield decreases the probability of tungsten, from the filament, being deposited on the thin aluminum window.

In the latter stages of this work it was found that the x-ray tube worked better without the tantalum shield, with the cathode at ground and the anode at a positive 8 kV. For this work a 12 kV high-voltage Sorenson supply was utilized.

### C. Operating Pressure of Sample Gas

The gaseous samples were studied at constant pressure during a given run. The gas pressures ranged from 5 to 10 microns in the target chamber and approximately  $10^{-5}$  mm pressure in the spectrometer housing. Independent pressure studies, Chapter III, page 56, suggest that contributions to the observed Auger spectra from inelastic scattering are negligible.

### D. Energy Calibration of Spectrum

#### 1. Sweep Calibration

The Auger spectra of the materials used in this study were recorded on energy sweeps of 2, 12, 30, 68 and 96 eV. The calibration of each of these sweeps had to be made, i.e., the increase in the sawtooth voltage over the 400 channels of the analyzer. Differences in energy between the Auger electron peaks in Ne K-LL and Ar L-MM spectra are accurately known; therefore, these were chosen to calibrate the energy sweeps. The Ne K-LL on a 68 eV and Ar L-MM on a 30 eV sweep are shown in Figures 9 and 10, respectively. The peak energies and differences are given in Tables IV and V. Figures 11a and 11b give the known peak energies versus the channel number for the 68 eV and 30 eV sweeps from which the energy per channel was determined.

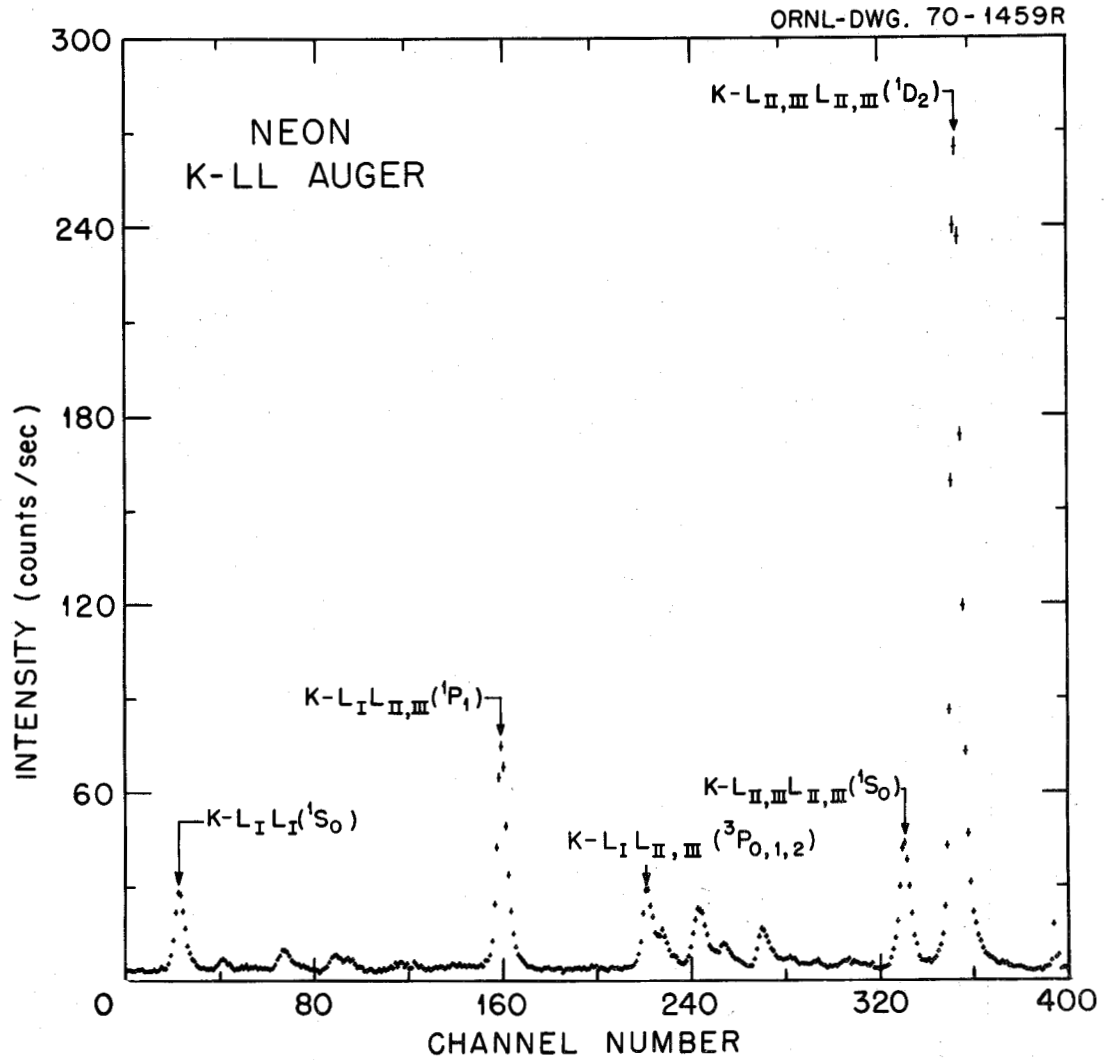


Figure 9. Neon K-LL Auger electron spectrum on a 68 eV sweep.

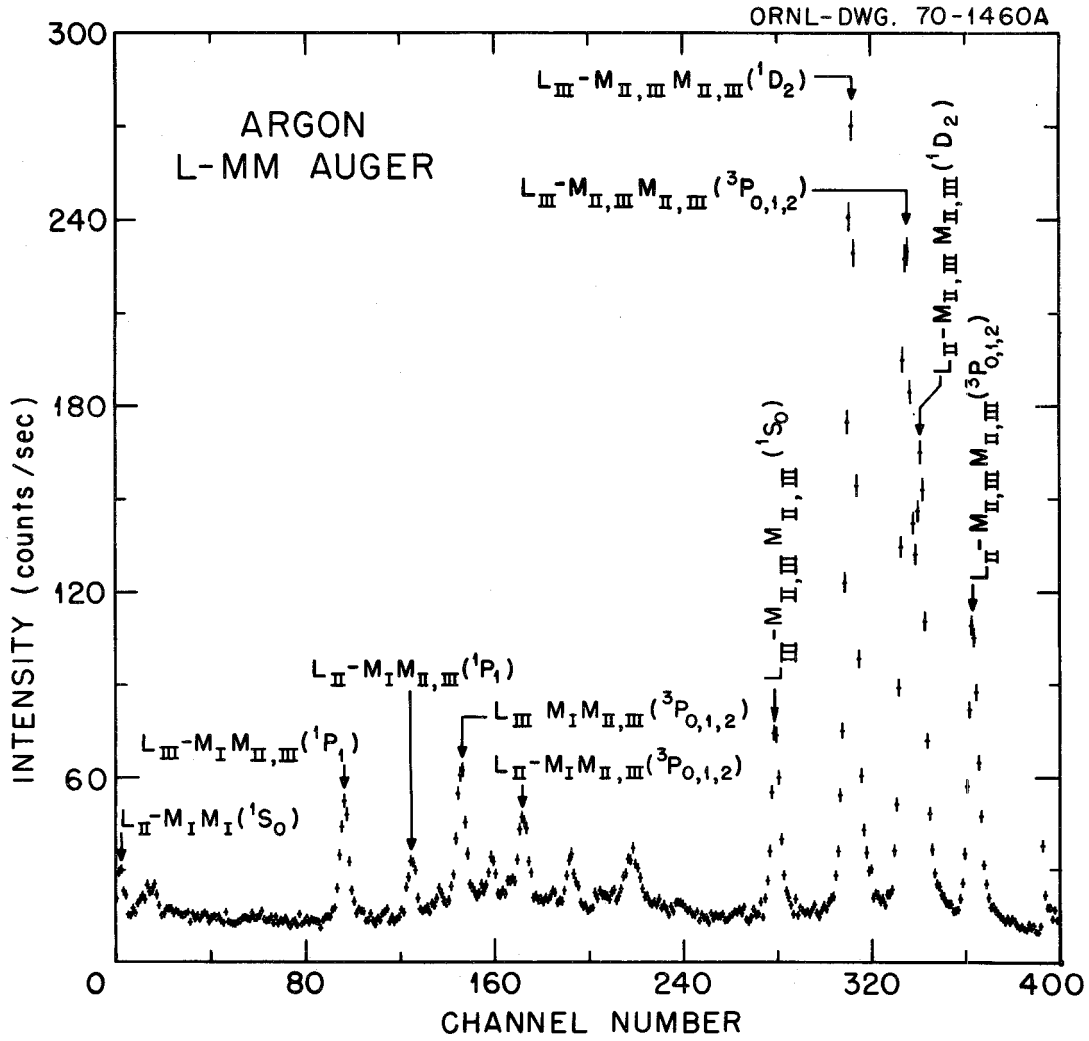


Figure 10. Argon L-MM Auger electron spectrum on a 30 eV sweep.

TABLE IV  
K-LL AUGER ELECTRON ENERGIES OF NEON

Transition	Absolute Energy (eV) <sup>23</sup>	$\Delta E$ From $^1D_2$ Line (eV)
K-L <sub>I</sub> L <sub>I</sub> ( $^1S_0$ )	748.1 $\pm$ 0.65	56.1 $\pm$ 0.1
K-L <sub>I</sub> L <sub>II,III</sub> ( $^1P_1$ )	771.5	32.7
K-L <sub>I</sub> L <sub>II,III</sub> ( $^3P_{0,1,2}$ )	782.0	22.2
K-L <sub>II,III</sub> L <sub>II,III</sub> ( $^1S_0$ )	800.5	3.7
K-L <sub>II,III</sub> L <sub>II,III</sub> ( $^1D_2$ )	804.15	0.0

TABLE V

## L-MM AUGER ELECTRON ENERGIES OF ARGON

Transition	Absolute Energy (eV) <sup>27</sup>	$\Delta E$ From $L_{III}-M_{II,III} M_{II,III}(^3P_{0,1,2})$ (eV)
$L_{II}-M_I M_I(^1S_0)$	179.93 $\pm$ 0.25	27.08 $\pm$ 0.02
$L_{III}-M_I M_{II,III}(^1P_1)$	187.16	19.85
$L_{II}-M_I M_{II,III}(^1P_1)$	189.30	17.71
$L_{III}-M_I M_{II,III}(^3P_{0,1,2})$	190.76	16.25
$L_{II}-M_I M_{II,III}(^3P_{0,1,2})$	192.90	14.11
$L_{III}-M_{II,III} M_{II,III}(^1S_0)$	200.87	6.14
$L_{III}-M_{II,III} M_{II,III}(^1D_2)$	203.26	3.75
$L_{III}-M_{II,III} M_{II,III}(^3P_{0,1,2})$	204.81	2.20
$L_{II}-M_{II,III} M_{II,III}(^1D_2)$	205.40	1.61
$L_{II}-M_{II,III} M_{II,III}(^3P_{0,1,2})$	207.01	0.00

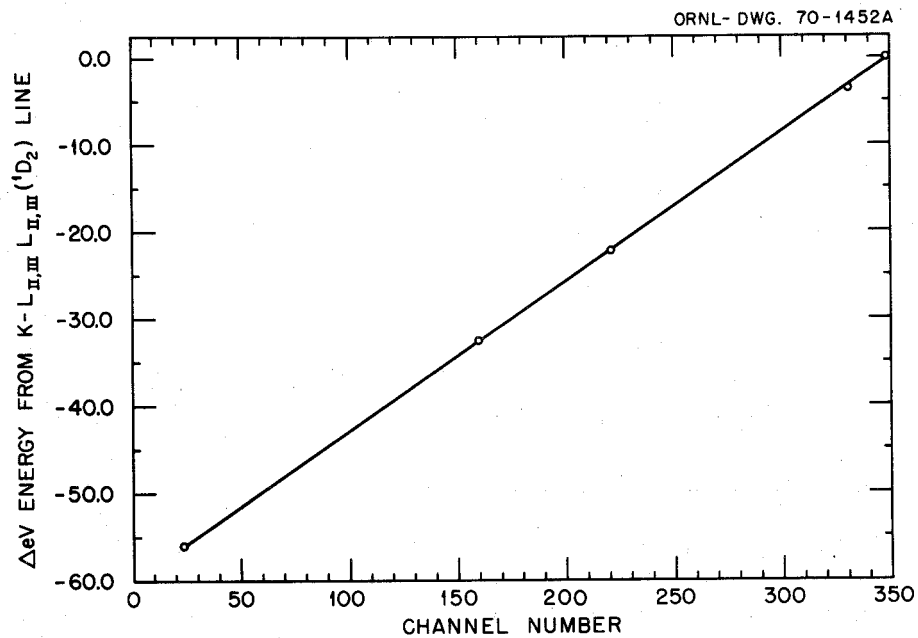


Figure 11a. 68 eV sweep calibration using a neon K-LL Auger electron spectrum.

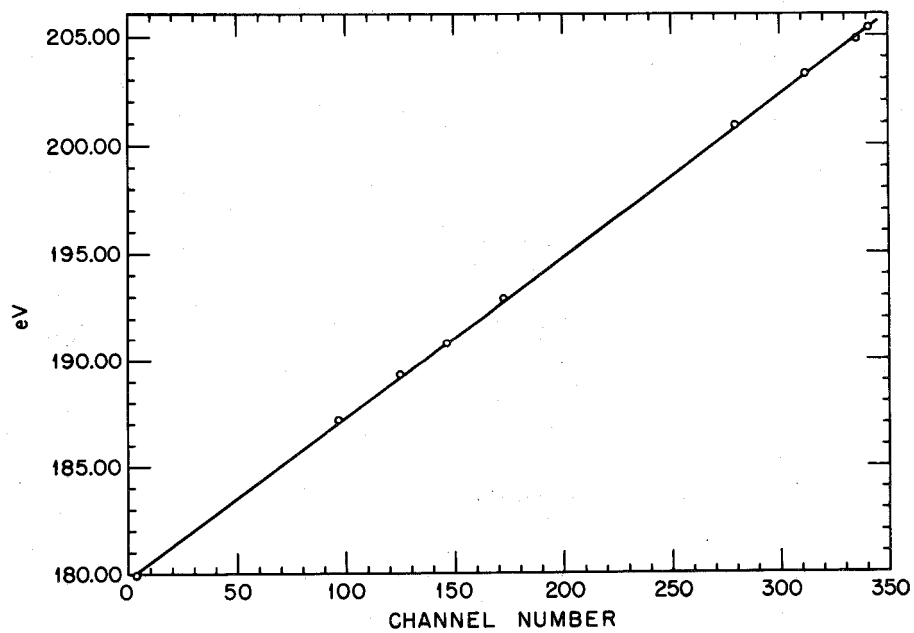


Figure 11b. 30 eV sweep calibration using argon L-MM Auger electron spectrum.

## 2. Energy Calibration of Sample

Energy calibrations for the peaks of the sample under investigation were made by using a Ne, Ar, and sample mixture. Under a constant pressure and electron beam intensity, the spectra of the individual components in the mixture were taken on a 12 eV sweep for 400 channels. The results for an oxygen calibration are shown in Figure 12. Prior to the recording of each spectrum, the voltage on the plates was determined. At this indicated plate voltage the minimum kinetic energy electron is detectable in channel zero of the analyzer. The relationship between the kinetic energy of the electron at channel zero,  $E_o$ , to the predetermined plate voltage,  $P$ , is given by equation (2-1).

$$E_o = \alpha P + V_o \quad (2-1)$$

$V_o$  is constant for each calibration, but is dependent upon the components of the gas mixture, the pressure of the mixture and the intensity of the ionizing electron beam. Alpha ( $\alpha$ ) is a proportionality constant whose value is dependent upon the energy sweep and the number of analyzer channels that were used.

In the oxygen calibration  $(E_o)_{Ne}$  and  $(E_o)_{Ar}$  are determined by knowing the energy of the peak, the channel at which the peak appears, and the sweep calibration. Alpha ( $\alpha$ ) can be found from equation (2-2). For the

$$\alpha = \frac{(E_o)_{Ne} - (E_o)_{Ar}}{P_{Ne} - P_{Ar}} \quad (2-2)$$

oxygen calibration of Figure 12,  $\alpha$  was determined to be 4.056. By knowing  $P_{O_2}$ ,  $(E_o)_{O_2}$  can be calculated from equation (2-3). Then by knowing

$$(E_o)_{O_2} = (E_o)_{Ne} - \alpha(P_{Ne} - P_{O_2}) \quad (2-3)$$

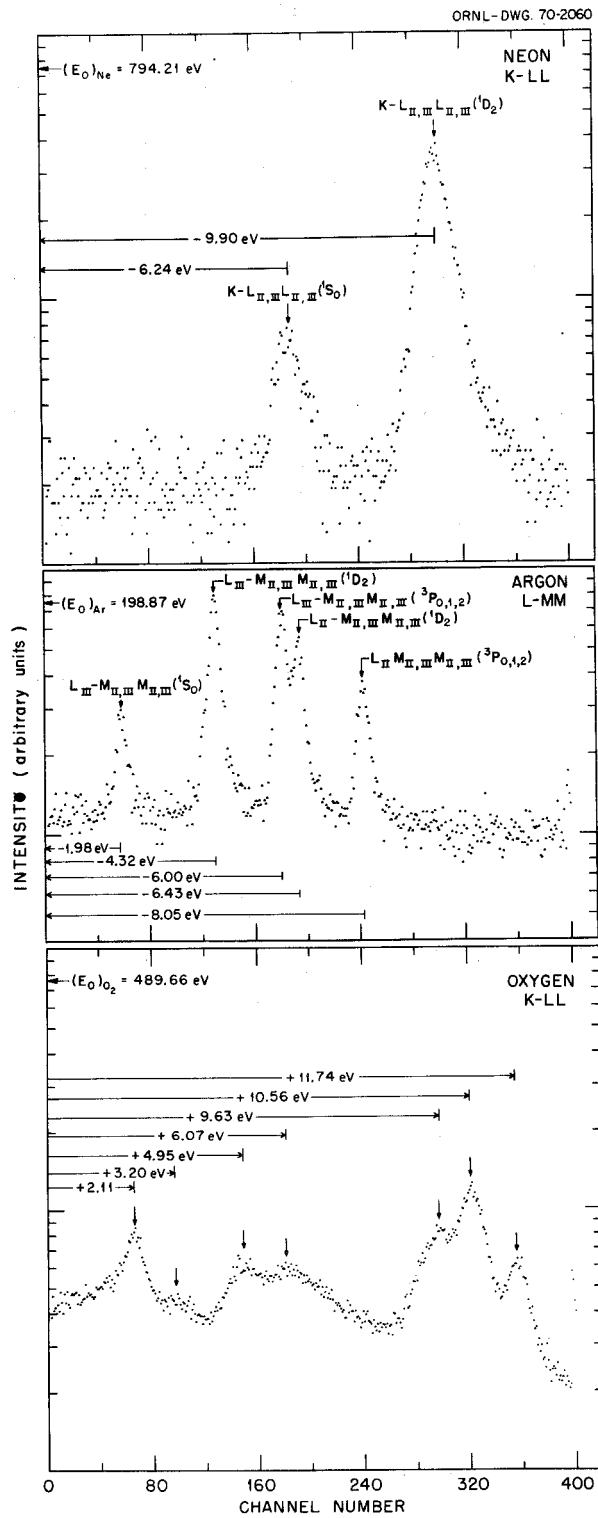


Figure 12. Calibration of molecular oxygen K-LL Auger electron peaks using neon, argon and oxygen mixture.

the sweep calibration, the channel at which the oxygen peaks appear, and  $(E_o)_{O_2}$ , the energy of the Auger electrons in the oxygen peaks can be found.

#### E. Chemical Materials

Table VI lists the gaseous materials studied and their percentage purities.

TABLE VI  
GASEOUS MATERIALS STUDIED AND THEIR  
PERCENTAGE PURITIES

Gas	Percentage Purity
O <sub>2</sub>	99.99 <sup>a</sup>
N <sub>2</sub>	99.999 <sup>a</sup>
CO	99.9 <sup>a</sup>
NO	99.8 <sup>a</sup>
CO <sub>2</sub>	99.995 <sup>a</sup>
H <sub>2</sub> O	re-purified <sup>b</sup>
CH <sub>4</sub>	99.99 <sup>c</sup>
CH <sub>3</sub> F	99.0 <sup>c</sup>
CH <sub>2</sub> F <sub>2</sub>	99.0 <sup>c</sup>
CHF <sub>3</sub>	98.0 <sup>c</sup>
CF <sub>4</sub>	99.7 <sup>c</sup>
SiH <sub>4</sub>	99.9999 <sup>a</sup>
SiF <sub>4</sub>	99.6 <sup>a</sup>

<sup>a</sup>The listed percentage purity is the purity specified by the manufacturer.

<sup>b</sup>Dissolved gases were removed from the distilled water by heating the liquid water to approximately 70° C in vacuo.

<sup>c</sup>Mass spectral data were taken on these compounds.

## CHAPTER III

### ANALYSES OF A K-LL AUGER SPECTRA INVOLVING THE VALENCE ELECTRONS

In analyzing a K-LL Auger spectrum of an atom or molecule excited by high energy electrons, one can use the following preliminary steps in order to identify the normal processes: (1) divide the spectrum into different energy regions according to the binding energy of the valence electrons that are involved in the Auger transition, and (2) determine the contribution of satellite lines with the help of auxiliary experiments (such as, the examination of the satellite lines found in the photoionization spectrum of the K-shell or the comparison of the Auger spectrum excited by different energy sources). By following the above procedure, one can ascertain information that is unattainable by other physical methods, such as the energy of different electronic states of doubly charged ions. With emphasis of interpretation placed on nitrogen, the Auger spectra of four diatomic molecules,  $N_2$ ,  $O_2$ , CO and NO, are discussed in detail. Also, the high resolution K-LL Auger spectra of more complex molecules are presented and analyzed in a similar fashion. All of the spectra were taken with at least a tenth of a percent resolution.

#### A. Diatomic Molecules

Shown in Figures 13-18 are the K-LL Auger spectra of each element in  $N_2$ ,  $O_2$ , CO and NO. The identified peaks are shown in each spectrum by arrows, and Tables VII-XII list the energies of the peaks associated with each figure. Each spectrum is divided into four energy regions. Basically, from highest to lowest electron kinetic energies, the main

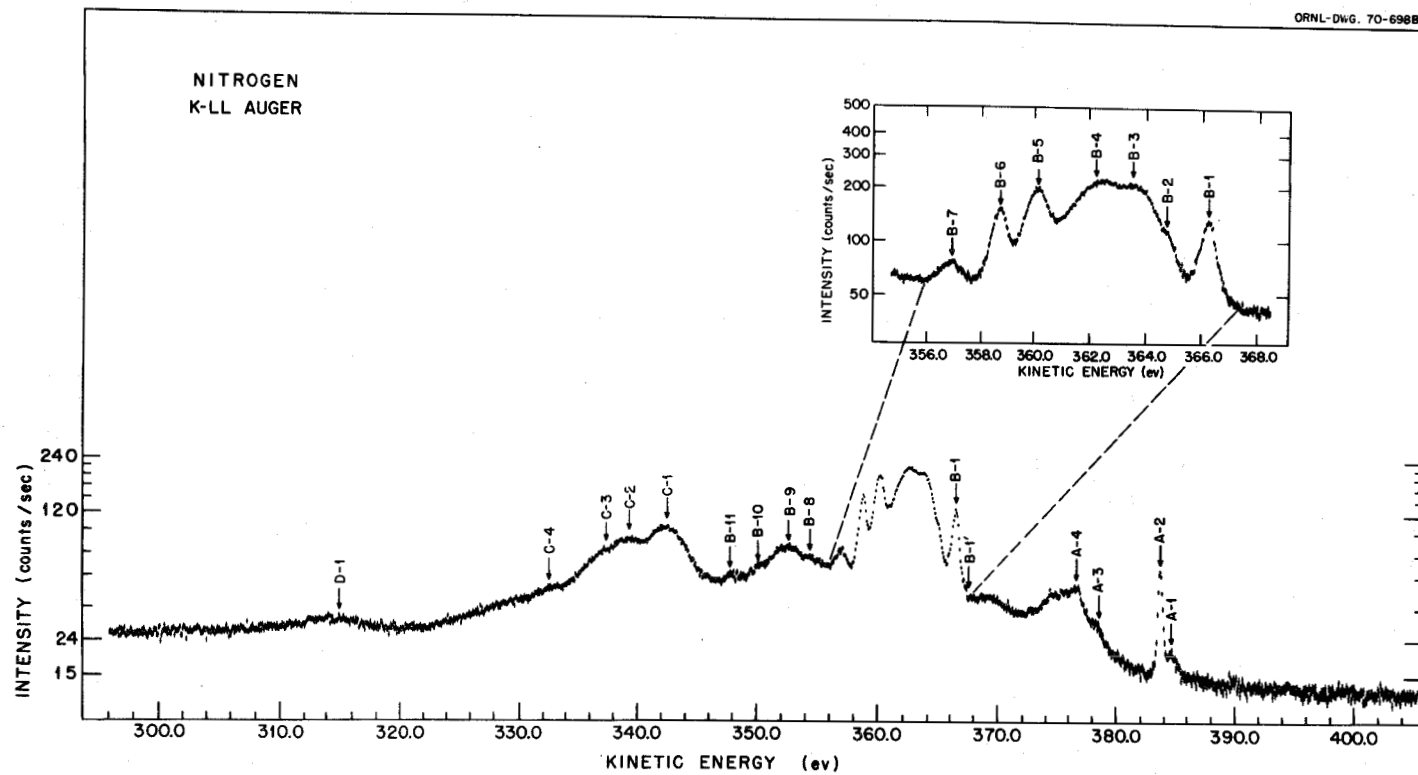


Figure 13. Molecular nitrogen K-LL Auger electron spectrum excited by electron impact.

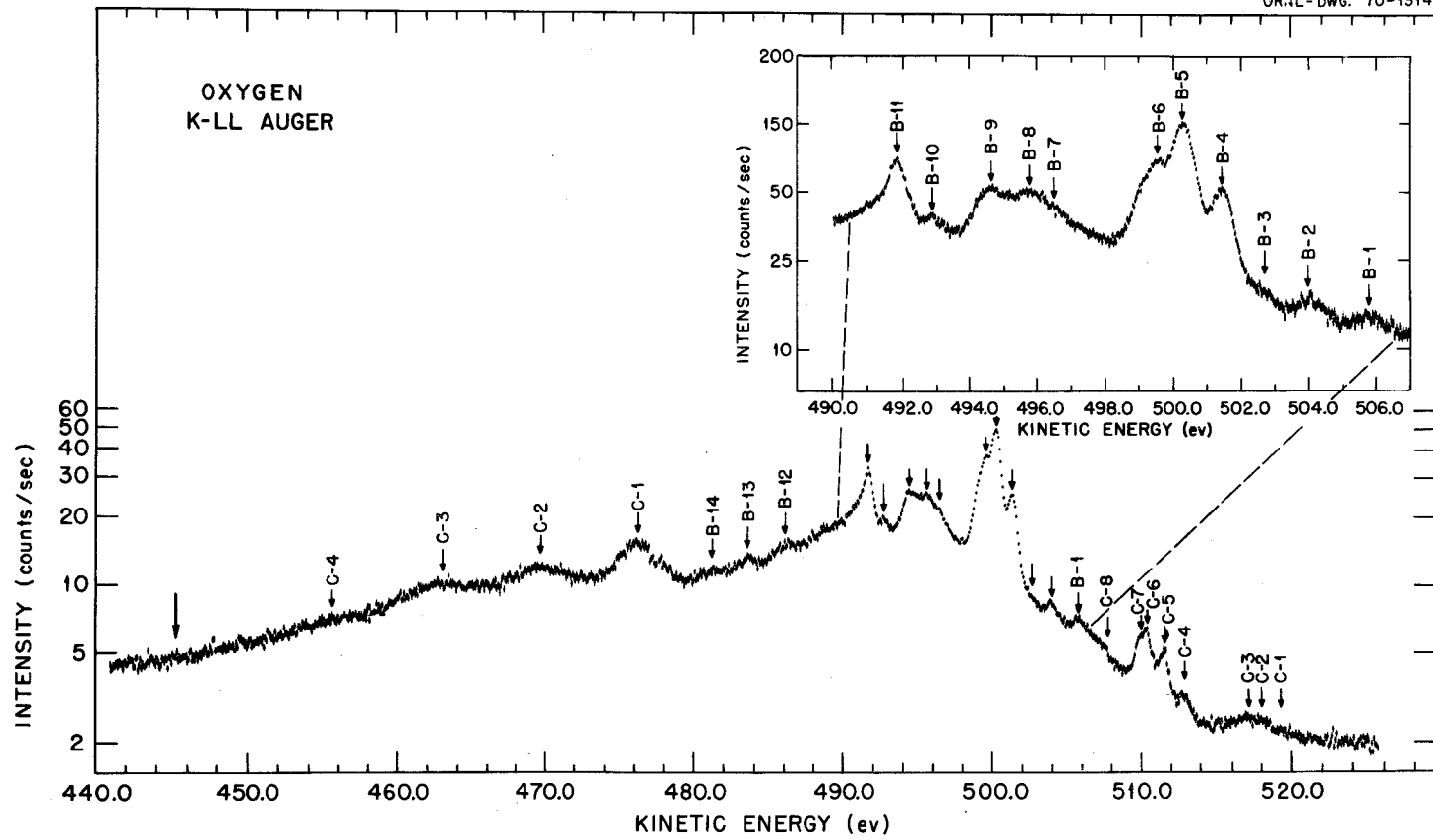


Figure 14. Molecular oxygen K-LL Auger electron spectrum excited by electron impact.

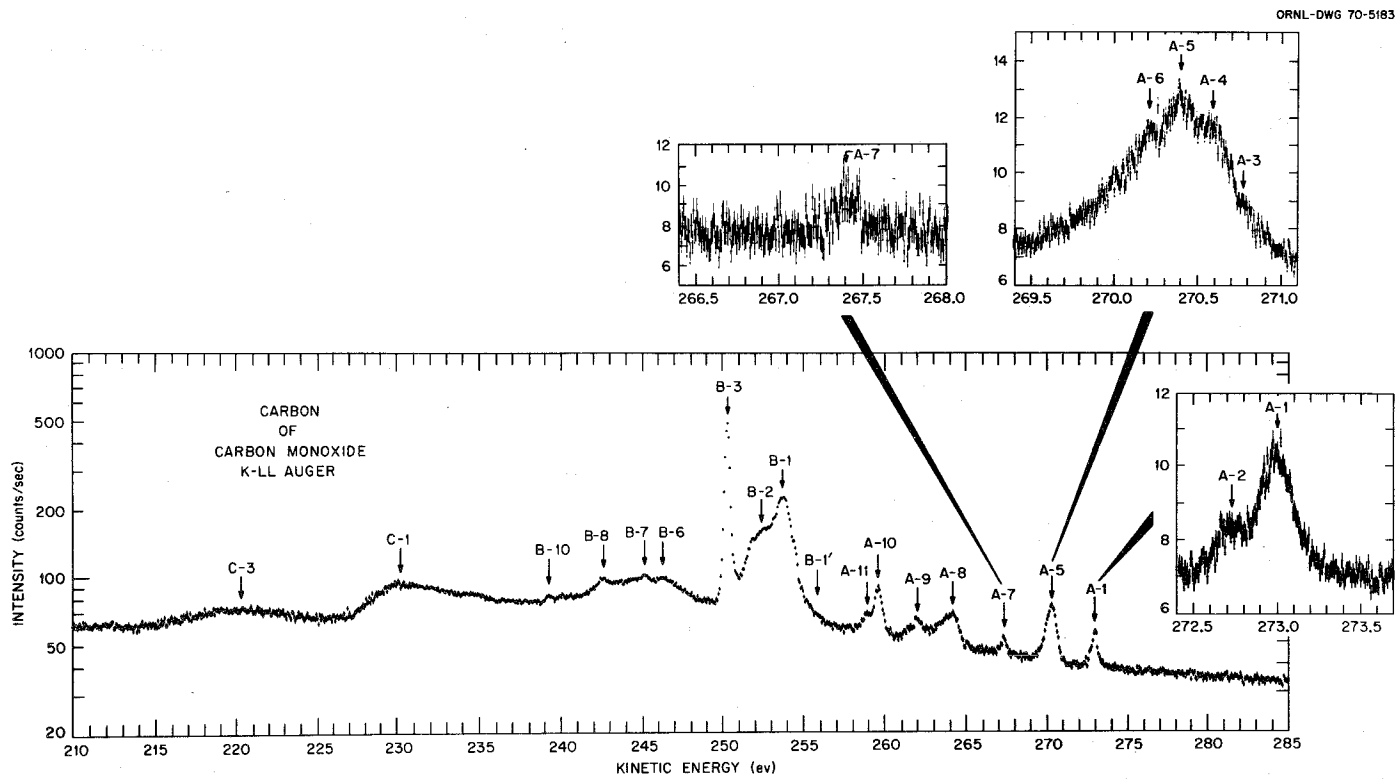


Figure 15. Carbon K-LL Auger electron spectrum of carbon monoxide excited by electron impact.

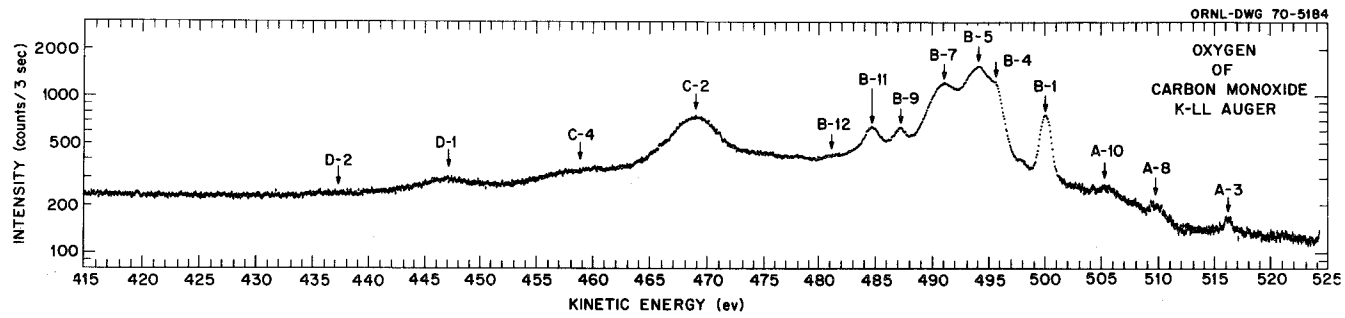


Figure 16. Oxygen K-LL Auger electron spectrum of carbon monoxide excited by electron impact.

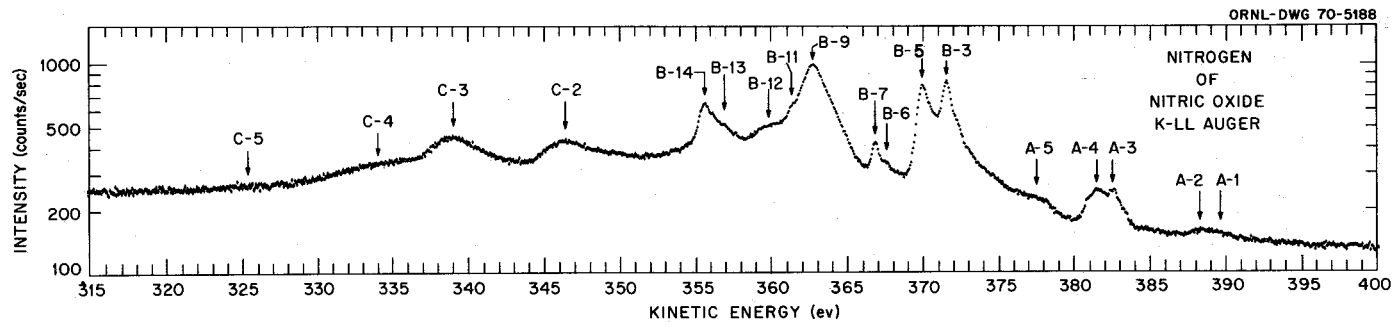


Figure 17. Nitrogen K-LL Auger electron spectrum of nitric oxide excited by electron impact.

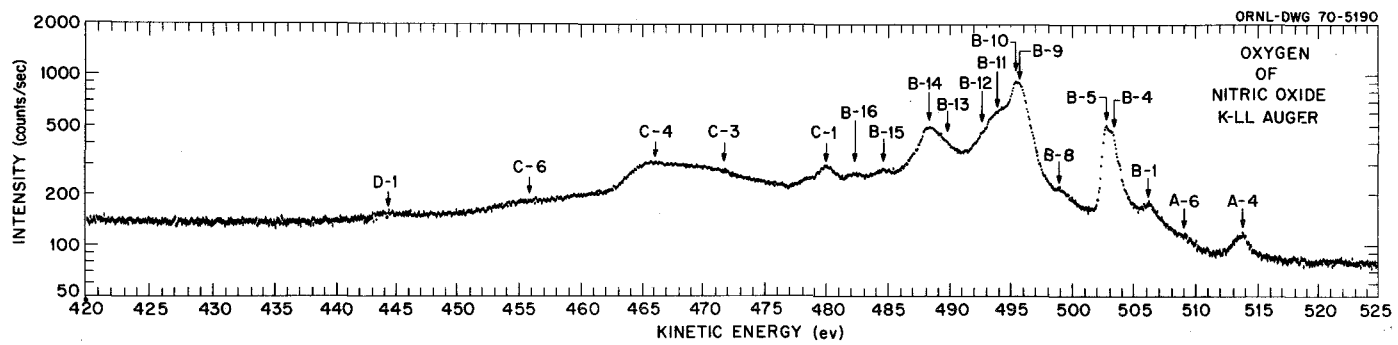


Figure 18. Oxygen K-LL Auger electron spectrum of nitric oxide excited by electron impact.

TABLE VII  
ELECTRON PEAK ENERGIES IN K-LL AUGER  
SPECTRUM OF MOLECULAR NITROGEN

Peak <sup>a</sup>	Absolute Energy (eV)
A-1	384.7 ± 0.4
A-2	383.8 ± 0.2
A-3	378.6 ± 0.5
A-4	376.7 ± 0.6
A-5	378.3 ± 0.5
A-6	375.0 ± 0.5
A-7	371.7 ± 0.6
B-1'	367.0
B-1	366.5 ± 0.2
B-2	365.0 ± 0.4
B-3	363.5 ± 0.5
B-4	362.5 ± 0.5
B-5	360.2 ± 0.2
B-6	358.7 ± 0.2
B-7	356.9 ± 0.3
B-8	354.7 ± 0.6
B-9	352.5 ± 0.6
B-10	350.4 ± 0.6
B-11	347.8 ± 0.6
C-1	342.4 ± 0.4
C-2	339.1 ± 0.5
C-3	337.4 ± 0.6
C-4	332.7 ± 0.7
D-1	315.0 ± 0.9

<sup>a</sup>All peaks except A-5, A-6 and A-7 were identified in the electron excited spectrum, Figure 13. A-5, A-6 and A-7 were seen in photon excited spectrum, Figure 21, page 54. The onset of a peak is indicated by a primed number.

TABLE VIII

ELECTRON PEAK ENERGIES IN K-LL AUGER  
SPECTRUM OF MOLECULAR OXYGEN

Peak <sup>a</sup>	Absolute Energy (eV)
A-1	519.4 ± 0.6
A-2	518.2 ± 0.6
A-3	517.1 ± 0.6
A-4	512.8 ± 0.4
A-5	511.6 ± 0.4
A-6	510.4 ± 0.3
A-7	510.0 ± 0.5
A-8	507.7 ± 0.5
A-9	511.9 ± 0.6
B-1'	506.8
B-1	505.9 ± 0.3
B-2	504.0 ± 0.3
B-3	502.7 ± 0.6
B-4	501.4 ± 0.2
B-5	500.3 ± 0.2
B-6	499.7 ± 0.3
B-7	496.4 ± 0.6
B-8	495.6 ± 0.5
B-9	494.6 ± 0.5
B-10	492.8 ± 0.5
B-11	491.8 ± 0.3
B-12	486.2 ± 0.6
B-13	483.8 ± 0.6
B-14	481.4 ± 0.7
C-1	476.5 ± 0.5
C-2	470.1 ± 0.6
C-3	463.3 ± 0.6
C-4	455.9 ± 0.9

<sup>a</sup>All peaks except A-9 were identified in the electron excited spectrum, Figure 14. A-9 was seen in the photon excited spectrum, Figure 26, page 64. The onset of a peak is indicated by a primed number.

TABLE IX

ELECTRON PEAK ENERGIES IN CARBON K-LL AUGER  
SPECTRUM OF CARBON MONOXIDE

Peak <sup>a</sup>	Absolute Energy (eV)
A-1	273.0 ± 0.2
A-2	272.7 ± 0.2
A-3	270.8 ± 0.2
A-4	270.6 ± 0.2
A-5	270.4 ± 0.2
A-6	270.2 ± 0.2
A-7	267.4 ± 0.2
A-8	264.3 ± 0.3
A-9	262.1 ± 0.3
A-10	259.7 ± 0.2
A-11	259.0 ± 0.3
B-1'	256.0 ± 0.3
B-1	254.0 ± 0.2
B-2	252.5 ± 0.4
B-3	250.4 ± 0.2
B-6	246.4 ± 0.4
B-7	245.3 ± 0.4
B-8	242.4 ± 0.4
B-10	239.3 ± 0.5
C-1	230.3 ± 0.8
C-3	220.9 ± 0.9

<sup>a</sup>All peaks were identified in Figure 15.  
The onset of a peak is indicated by a primed  
number.

TABLE X  
ELECTRON PEAK ENERGIES IN OXYGEN K-LL AUGER  
SPECTRUM OF CARBON MONOXIDE

Peak <sup>a</sup>	Absolute Energy (eV)
A-3	516.6 ± 0.4
A-8	510.1 ± 0.5
A-10	505.7 ± 0.5
B-1'	501.6
B-1	500.4 ± 0.2
B-4	496.1 ± 0.4
B-5	494.5 ± 0.4
B-7	491.5 ± 0.3
B-9	487.6 ± 0.3
B-11	485.1 ± 0.3
B-12	481.5 ± 0.7
C-2	469.4 ± 0.5
C-4	459.1 ± 0.7
D-1	447.2 ± 0.6
D-2	437.4 ± 0.9

<sup>a</sup>All peaks were identified in Figure 16. The onset of a peak is given by a primed number.

TABLE XI

ELECTRON PEAK ENERGIES IN NITROGEN K-LL  
AUGER SPECTRUM OF NITRIC OXIDE

Peak <sup>a</sup>	Absolute Energy (eV)
A-1	389.8 ± 0.6
A-2	388.5 ± 0.6
A-3	382.5 ± 0.4
A-4	381.2 ± 0.4
A-5	377.6 ± 0.6
B-1'	376.1
B-1	374.8 ± 0.4
B-2	373.1 ± 0.4
B-3	371.7 ± 0.2
B-5	370.0 ± 0.3
B-6	367.6 ± 0.5
B-7	366.9 ± 0.3
B-10	362.7 ± 0.3
B-11	361.5 ± 0.5
B-12	360.0 ± 0.6
B-13	357.1 ± 0.6
B-14	355.8 ± 0.3
C-2	346.6 ± 0.5
C-3	339.1 ± 0.5
C-4	334.2 ± 0.9
C-5	325.5 ± 0.9

<sup>a</sup>All peaks except B-1 and B-2 were identified in the electron excited spectrum, Figure 17. B-1 and B-2 were characterized in the photon excited spectrum, Figure 33, page 80. The onset of a peak is indicated by a primed number.

TABLE XII

ELECTRON PEAK ENERGIES IN OXYGEN K-LL  
AUGER SPECTRUM OF NITRIC OXIDE

Peak <sup>a</sup>	Absolute Energy (eV)
A-4	514.6 ± 0.4
A-6	509.9 ± 0.6
B-1'	508.9
B-1	507.2 ± 0.4
B-4	503.3 ± 0.2
B-5	502.9 ± 0.2
B-8	499.2 ± 0.6
B-9	496.0 ± 0.2
B-10	495.5 ± 0.6
B-11	494.0 ± 0.6
B-12	492.5 ± 0.6
B-13	489.8 ± 0.6
B-14	488.3 ± 0.4
B-15	485.0 ± 0.5
B-16	482.4 ± 0.5
C-1	480.1 ± 0.3
C-3	471.5 ± 0.9
C-4	466.1 ± 0.9
C-6	456.0 ± 0.9
D-1	444.5 ± 0.8

<sup>a</sup>All peaks were identified in Figure 18.  
B-1' was estimated from Figure 33, page 80.

contributions to the four divisions are: (1) A - readjustments to a 1s vacancy by an Auger process involving electrons in molecular orbitals from autoionized and monopole excited states; (2) B - readjustments to a 1s vacancy by an Auger process involving weakly bound electrons, w; (3) C - readjustments involving both weakly, w, and tightly, s, bound electrons; and (4) D - readjustments involving essentially only tightly bound electrons, s. For the location of the Auger electron energies found in region A, 1s-absorption and 1s-photoelectron data are used. The absolute magnitude of the energies in regions B, C and D can be located by employing equation (1-4) or Table I, pages 10-11. In practice, however, region B is the only region that is effectively located by employing one of the above; C and D are more realistically found by using equations (3-4), (3-5) and (3-6) of this chapter, page 88.

#### 1. Analysis of Region A - High Energy Satellite Lines

Auger electrons produced in region A result mainly from the decay of autoionized and monopole excited states by an Auger transition. As will be recalled from Chapter I, page 7, an autoionized state is formed by resonance excitation of a 1s (or K) electron into an unoccupied molecular orbital; a monopole excited state is formed by the excitation of a valence electron into an excited molecular orbital due to the sudden formation of an inner-shell vacancy. If monochromatic photons greater than the 1s binding energy are used to excite the K-LL Auger spectrum, resonance absorption will not occur. Thus, the Auger spectrum arising from photon excitation will be absent of lines that result from autoionization transitions. Monopole excited states will form with either electron or x-ray

excitation. Thus, the decay of these latter states will appear in an electron and an x-ray excited Auger spectrum. However, by exciting the K-LL Auger spectrum with electrons and photons, high energy lines can be identified and in some cases characterized, which in turn aids in the identification of the highest energy normal Auger process.

a. Nitrogen. The electron configuration of nitrogen is  $(1s\sigma_g)^2(1s\sigma_u)^2(2s\sigma_g)^2(2s\sigma_u)^2(2p\pi_u)^4(2p\sigma_g)^2$ . The molecular orbital diagram is given in Figure 19. From the 1s-absorption data of Nakamura, et al,<sup>41</sup> using synchrotron irradiation, eight unoccupied molecular orbitals are filled by resonance absorption giving rise to eight initial autoionization states of 400.2, 405.6, 406.5, 406.7, 407.7, 407.9, 408.2 and 408.5 eV. The 1s to  $2p\pi_g(1\Pi_u)$  absorption at 400.2 eV, represented in Figure 20a, is the strongest in intensity (by a factor of ten above any of the other transitions). If we assume similar autoionization states can be formed by using a high energy electron beam, Auger electron energies would be expected at 383.5, 388.9, 389.8, 390.0, 391.0, 391.2, 391.5 and 391.8 eV. These energies are calculated by using equation (3-1), where  $E_A(A)$  is the

$$E_A(A) = E^* - E_{X_2+1} \quad (3-1)$$

Auger electron energy found in region A,  $E^*$  is the resonance absorption energy -- the energy available for the Auger transition -- and  $E_{X_2+1}$  is the energy of the electronic state of the singly charged ion. In the above calculations the energy of the  $2p\pi_u$  orbital, 16.7 eV, was used. Because of the absence in Figure 13, page 37, of high energy Auger electron energies above 385 eV, there appears to be only one autoionization electronic state,  $1\Pi_u$ , appreciably populated by resonance absorption.

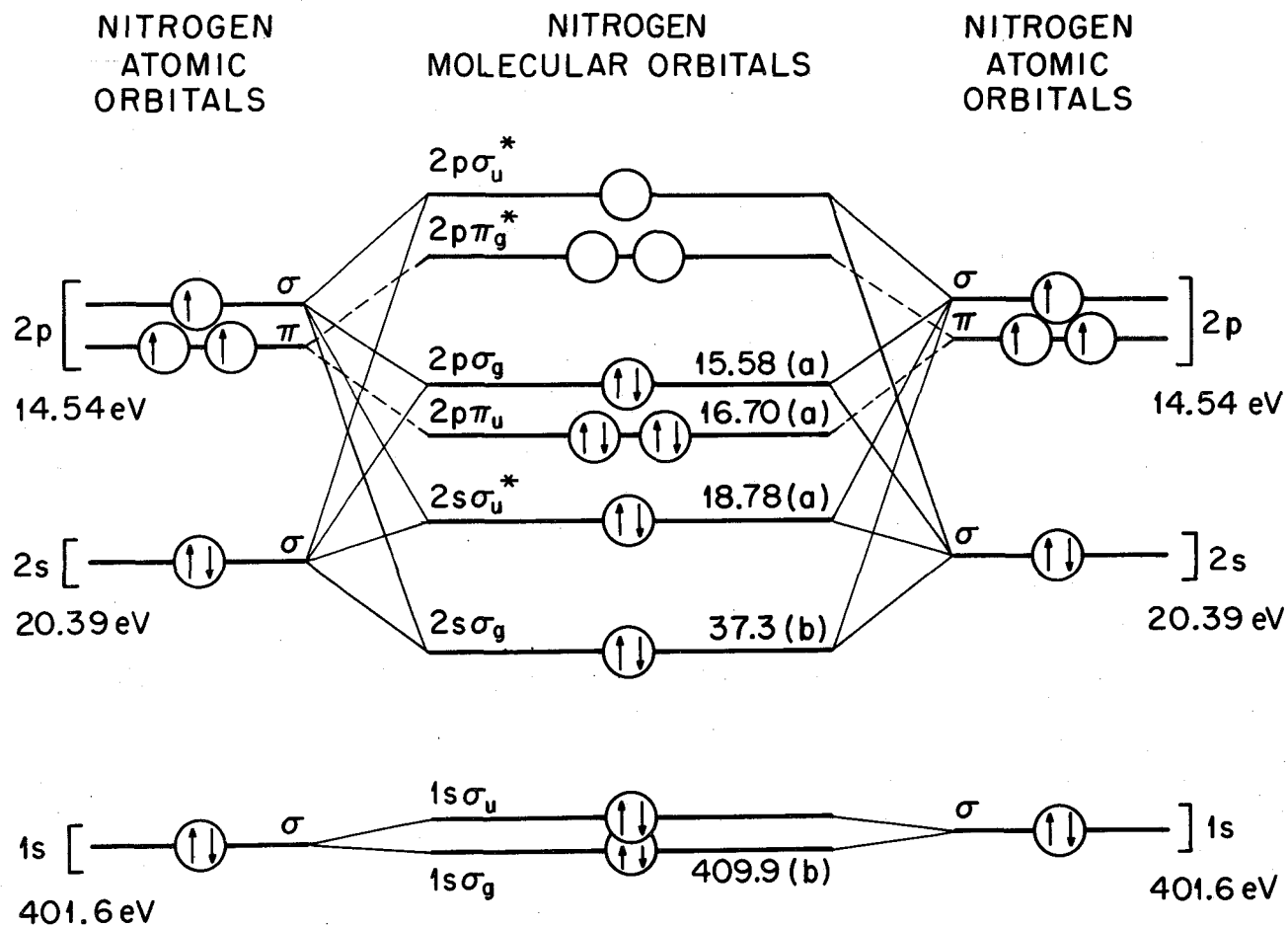


Figure 19. Molecular orbital diagram for nitrogen.

(a), obtained from reference 37; (b), obtained from reference 11.

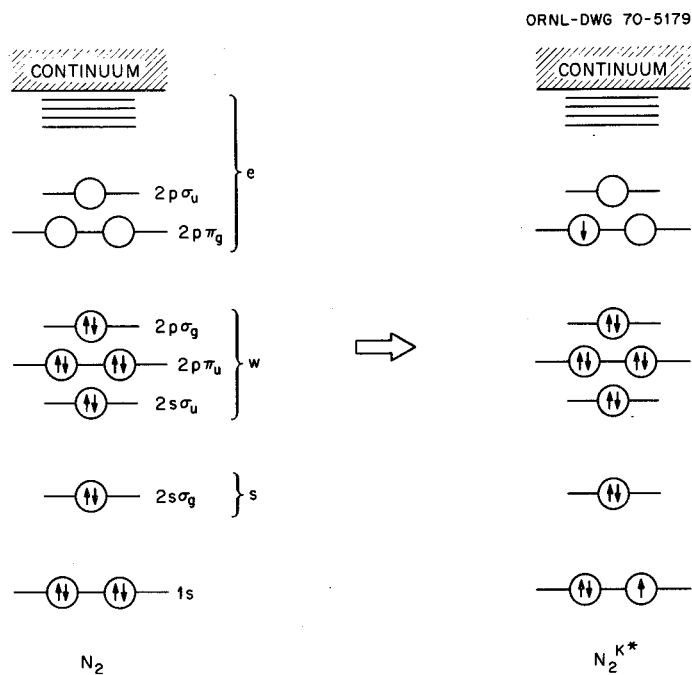


Figure 20a. Formation of  $N_2^{K^*}$  by absorption of a  $1s(K)$  electron into the empty  $2p\pi_g$  level.

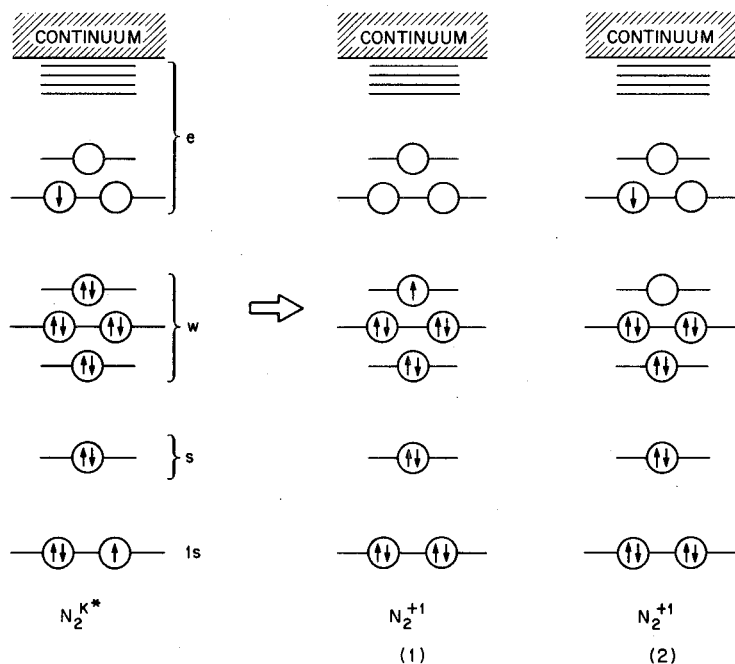


Figure 20b. Decay of  $N_2^{K^*}$ .

(1), outer-excited process; (2), inner-excited process.

The autoionization states will be represented as  $X_2^{K*}$ , i.e., for nitrogen,  $N_2^{K*}$ . The two decay modes of  $N_2^{K*}$  by autoionization, shown in Figure 20b, are classified as to whether or not the electron in the excited molecular orbital,  $2p\pi_g$  in the case of  $N_2$ , participates in the transition. For example, for nitrogen, when the excited molecular orbital participates in the Auger transition the process will be labeled  $1s(2p\pi_g)^{+1} - (2p\pi_g)w$  and will be referred to as an "outer-excited" autoionization transition; and, a process in which the  $2p\pi_g$  electron remains as a "spectator" will be labeled  $1s(2p\pi_g)^{+1} - ww$  and will be referred to as an "inner excited" transition (again,  $w$  signifies the weakly bonding electrons). As pointed out for nitrogen by Carlson, et al,<sup>9</sup> "inner-excited" autoionization transitions are basically normal K-LL Auger processes occurring under the electrostatic shell of the spectator  $2p\pi_g$  electron (see Figure 20b).

The data points designated by (+) in Figure 21 are derived by reproducing Figure 13, page 37, without its background. The Auger electron energies A-1 through A-4 and the shaded area of Figure 21 have been assigned to autoionization transitions. Table XIII compares the energies of the resultant singly charged ion  $E_{N_2+1}$ , as calculated from equation (3-1), with known values. Qualitatively, the general appearance of the "inner-excited" structure A-3 and A-4 through 370 eV should be compared with the diagram lines B-1 through B-6 (the latter lines are shifted on the order of 10 eV higher in energy).

If the assignments of peaks A-1 through A-4 and the shaded area of Figure 21 are correct, the processes that result in this structure should be absent if the energy for resonance absorption ( $1s \rightarrow 2p\pi_g$ ) is not available. Therefore, if monochromatic photons of energy above the  $1s$  binding

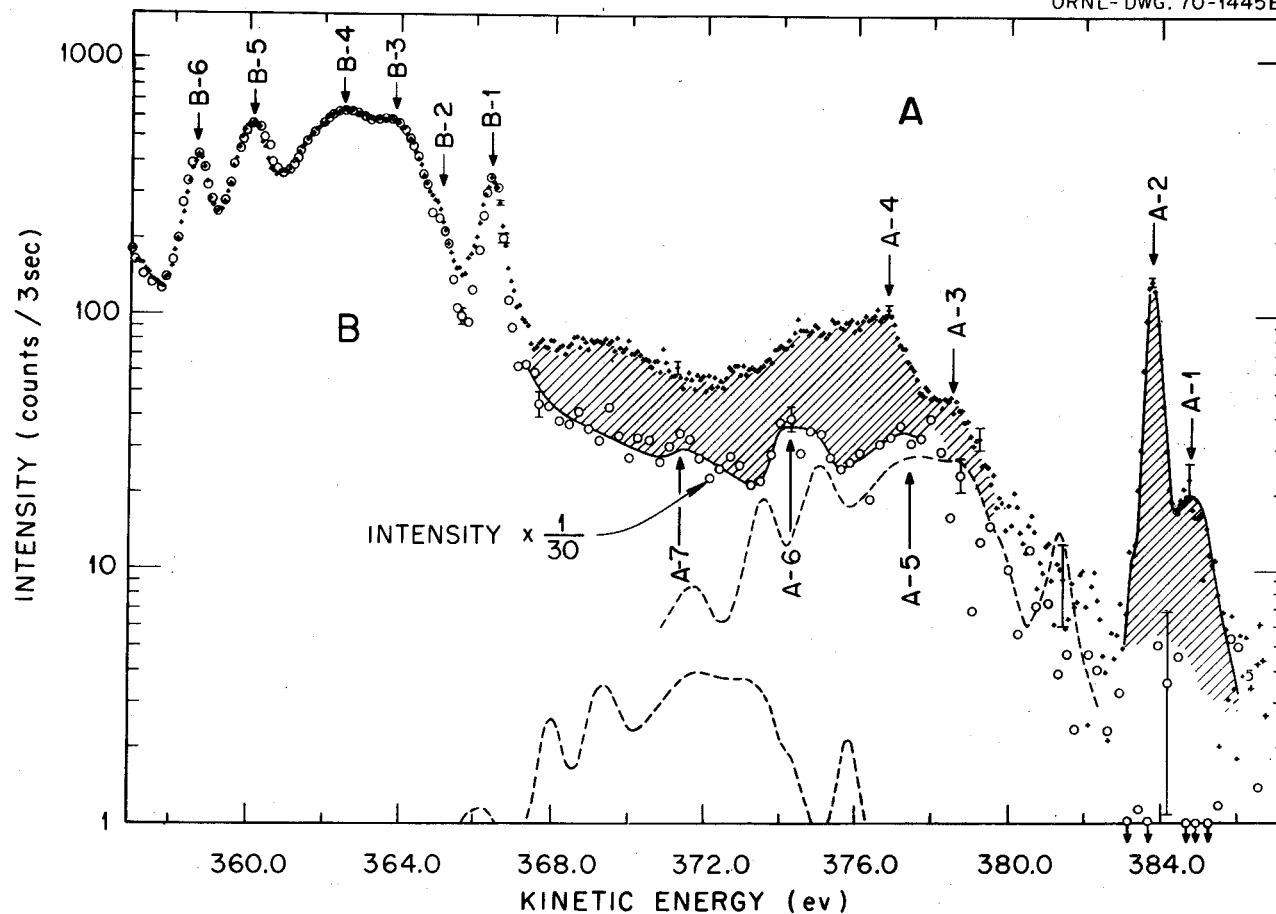


Figure 21. High energy portion of the K-LL Auger electron spectrum of molecular nitrogen excited by electrons and aluminum  $K_{\alpha}$  photons.

plus data points (+) represent the electron excited spectrum of molecular nitrogen, circle data points (o) represent the AlK excited spectrum, dashed lines (--) represent the expected decay of  $N_2 K^{+*}$  states.

TABLE XIII

ASSIGNMENTS OF THE PEAKS APPEARING IN THE HIGH ENERGY SATELLITE REGION OF THE K-LL AUGER SPECTRUM OF MOLECULAR NITROGEN

Peak <sup>a</sup>	Initial State <sup>b</sup>	$E_{N_2+1}$ from This Work (eV) <sup>c</sup>	$E_{N_2+1}$ from Other Auger Data (eV)	$E_{N_2+1}$ from Other Sources (eV) <sup>d</sup>	Assignment <sup>e</sup>
A-1	$N_2^{K^*}$	15.5		15.576 ( $X^2\Sigma_g^+$ ) <sup>42</sup>	Outer-excited
A-2	$N_2^{K^*}$	16.4	16.5, <sup>8</sup> 16.0 <sup>11</sup>	16.693 ( $A^2\Pi_u$ ) <sup>42</sup>	Outer-excited
A-3	$N_2^{K^*}$	21.6		20.7 <sup>43</sup> 21.1 ( $^4\Sigma_u^+$ ) <sup>44</sup> 21.9 ( $^4\Delta_u$ ) <sup>44</sup> 23.0 ( $^-\Sigma_u$ ) <sup>44</sup>	Inner-excited
A-4	$N_2^{K^*}$	23.5		23.8 ( $^4\Pi_g$ ) <sup>44</sup> 24.6 ( $D^2\Pi$ ) <sup>45</sup> 25.0 ( $C^+\Sigma_u$ ) <sup>11,45</sup>	Inner-excited
A-5	$N_2^{K+^*}$				
A-6	$N_2^{K+^*}$				
A-7	$N_2^{K+^*}$				

<sup>a</sup>All peaks appear in Figure 21. Peaks A-1, A-2, A-3 and A-4 also appear in Figure 13, page 37.

<sup>b</sup> $N_2^{K^*}$  is the autoionization state of nitrogen populated by resonance absorption of the 1s electron into an excited molecular orbital. In the case of nitrogen apparently only the  $2p\pi_g$  is populated.  $N_2^{K+^*}$  is an excited state of a nitrogen ion with a hole in the 1s level.

<sup>c</sup> $E_{N_2+1}$  is the energy of the nitrogen positive-one ion relative to the ground electronic state of a neutral nitrogen molecule. The different  $E_{N_2+1}$  values were calculated from equation (3-1), page 50.

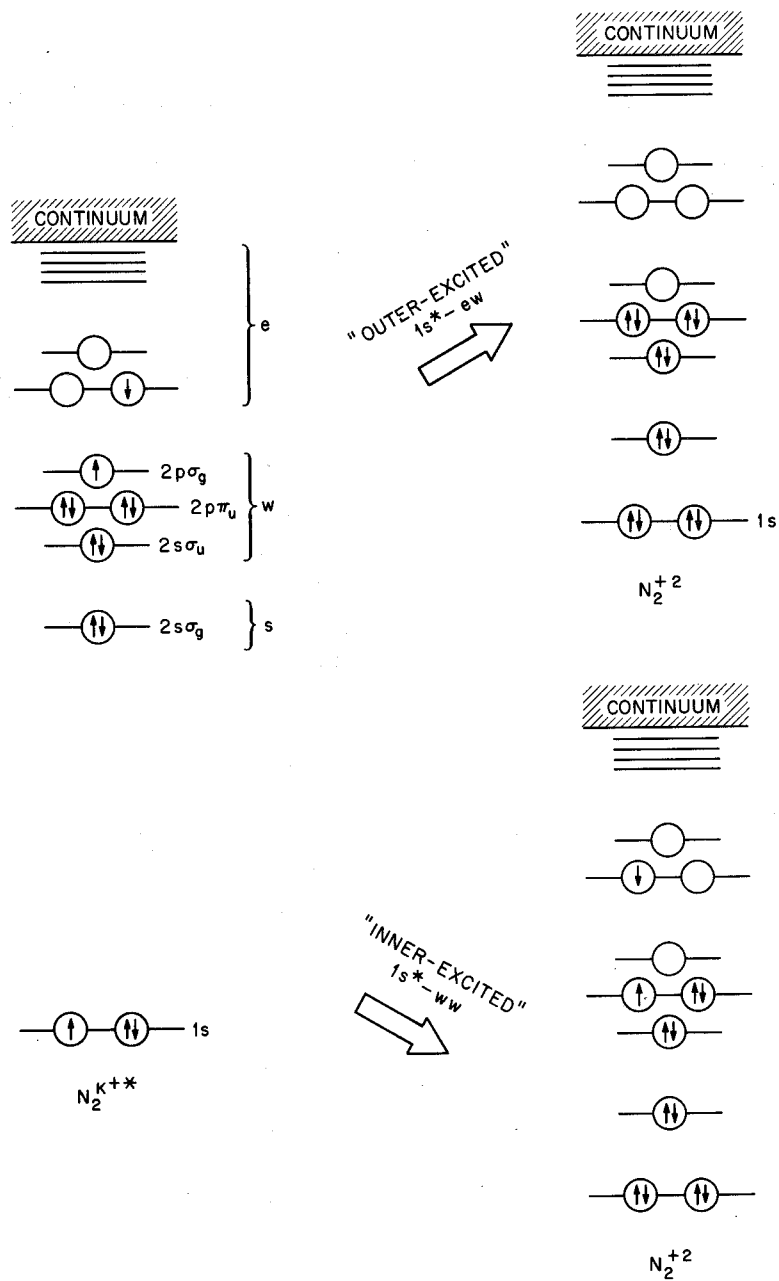
<sup>d</sup>The final electronic state is given in parenthesis.

<sup>e</sup>Peak A-1 probably results from a  $1s(2p\pi_g)^{+1} - 2p\pi_g 2p\sigma_g(X^2\Sigma_g^+)$  transition. Peak A-2 results from a  $1s(2p\pi_g)^{+1} - 2p\pi_g 2p\pi_u(A^2\Pi_u)^g$  transition. Peaks A-3 and A-4 are assigned to  $1s(2p\pi_g)^{+1}$ -ww processes.

energy of nitrogen are used to excite the K-LL Auger spectrum of nitrogen, the peaks attributed to autoionization should disappear. The high energy portion of the aluminum  $K_{\alpha}$  excited molecular nitrogen Auger spectrum (0 - data points) of Figure 21 with background removed is superimposed on the electron excited spectrum (+ - data points). The reader is directed to obvious disappearance of A-1 and A-2, the "outer-excited" peaks, and to the decrease in the intensity of the "inner-excited" structure between A-3 and 370 eV.

The remaining peaks, A-5, A-6 and A-7, apparently do not result from resonance absorption, but rather from a readjustment to a  $1s$ -vacancy of an excited nitrogen ion, the monopole excited  $N_2^{K+*}$ . The decay modes of  $N_2^{K+*}$  by an Auger process are represented in Figure 22. Knowledge of  $N_2^{K+*}$  states can be obtained from the  $1s$ -photoelectron spectrum of nitrogen given in Figure 23. The peaks on the low energy side of the  $1s$ -photoelectron peak can be attributed to the formation of monopole excited states. In addition, structure due to excitations in neutral nitrogen molecules can be found. Excitations of neutral nitrogen in the  $1s$ -photoelectron spectrum can be accounted for by: (1) studying the  $1s$ -photoelectron spectrum as a function of pressure and (2) studying the inelastic scattered electrons at the same pressure and energy as that used in the photoelectron run. The two pressure investigations gave consistent results. The pressure correction for collision losses in neutral nitrogen is represented in (2) of Figure 23. By subtracting contributions for these collision losses different  $N_2^{K+*}$  states could be ascertained. The contribution of monopole excited states in nitrogen is represented in (3) of Figure 23. The energy analysis of Figure 23 is given in Table XIV. Figure 24

ORNL-DWG 70-5178

Figure 22. Decay modes of  $N_2^{K+*}$ .

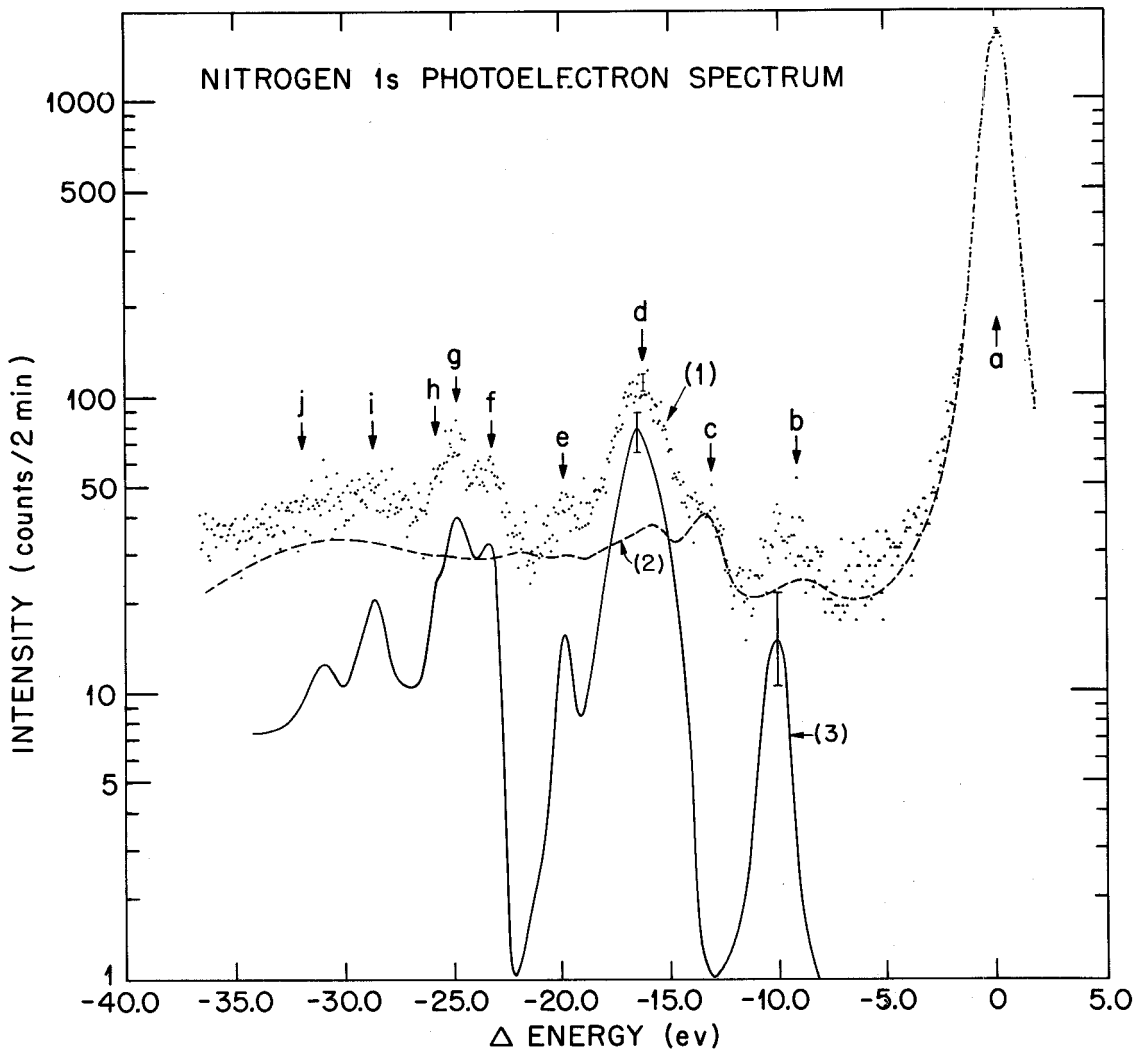


Figure 23. The 1s photoelectron spectrum of nitrogen.

1, raw data; 2, pressure correction for collision losses in neutral nitrogen; 3,  $N_2^{K+*}$  states.

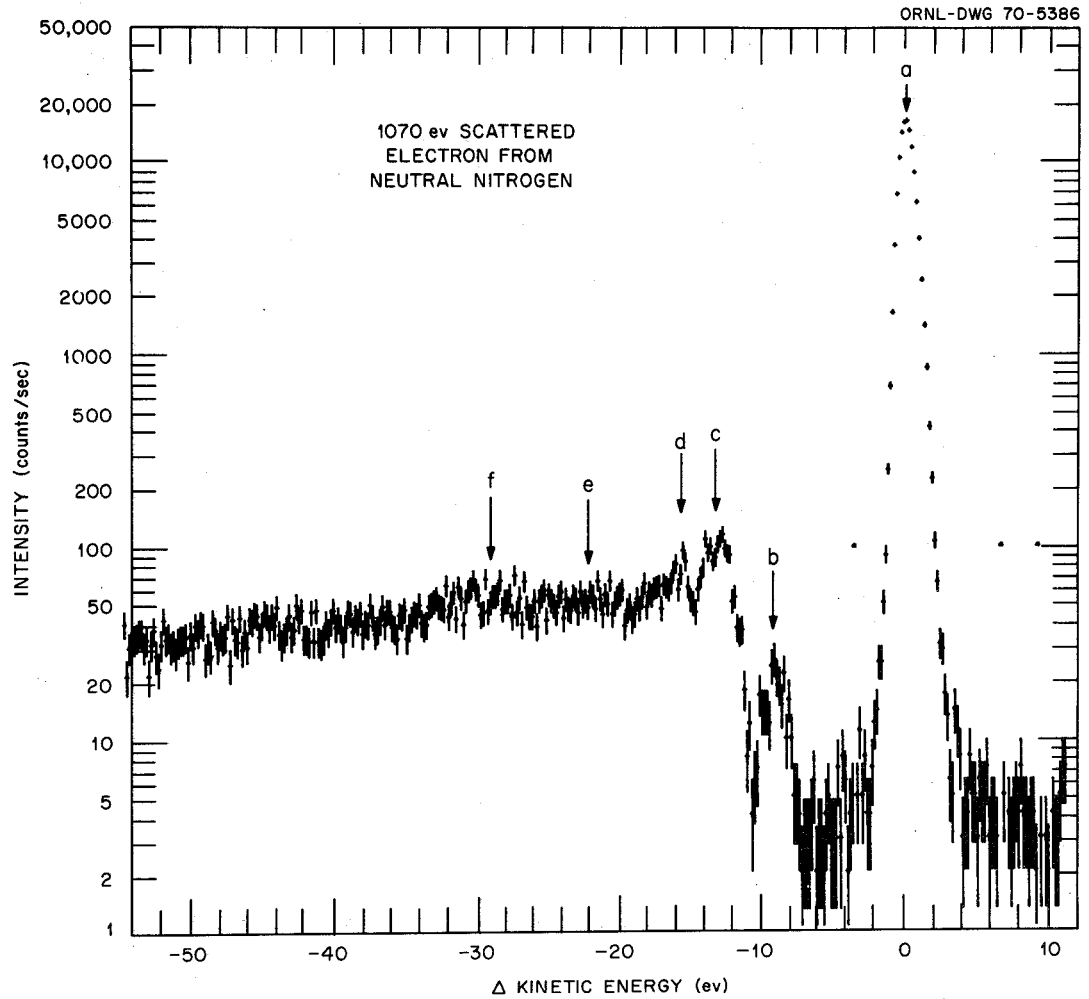


Figure 24. 1070 eV electrons elastically and inelastically scattered from neutral nitrogen molecules at 5 microns gas pressure.

TABLE XIV

RELATIVE ENERGIES AND INTENSITIES OF THE OBSERVED PEAKS IN  
THE 1s-PHOTOELECTRON SPECTRUM OF MOLECULAR NITROGEN

Peak <sup>a</sup>	Energy from a <sup>b</sup> (eV)	Intensity Relative to a <sup>c</sup>	Assignment <sup>d</sup>
a	0.0	100.	N <sub>2</sub> K+
b	-10.0 ± 0.3	0.9	N <sub>2</sub> K+*
c	-13.2 ± 0.5		N <sub>2</sub> *
d	-16.3 ± 0.4	4.6 ± 1.2	N <sub>2</sub> K+*
e	-19.8 ± 0.4	0.8	N <sub>2</sub> K+*
f	-23.3 ± 0.3	1.9	N <sub>2</sub> K+*
g	-24.9 ± 0.3	2.2	N <sub>2</sub> K+*
h	-25.9 ± 0.5	1.3	N <sub>2</sub> K+*
i	-28.7 ± 0.4	1.2	N <sub>2</sub> K+*
j	-31.1 ± 0.5	0.8	N <sub>2</sub> K+*

<sup>a</sup>Peaks were observed in Figure 23.

<sup>b</sup>Peak c is pressure dependent.

<sup>c</sup>The peak intensities were corrected for unelastic scattering from neutral nitrogen.

<sup>d</sup>N<sub>2</sub> K+ represents a nitrogen ion with a vacancy in the 1s-level. N<sub>2</sub> K+\* represents a monopole excited state of N<sub>2</sub> K+, N<sub>2</sub> represents an excited nitrogen neutral molecule.

illustrates the elastic and inelastic scattered electrons from neutral nitrogen, and Table XV gives the results of the scattered electron measurements. From the analysis of Figure 23, states of  $N_2^{K+*}$  appear at -10.0, -16.3, -19.8, -23.3, -24.4 and -25.9 eV above  $N_2^{K+}$  with the peak at -16.3 of greatest intensity.

Since the charge on the resulting ion from readjustments to  $N_2^{K+*}$  is plus two, one might expect to see the normal lines (B-1 through B-7) shifted some 10.0, 16.3, 20.0, 23.3 eV, etc. to higher energy at 0.9, 4.6, 0.8, 1.9, etc. percent of their original intensity. The apparent shift of B-1 through B-7 some 10.0 and 16.3 eV is consistent with the observed structure, A-5, A-6 and A-7, excited by x-rays (see dashed lines in Figure 21, page 54, for curve fitting following the shift of B-1 through B-7 to higher energy).

b. Oxygen. The electronic configuration of neutral oxygen is  $(1s\sigma_g)^2(1s\sigma_u)^2(2s\sigma_g)^2(2s\sigma_u)^2(2p\sigma_g)^2(2p\pi_u)^4(2p\pi_g)^2$ . Figure 25 gives the molecular orbital diagram of oxygen with the associated binding energies of the different orbitals. Since the  $2p\pi_g$  level is half filled and no ls-absorption data is available, the formation of the initial autoionization state (or states) is not clear in the case of oxygen. Any assignments of the autoionization Auger transitions to different final electronic states of singly charged oxygen cannot be made. However, classification of the structure as to inner- or outer-excited autoionization transitions is considered.

The points (+) of Figure 26 are obtained by expanding Figure 14, page 38, and subtracting the background. If A-1, A-2 and A-3 are attributed to outer-excited autoionization processes in which the excited

TABLE XV

RELATIVE ENERGIES AND INTENSITIES OF THE INELASTIC  
SCATTERED ELECTRONS FROM NEUTRAL NITROGEN  
AT APPROXIMATELY 5 MICRONS PRESSURE

Peak <sup>a</sup>	Energy From a (eV)	Intensity Ratio Relative to a	Known Energy From a <sup>b</sup> (eV)
a	0.0	100.	
b	-9.1 ± 0.3	0.3	-9.16
c	-12.8 ± 0.4	3.4	-12.93
d	-13.8 ± 0.4	3.0	
e	-16.0 ± 0.4	1.8	
f	-18.8 ± 0.7	1.4	
g	-22.6 ± 0.4	1.1	
h	-29.2 ± 0.7	1.0	

<sup>a</sup>Peaks were observed in Figure 24.

<sup>b</sup>The -9.16 and -12.93 eV were the most intense inelastic scattered peaks that occurred in the spectrum measured by Lassetre et al, reference 46. Other peaks of lower intensity were observed at -12.26 and -13.21 eV.

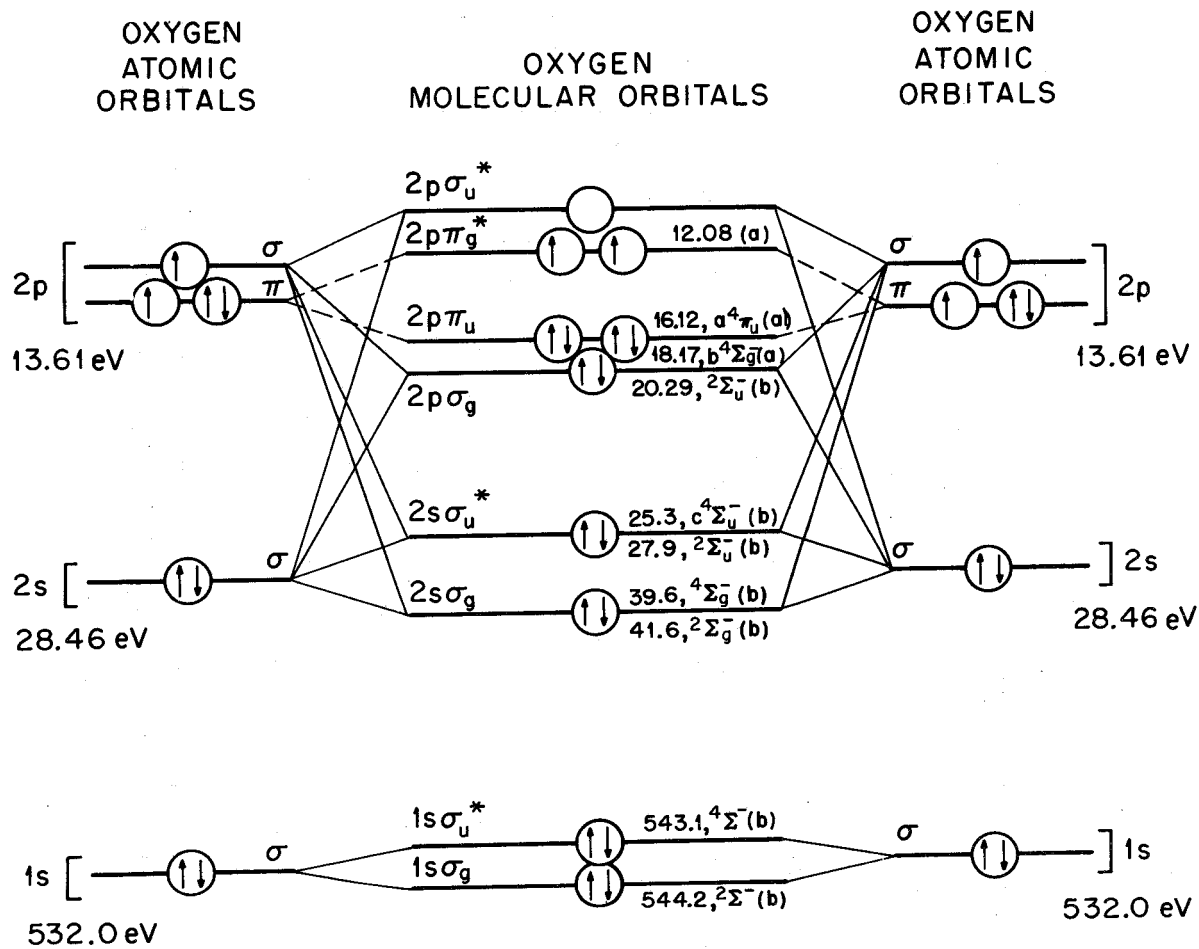


Figure 25. Molecular orbital diagram for oxygen.

(a), obtained from reference 47; (b), obtained from reference 11.

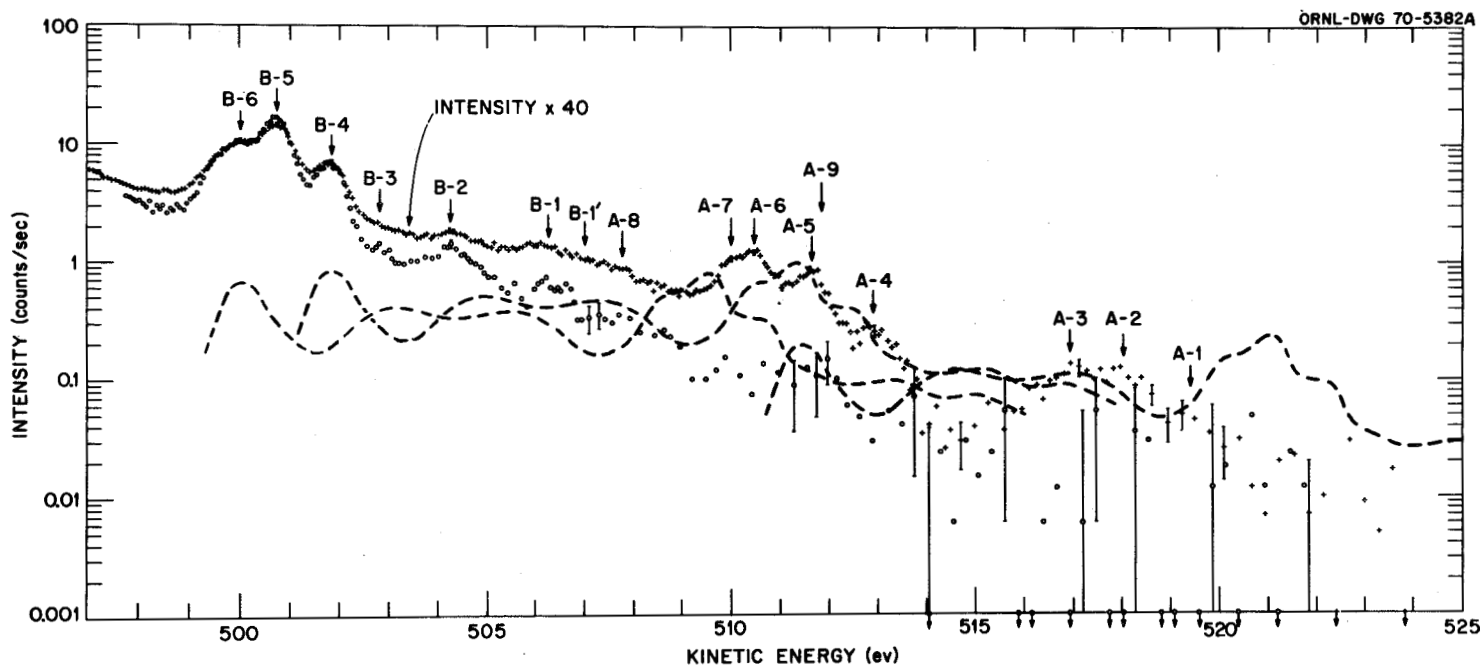


Figure 26. High energy portion of the K-LL Auger electron spectrum of molecular oxygen excited by electrons and aluminum  $K_{\alpha}$  photons.

plus data points (+) represent the electron excited spectrum of molecular oxygen, circle data points (o) represent the  $AlK_{\alpha}$  excited spectrum, dashed lines (--) represent the expected decay of  $O_2 K^{+*}$  states.

molecular orbital participates in the transition, A-4 through A-8 could result from inner-excited transitions. Since the inner-excited transitions can be imagined as normal Auger processes occurring under an occupied excited shell, a comparison of the likeness of B-4, B-5 and B-6 (the normal lines) to A-5, A-6 and A-7 (which are shifted on the order of 10 eV higher in energy) assists in the above assignment.

The Auger data excited with aluminum  $K_{\alpha}$  radiation is shown in Figure 26 (0 - points) superimposed on the electron excited spectrum (+ - points). A-4 through A-7 have disappeared with x-ray excitation, but the disappearance of A-1 and A-3 could not be determined because the statistics were not sufficient. Table XVI summarizes the results of the autoionization structure seen for oxygen.

Figure 27 illustrates the 1s-photoelectron spectrum of oxygen excited by aluminum  $K_{\alpha}$  radiation, and Table XVII gives the energy results of the observed structure. Three peaks, -8.5, -10.5 and -22.3 eV of 5.7, 7.6 and 2.7 percent relative intensity to the 1s line, could be identified with monopole excited states of oxygen. The expected decay of these three states to different electronic states of  $O_2^{+2}$  by an Auger transition that involves the excited molecular orbital is shown by the dashed structure of Figure 26. The dashed structure does not coincide with any of the 0 - points. However, the excited molecular orbital can remain occupied, and more tightly bound electrons beneath this orbital can be involved in the decay of  $O_2^{K+*}$  states (see Figure 22, page 57, for the representation of the two decay modes of  $N_2^{K+*}$  states). Krause, et al,<sup>20</sup> have demonstrated for neon that processes involving the spectator electron in the Auger transition account for

TABLE XVI

ASSIGNMENTS OF THE PEAKS APPEARING IN THE HIGH ENERGY  
SATELLITE REGION OF THE K-LL AUGER  
SPECTRUM OF MOLECULAR OXYGEN

Peak <sup>a</sup>	Energy From A-1 (eV)	Assignment
A-1	0.0	Outer-excited
A-2	-1.2	Outer-excited
A-3	-2.3	Outer-excited
A-4	-6.6	Inner-excited
A-5	-7.8	Inner-excited
A-6	-9.0	Inner-excited
A-7	-9.4	Inner-excited
A-8	-11.6	Inner-excited

<sup>a</sup>Peaks were obtained from Figures 14 and 26,  
pages 38 and 64, respectively.

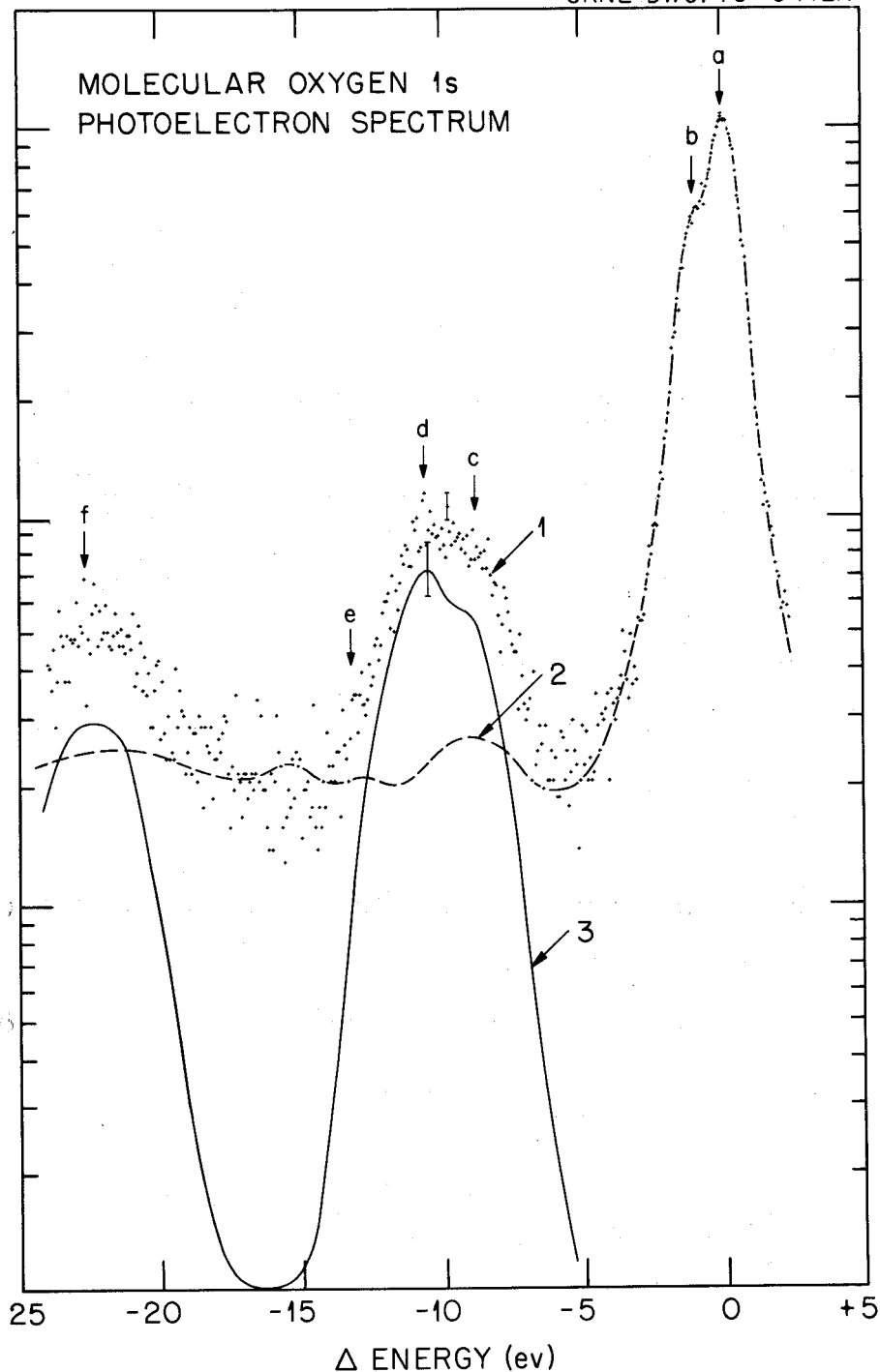


Figure 27. The 1s photoelectron spectrum of oxygen.

1, raw data; 2, pressure correction for collision losses in neutral oxygen; 3,  $O_2^{K+*}$  states.

TABLE XVII

RELATIVE ENERGIES AND INTENSITIES OF THE OBSERVED  
PEAKS IN THE 1s PHOTOELECTRON SPECTRUM  
OF MOLECULAR OXYGEN

Peak <sup>a</sup>	Energy From a <sup>b</sup> (eV)	Intensity Relative to a <sup>c</sup>	Assignment <sup>d</sup>
a	0.0	100.	O <sub>2</sub> <sup>K+</sup>
b	-1.2 ± 0.3		O <sub>2</sub> <sup>K+</sup>
c	-8.5 ± 0.4	5.8	O <sub>2</sub> <sup>K+*</sup>
d	-10.5 ± 0.4	7.6	O <sub>2</sub> <sup>K+*</sup>
e	-15.8 ± 0.6		O <sub>2</sub> <sup>*</sup>
f	-22.3 ± 0.6	2.7	O <sub>2</sub> <sup>K+*</sup>

<sup>a</sup>Peaks were observed in Figure 27.

<sup>b</sup>Peak e was pressure dependent.

<sup>c</sup>The peak intensities were corrected for inelastic scattering from neutral oxygen.

<sup>d</sup>O<sub>2</sub><sup>K+</sup> represents an oxygen ion with a vacancy in the 1s-level. O<sub>2</sub><sup>K+\*</sup> represents a monopole excited O<sub>2</sub><sup>K+</sup>. O<sub>2</sub><sup>\*</sup> represents an excited neutral molecule.

only 20 percent for the frequency of filling the K-vacancy with a monopole excited state. Thus, the remaining Auger structure of Figure 26 can be accounted for by reducing the dashed lines by one-fifth of their intensity.

The origin of the structure B-1 and B-2 is still questionable; i.e., they could result from the decay of monopole excited states by an "inner-excited" Auger process. The first excited state of molecular oxygen with an electron paired in the  $2p\pi_g$  orbital lies approximately 4.5 eV above the ground state.<sup>48</sup> Shifting the dashed structure of Figure 26 by this amount does not coincide with B-1 and B-2. Calculations on neon<sup>49</sup> indicate that the decay of monopole excited states by "inner-excited" transitions will lie 20 eV lower in energy to the decay involving the electron in the excited molecular orbital. Apparently B-1 and B-2 result neither from the decay of autoionization nor monopole excited states but from the decay of  $O_2^{K+}$ ,  $^4\Sigma^-$  and  $^2\Sigma^-$  initial states.

c. Carbon monoxide. The electronic configuration of neutral carbon monoxide is  $(1s_o)^2(1s_c)^2(2s\sigma^b)^2(2s\sigma^*)^2(2p\pi^b)^4(2p\sigma^b)^2$ . Figure 28 gives the molecular orbital diagram of carbon monoxide with the binding energies of the different orbitals. Figure 29 illustrates the high energy side of Figures 15 and 16, pages 39 and 40, excited by electrons (+ - points) and aluminum  $K_{\alpha}$  photons (0 - points). The absolute energy and energy separations observable in the carbon spectrum offer a unique opportunity to study vibrational structure by Auger spectroscopy. The region in which the vibrational structure can be determined has been seen in more detail by Siegbahn.<sup>11</sup> Table XVIII compares the data obtained from Figure 29 with

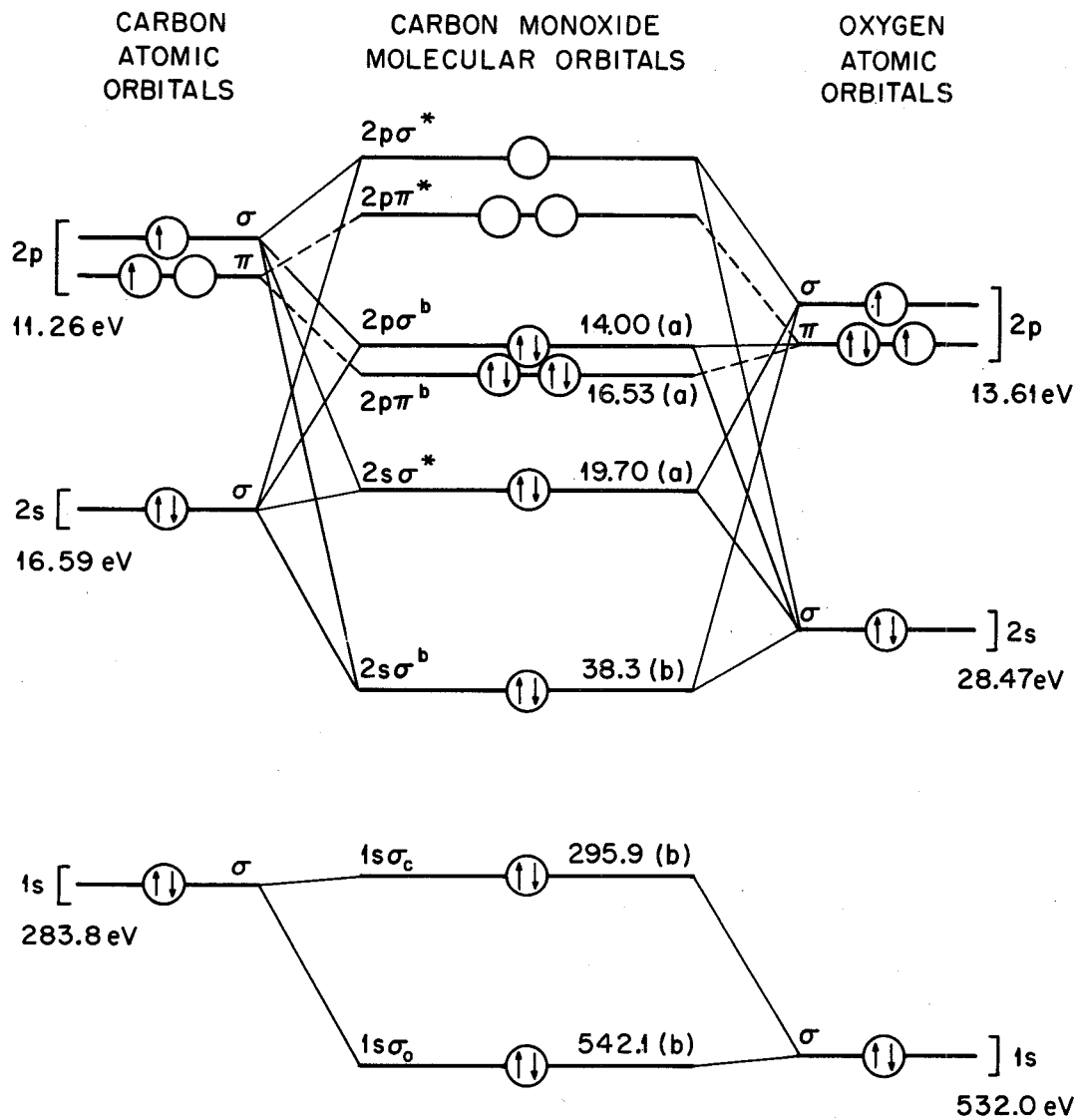


Figure 28. Molecular orbital diagram for carbon monoxide.

(a), obtained from reference 37; (b), obtained from reference 11.

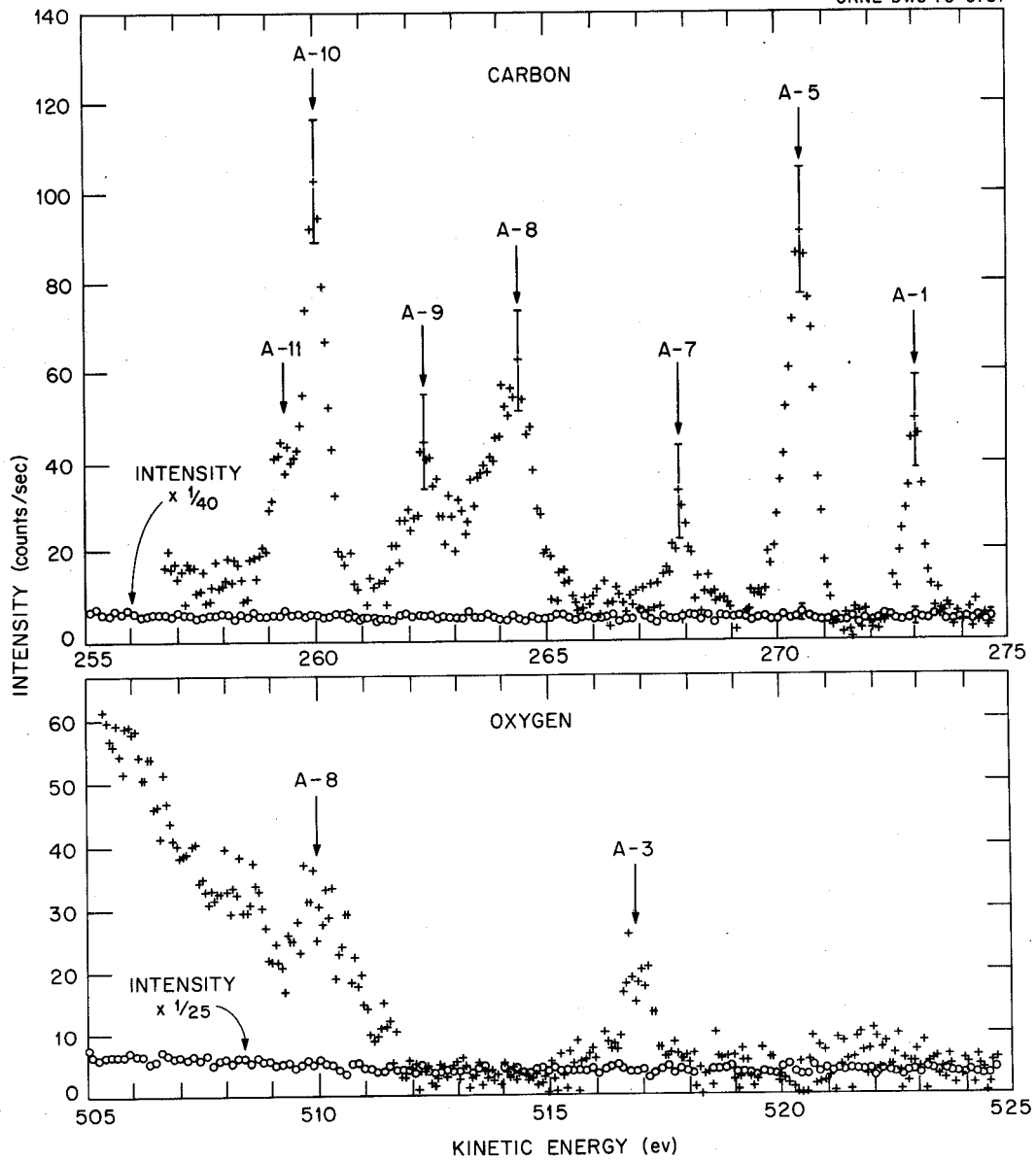


Figure 29. High energy portion of the carbon and oxygen K-LL Auger spectra of carbon monoxide excited by electrons and aluminum  $K_{\alpha}$  photons.

plus data points (+) represent the electron excited spectra of carbon monoxide, circle data points (o) represent the AlK<sub>α</sub> excited spectra.

TABLE XVIII

ASSIGNMENTS OF THE PEAKS APPEARING IN HIGH ENERGY  
SATELLITE REGION OF THE K-LL AUGER  
SPECTRA OF CARBON MONOXIDE

Peak <sup>a</sup>	Energy From A-1 in Carbon Spectrum <sup>b</sup> (eV)	Energy from A-8 in Oxygen Spectrum <sup>b</sup>	Results of Siegbahn <sup>c</sup> (eV)	Assignment <sup>d</sup>
A-1	0.00	----	0.00	Outer-excited
A-2	-0.28 ± 0.3	----	-0.26 ± 0.02	Outer-excited
A-3	-2.20 ± 0.07	(-2.2) +6.5	----	Outer-excited
A-4	-2.40 ± 0.06	----	(0.00) -2.51 ± 0.02	Outer-excited
A-5	-2.60 ± 0.06	----	(-0.19 ± 0.01)	Outer-excited
A-6	-2.80 ± 0.06	----	(-0.38 ± 0.01)	Outer-excited
A-7	-5.60 ± 0.06	----	-5.65 ± 0.04	Outer-excited
A-8	-8.7 ± 0.3	(-8.7) 0.0	-8.7 ± 0.3	Inner-excited
A-9	-10.9 ± 0.3	----	-10.9 ± 0.3	Inner-excited
A-10	-13.3 ± 0.2	(-13.2) -4.4	-13.3 ± 0.3	Inner-excited
A-11	-14.0 ± 0.3	----	-13.9 ± 0.3	Inner-excited

<sup>a</sup>Peaks were observed in Figure 29.

<sup>b</sup>Energy of peaks obtained from insert of Figure 29. Dashed line indicates no peak observed in the oxygen spectrum.

<sup>c</sup>Data were obtained from Reference 11.

<sup>d</sup>Peaks A-1 and A-2 probably result from a  $1s_c(e)^{+1} - e 2p\sigma_g (X^2\Sigma^+)$  transition, peaks A-3, A-4, A-5 and A-6 from  $1s_c(e)^{+1} - e 2p\pi_g (A^2\Pi)$ , and A-7 from  $1s_c(e)^{+1} - e 2s\sigma_u (B^2\Sigma^+)$ . A-8 through A-11 are probably inner-excited autoionization transitions where the excited e orbital remains occupied during the transition, although the delay of a monopole excited state might account for the peak A-9.

Siegbahn's results.<sup>11</sup> The observance of vibrational structure with peaks of 0.19 eV FWHM allows one to set an upper limit on the lifetime of the excited autoionized state of  $2 \times 10^{-15}$  sec.

By comparing the x-ray with the electron excited spectrum, peaks A-1 through A-11 disappear; therefore, they are assumed to result from autoionization. Unfortunately no ls-absorption data are available, and energies of the final electronic states can not be calculated and compared with known energies. However, A-1 (A-1 and A-2), A-4 (A-4 through A-6) and A-7 most probably result from the removal of  $2p\sigma^b$ ,  $2p\pi^b$  and  $2s\sigma^*$  molecular orbitals in forming the different final  $X^2\Sigma^+$ ,  $A^2\Pi$  and  $B^2\Sigma^+$  electronic states of  $CO^{+1}$ ; therefore, these transitions would be classified as "outer-excited" autoionization processes. The difference in energy between A-1 and A-4 and between A-1 and A-7 agree well with the spectroscopic differences between the  $X^2\Sigma^+ - A^2\Pi$  (2.57) and  $X^2\Sigma^+ - B^2\Sigma^+$  (5.69) states.<sup>50</sup> A-8, A-9 and A-10 could result from "inner-excited" Auger transitions taking place under an occupied excited orbital (see the similarity between the normal lines, B-1, B-2 and B-3, and the "inner-excited" lines, A-8, A-9 and A-10, except that the latter appear on the order of 10 eV higher in energy).

It has been observed in both our and Siegbahn's<sup>11</sup> experiments a small peak above the  $v = 0$  state of the  $A^2\Pi$  electronic state. The appearance of the vibrational peak A-3 could result from the decay of a vibrationally excited initial excited state to the ground vibrational state of the  $A^2\Pi$  electronic state of  $CO^{+1}$ . This is analogous to a "hot" band.<sup>51</sup>

The following two Figures, 30 and 31, show the 1s-photoelectron spectra of carbon and oxygen in CO. The values for the photoelectron data are given in Tables XIX and XX. Since monopole excited states do form, one would expect some contributions from the decay in the region A of the Auger spectrum to occur. However, results due to the decay of monopole excited states are inconclusive.

d. Nitric oxide. The electron configuration of nitric oxide is  $(1s_{\text{O}})^2(1s_{\text{N}})^2(2s\sigma^b)^2(2p\sigma^b)^2(2p\pi^b)^4(2p\pi^*)^1$ . Figure 32 gives the molecular orbital diagram of nitric oxide accompanied by the binding energies of the different orbitals. Figure 33 illustrates the high energy side of the K-LL Auger spectrum of nitric oxide (Figures 17 and 18, pages 41 and 42) excited with electrons (+ points) and x-rays (O points). Table XXI lists the possible assignments of the observed peaks. As in the case of molecular oxygen, there are many possible initial and final states; and, because no 1s-absorption data is available, assignment involving final states of the plus one ion is impossible. If A-1 and A-2 which are present in the nitrogen spectrum are assigned to outer-excited transitions, then A-3 through A-7 would arise from inner-excited transitions.

In comparing the oxygen and nitrogen spectra in region A, there appears to be a greater intensity of autoionization transitions in the nitrogen spectrum. This is consistent with the atomic population of the  $2p\pi^*$  molecular orbital which has been shown by SCF calculations<sup>52</sup> and photoelectron spectroscopy<sup>53</sup> to have approximately 64 percent nitrogen character.

Since peaks B-1 and B-2 do not disappear in the x-ray excited spectrum, their origin is other than the decay of an autoionization state. B-1 and B-2

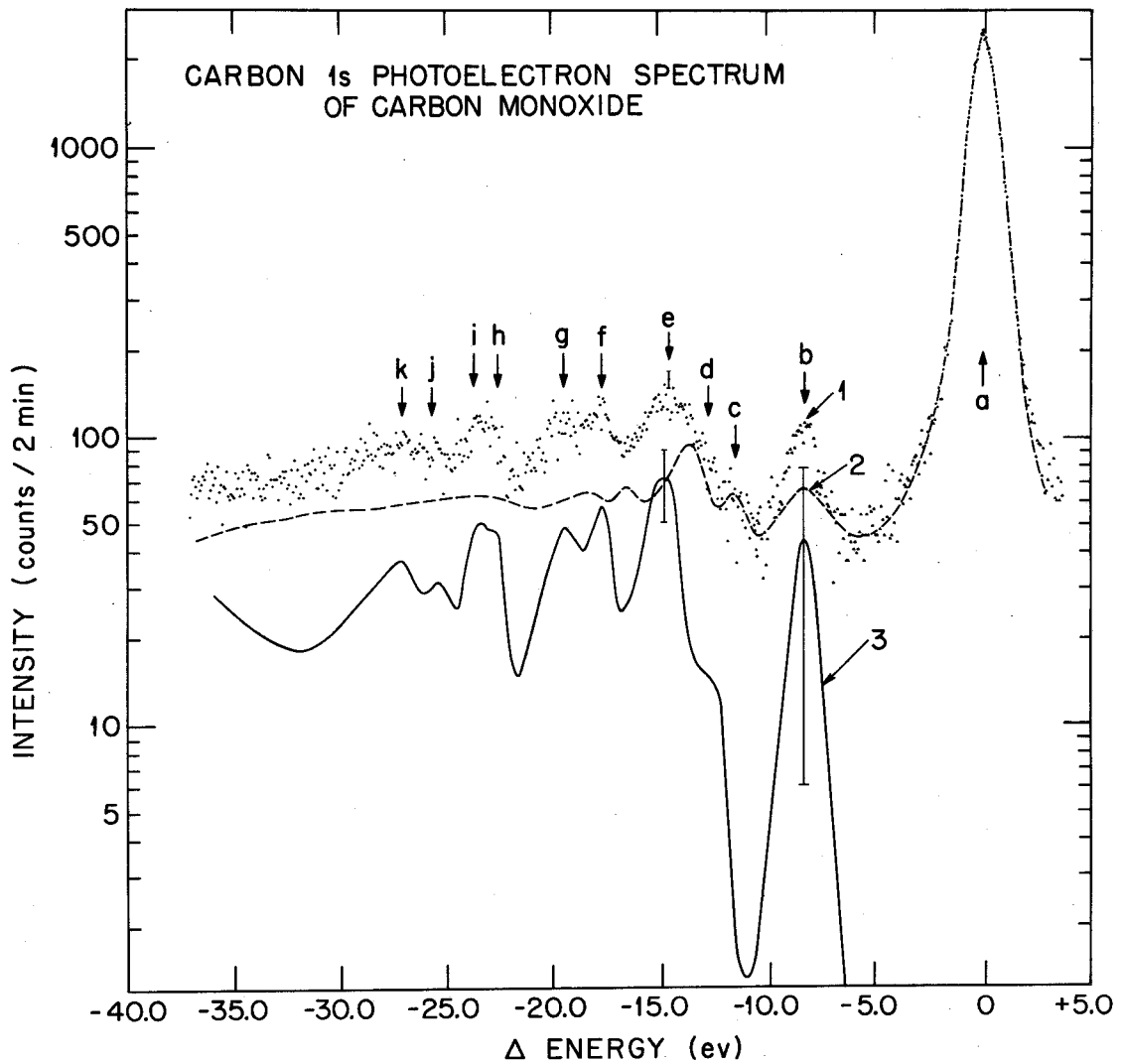


Figure 30. The carbon 1s-photoelectron spectrum of carbon monoxide.

1, raw data; 2, pressure correction for collision losses in neutral molecule; 3, C<sup>K+</sup>O states.

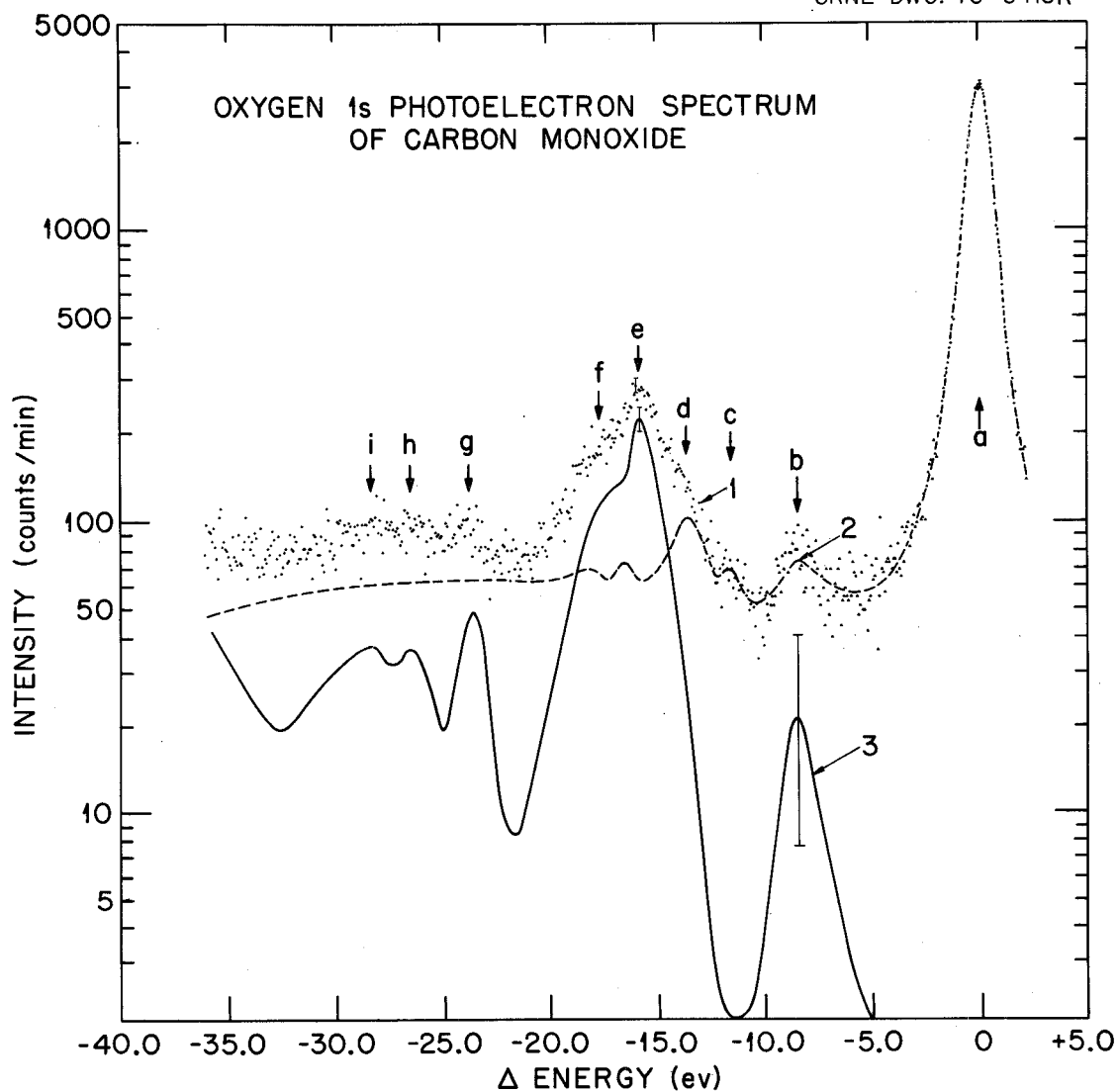


Figure 31. The oxygen 1s-photoelectron spectrum of carbon monoxide.

1, raw data; 2, pressure correction for collision losses in neutral molecule; 3, CO<sup>K+\*</sup> states.

TABLE XIX

RELATIVE ENERGIES AND INTENSITIES OF THE OBSERVED PEAKS IN THE  
CARBON 1s-PHOTOELECTRON SPECTRUM OF CARBON MONOXIDE

Peak <sup>a</sup>	Energy from a (eV)	Intensity Relative to a	Assignment <sup>b</sup>
a	0.0	100.	$C^{K+}O$
b	-8.5	1.8	$C^{K+*}O$
c	-11.6		$CO^*$
d	-12.9	0.6	$C^{K+*}O$
e	-14.9	2.9	$C^{K+*}O$
f	-18.0	2.4	$C^{K+*}O$
g	-19.8	2.0	$C^{K+*}O$
h	-23.0	2.0	$C^{K+*}O$
i	-23.8	2.0	$C^{K+*}O$
j	-25.0	1.2	$C^{K+*}O$
k	-27.5	1.5	$C^{K+*}O$

<sup>a</sup>Peaks were observed in Figure 30.

<sup>b</sup> $C^{K+}O$  represents a carbon monoxide molecule with a vacancy in the carbon 1s level without any additional excitation.  
 $C^{K+*}O$  represents a carbon monoxide molecule with a carbon 1s-vacancy but with additional excitation of valence electrons.  
 $CO^*$  represents a neutral excited carbon monoxide molecule.

TABLE XX

RELATIVE ENERGIES AND INTENSITIES OF THE OBSERVED PEAKS IN THE  
OXYGEN 1s-PHOTOELECTRON SPECTRUM OF CARBON MONOXIDE

Peak <sup>a</sup>	Energy from a (eV)	Intensity Relative to a	Assignment <sup>b</sup>
a	0.0	100.	CO <sup>K+</sup>
b	-8.6	0.6	CO <sup>K+*</sup>
c	-11.9		CO <sup>*</sup>
d	-14.0		CO <sup>*</sup>
e	-15.9	7.5	CO <sup>K+*</sup>
f	-18.0	3.8	CO <sup>K+*</sup>
g	-23.7	1.5	CO <sup>K+*</sup>
h	-26.4	1.2	CO <sup>K+*</sup>
i	-28.5	1.2	CO <sup>K+*</sup>

<sup>a</sup>Peaks were observed in Figure 31.

<sup>b</sup>CO<sup>K+</sup> represents a carbon monoxide molecule with a vacancy in the oxygen 1s level without any additional excitation. CO<sup>K+\*</sup> represents a carbon monoxide molecule with an oxygen 1s-vacancy but with additional excitation of valence electrons. CO<sup>\*</sup> represents a neutral excited carbon monoxide molecule.

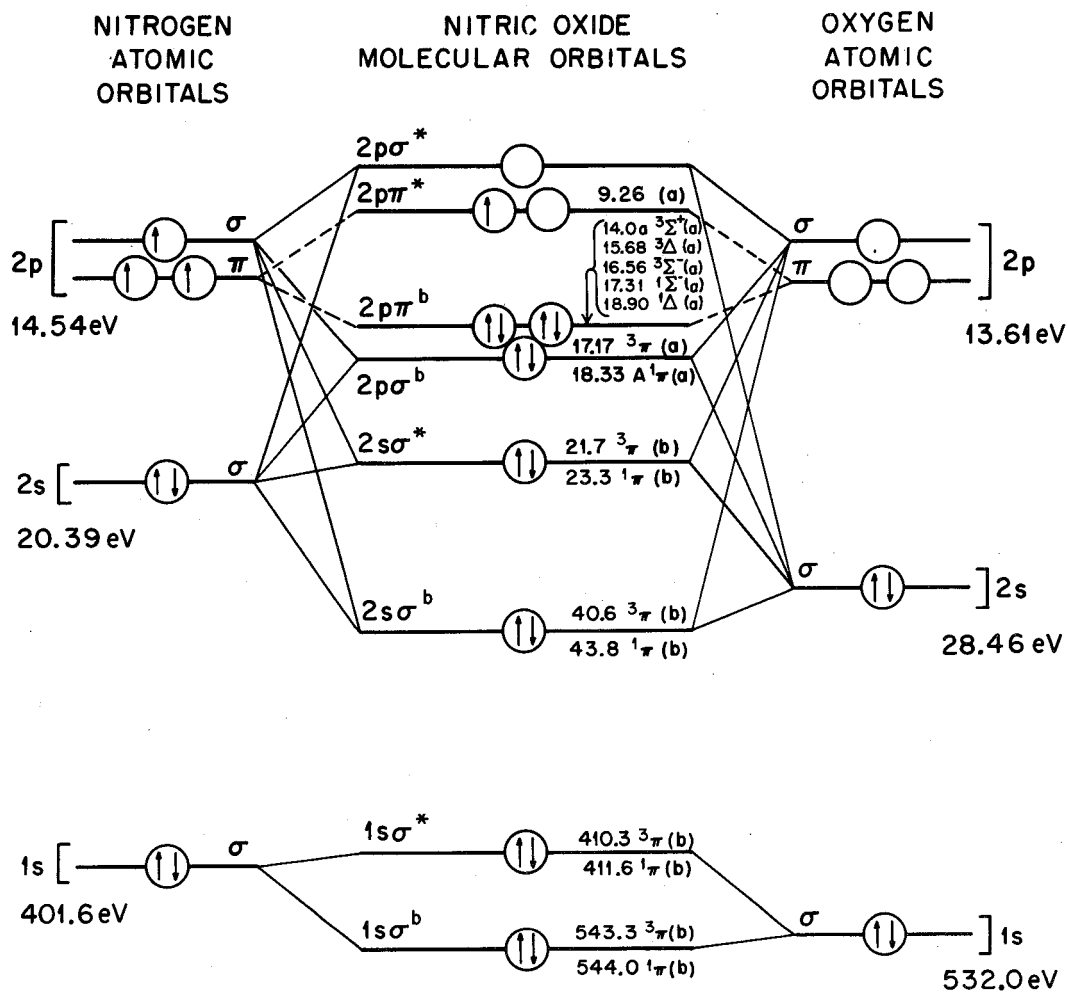


Figure 32. Molecular orbital diagram for nitric oxide.

(a), obtained from reference 54; (b), obtained from reference 11.

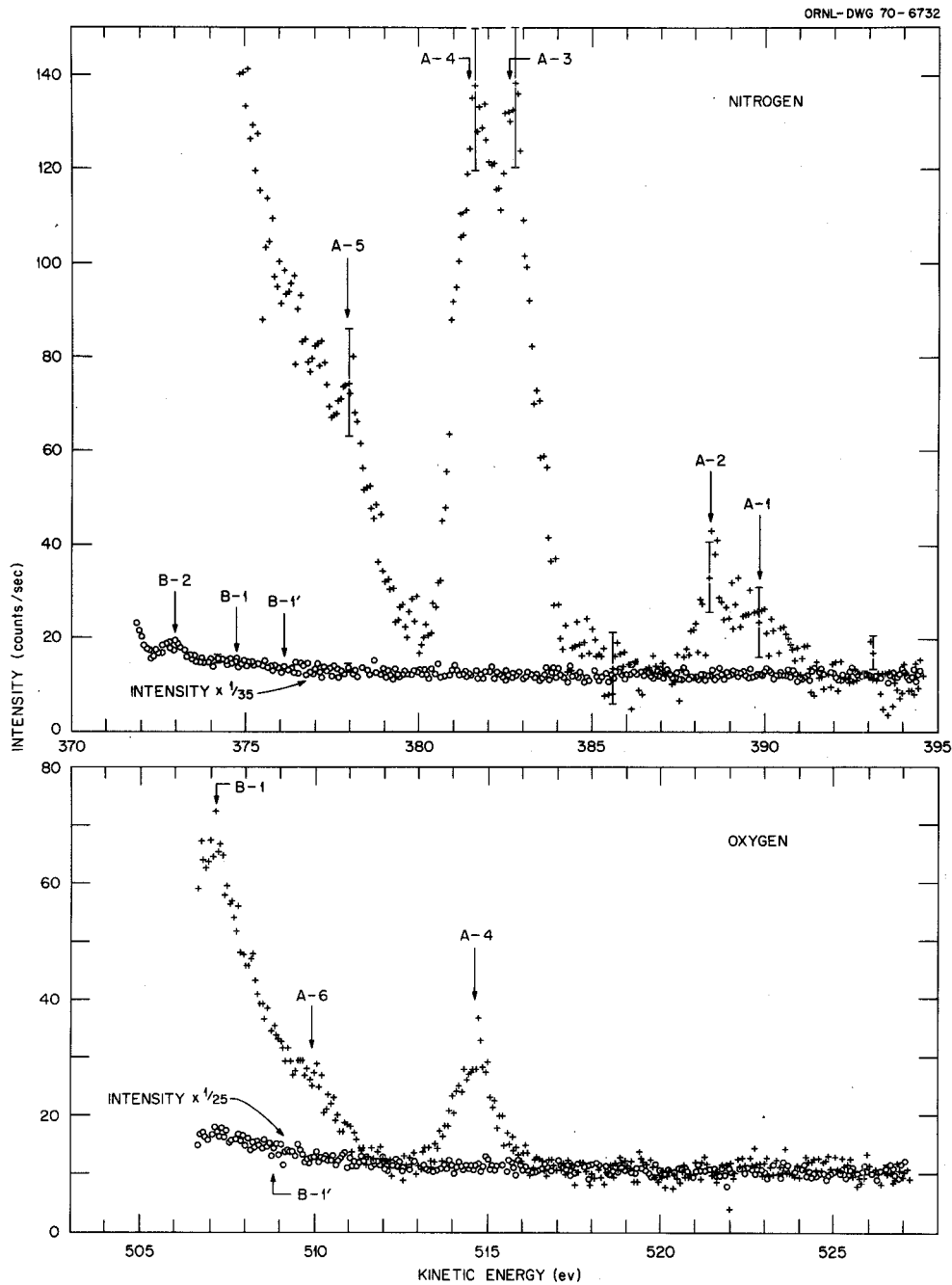


Figure 33. High energy portions of the Auger electron spectra of nitric oxide excited by electrons and aluminum  $K_{\alpha}$  photons.

plus data points (+) represent the electron excited spectra of nitric oxide, circle data points (o) represent the  $AlK_{\alpha}$  excited spectra.

TABLE XXI

ASSIGNMENTS OF THE PEAKS APPEARING IN HIGH ENERGY SATELLITE  
REGION OF THE K-LL AUGER SPECTRA OF NITRIC OXIDE

Peak <sup>a</sup>	Energy From A-1 in Nitrogen Spectrum (eV)	Energy From A-4 in Oxygen Spectrum (eV)	Assignment
A-1	0.0	----	Outer-excited
A-2	-1.3 ± 0.4	----	Outer-excited
A-3	-7.3 ± 0.4	----	Inner-excited
A-4	-8.6 ± 0.4	(-8.6) 0.0	Inner-excited
A-5	-12.2 ± 0.7	----	Inner-excited
A-6	----	(-13.3) 4.7	Inner-excited

<sup>a</sup>Peaks were observed in Figure 33.

could arise from normal Auger processes or from the decay of monopole excited states, although their origin has not as yet been determined. However, by recording the nitrogen 1s- and oxygen 1s-photoelectron spectra of NO, the energy of the monopole excited states can be found. Positioning of these monopole states into Figure 33 could aid in the identification of B-1 and B-2.

## 2. Analysis of Regions B, C and D - The Diagram Lines

The principal contribution of the structure that is seen in regions B, C and D can be attributed to normal Auger processes - Auger transitions that result from electron readjustments to an ion with a K vacancy that has been formed without excitation of any of the other orbitals. In the case of nitrogen this state is designated as  $N_2^{K+}$ . The decay of  $N_2^{K+}$  by the Auger process results in the formation of "normal" or "diagram" lines. Also in the analysis of the regions B through D one must be cognizant of processes that arise from the decay by an Auger process of initially multiply charged ions that have been formed by monopole ionizations, e.g.,  $N_2^{KL++}$  initial states. Readjustments to  $N_2^{KL++}$  result in low energy "satellite" electrons to the diagram lines. Still smaller contributions due to the excited processes resulting from transitions involving (1) autoionized states, (2) monopole excited states, (3) excited states caused by the Auger electron and (4) "double" Auger processes can occur in these three regions. The processes involving autoionized and monopole excited states ((1) and (2) above) normally occur in region A, but when the excited molecular orbital remains occupied, and more tightly bound electrons are involved in the decay, these processes are shifted to lower energy under the diagram line structure.

a. Nitrogen. The decay of  $N_2^{K+}$  and  $N_2^{KL++}$  states by Auger processes involving weakly bound  $2p\sigma_g$ ,  $2p\pi_u$  and  $2s\sigma_u$  electrons are illustrated in Figures 34a and 34b, respectively. Such transitions result in most of the structure seen in region B between 348 and 368 eV of Figure 13, page 37. The more intense lines B-1 through B-7 are attributed to normal ls-wv processes. Since these processes result from the formation of  $N_2^{+2}$  ions, the energy of the different electronic states of the doubly charged ion,  $E_{N_2^{+2}}$ , can be calculated by use of equation (3-3).

$$E_{X_2^{+2}} = E_A(B) - E_{1s}(X_2) \quad (3-3)$$

This is equation (1-4), page 11, rewritten.  $E_A(B)$  is the Auger electron energy for the ls-wv process,  $E_{1s}(X_2)$  is the ls-binding energy of the molecule  $X_2$ , and  $E_{X_2^{+2}}$  is the energy of the doubly charged ion (for nitrogen  $E_{X_2^{+2}} = E_{N_2^{+2}}$ ). The possible electronic states for  $N_2^{+2}$  with wv vacancies are:

$$\begin{aligned} &(2p\sigma_g)^{-1}(2p\sigma_g)^{-1} - 1\Sigma_g^+ \\ &(2p\sigma_g)^{-1}(2p\pi_u)^{-1} - 1\Pi_u, 3\Pi_u \\ &(2p\pi_u)^{-1}(2p\pi_u)^{-1} - 1\Sigma_g^+, 3\Sigma_g^-, 1\Delta_g \\ &(2p\pi_u)^{-1}(2s\sigma_u)^{-1} - 1\Pi_g, 3\Pi_g \\ &(2p\sigma_g)^{-1}(2s\sigma_u)^{-1} - 1\Sigma_u^+, 3\Sigma_u^+ \\ &(2s\sigma_u)^{-1}(2s\sigma_u)^{-1} - 1\Sigma_g^+ \end{aligned}$$

The  $E_{N_2^{+2}}$  values obtained from equation (3-3) by using the Auger data from Table VII, page 43, and  $E_{1s}(N_2) = 409.9 \text{ eV}^{11}$  are listed in Table XXII along with other experimental<sup>8,11</sup> and calculated values.<sup>22</sup>

ORNL-DWG 70-5181

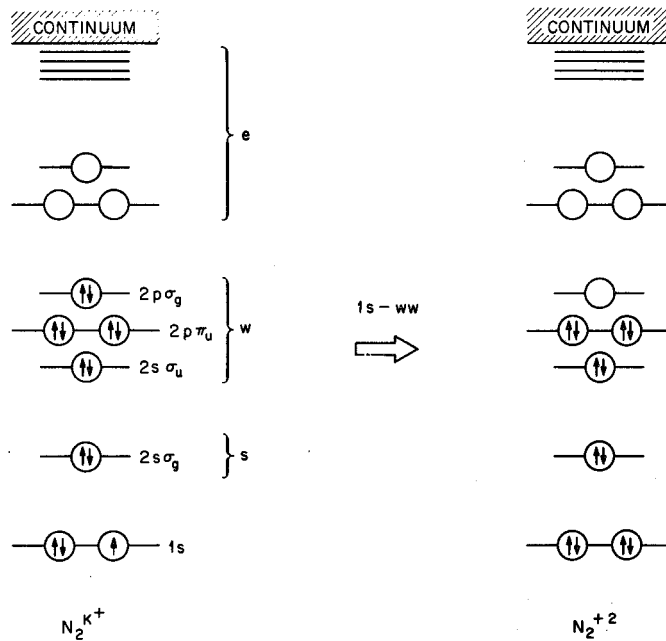


Figure 34a. Normal Auger processes resulting in diagram lines from the decay of  $N_2^{K^+}$ .

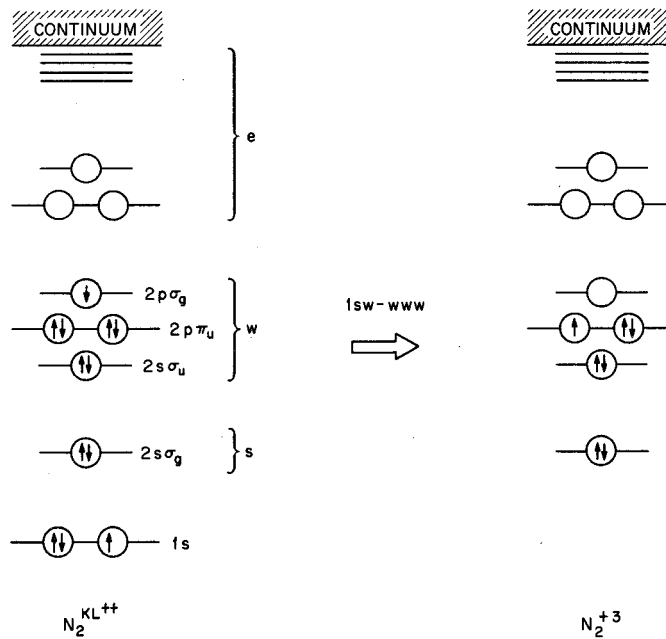


Figure 34b. Satellite Auger processes resulting in low energy satellite lines from the decay of  $N_2^{KL^{++}}$  states.

TABLE XXII

ASSIGNMENTS OF THE PEAKS IN DIAGRAM LINE REGION OF THE MOLECULAR NITROGEN K-LL AUGER SPECTRUM

Peak <sup>a</sup>	Probable Initial State <sup>b</sup>	Possible Final Electronic State <sup>c</sup>	$E_{N_2+2}$ <sup>d</sup> (eV)	Results of Stalherm <sup>8</sup> (eV)	Results of Siegbahn <sup>11</sup> (eV)	Calculations <sup>e</sup> (eV)
B-1'	$N_2^{K+}$		42.9 < 42.7 >			
		$X^3\Pi_u$			(0.0)	(-0.1)
B-1	$N_2^{K+}$	$X^1\Sigma_g^+$	43.3 (0.0)	43.3 (0.0)	(0.3)	42.73 (0.0)
		$A^1\Sigma_g^-$				(1.0)
B-2	$N_2^{K+}$	$b^1\Pi_u$	44.9 (1.5 ± 0.3)		(1.8)	(1.3)
B-3	$N_2^{K+}$	$A^{11}3\Sigma_u^+$	46.4 (3.0 ± 0.3)	(2.9)	(3.1)	(2.5)
B-4	$N_2^{K+}$	$A^3\Pi_g$	47.4 (4.0 ± 0.3)	(3.9)	(4.4)	(3.5)
B-5	$N_2^{K+}$	$C^1\Pi_g$	49.7 (6.3 ± 0.1)	(6.4)	(6.8)	(5.9)
		$B^3\Pi_g$				(7.9)
B-6	$N_2^{K+}$	$d^1\Sigma_u^+$	51.2 (7.8 ± 0.1)	(7.9)	(8.1)	(7.9)
B-7	$N_2^{K+}$	$e^1\Sigma_g^+$	53.0 (9.6 ± 0.1)	(9.5)	(10.0)	(9.8)
B-8						
B-9						

TABLE XXII (continued)

Peak <sup>a</sup>	Probable Initial State <sup>b</sup>	Possible Final Electronic State <sup>c</sup>	$E_{N_2^{+2}}$ <sup>d</sup> (eV)	Results of Stalherm <sup>8</sup> (eV)	Results of Siegbahn <sup>11</sup> (eV)	Calculations <sup>e</sup> (eV)
B-10						
B-11						
C-1	$N_2^{K+}$					
C-2						
C-3						
C-4						
D-1	$N_2^{K+}$	$1\Sigma_g^+$	94.9 (+51.5 ± 0.8)	(+53.0)		

<sup>a</sup>The electron energies of these peaks are listed in Table VII, page 43. B-1' is the onset of the normal Auger line B-1.

<sup>b</sup> $N_2^{K+}$  signifies a molecular nitrogen ion with a hole in 1s-level. Peaks with corresponding blank spaces in this column probably arise from decay of  $N_2^{KL^{++}}$  initial states, although these peaks could result from excitations caused by the normal Auger electrons.

<sup>c</sup>These are final electronic states of a doubly charged molecular ion of nitrogen.

<sup>d</sup> $E_{N_2^{+2}}$  are the energies of the electronic states of doubly charged nitrogen ion relative to the ground electronic state of neutral nitrogen. These values were determined from equation (3-3), page 83. The values given in parentheses are relative to the B-1 line. The value of 42.9 eV represents the minimum energy required for double electron removal from the ground state of a neutral nitrogen molecule. The value listed in brackets, 42.7 eV, was obtained for the appearance potential of  $N_2^{+2}$  from electron impact studies (reference 55). Another double ionization was witnessed at 43.8 eV by Dorman and Morrison.

<sup>e</sup>These values were obtained from reference 22.

Although the peaks B-8 through B-11 of Figure 13, page 37, could result from processes involving  $N_2^{K+}$ , one suspects these lines to be due to satellite lines, probably from Auger readjustments to  $N_2^{KL++}$ . However, this structure could result from other excited processes, i.e., (1) through (4) on page 82. Of these smaller contributions only those transitions due to double Auger processes can be completely eliminated. These processes have been shown to account for 7.5 percent of the decay of a  $Ne^{K+}$  ion;<sup>18</sup> however, they will appear as a continuous distribution of energy below the normal Auger lines (i.e., at lower Auger electron energies than occur in region D). Calculations<sup>49</sup> on atomic systems show that (1), (2) and (3) will occur in the three regions B, C and D although, from experimental results in the K-LL Auger spectrum of neon, such transitions appear to be low in intensity.<sup>20</sup>

Use of an excitation source, either electrons or photons whose energy is close to the binding energy where the initial vacancy occurred, has been shown to be useful in reducing the percentages of initial multiply charged ions in neon<sup>17,56,57</sup> and argon.<sup>56</sup> Thus, choice of a source just above the 1s binding energy of molecular nitrogen could aid in the identification of not only the structure B-8 through B-11, but also substantiate the assignment of B-1 through B-7.

The regions C and D have been designated as the regions in which one would expect 1s-ws and 1s-ss normal Auger processes to occur, respectively. Calculations as to where 1s-ws and 1s-ss processes would appear relative to the main diagram lines in region B can be related to the difference in energy of the various ways of removing two electrons from a

neutral molecule. Consider an atom or molecule with shells 1, 2... where 1 represents the least tightly bound orbital, 2 the next tightly bound, etc. If coupling in the final states of the doubly charged ion are ignored, the position of the Auger lines resulting from vacancies in the first two orbitals may be taken as

$$E_1 - E_2 = \epsilon_2 - \epsilon_1 \quad (3-4)$$

$$E_1 - E_3 = 2(\epsilon_2 - \epsilon_1) + c(\epsilon_2 - \epsilon_1) \quad (3-5)$$

where  $E_1$ ,  $E_2$  and  $E_3$  are the Auger lines or bands with  $E_1$  representing the highest kinetic energy Auger process, and  $c$  is a factor which is related to changes in the configurations as electrons are successively removed.  $c$  may be obtained empirically or from a model. For example, if one considers an atom to be a series of rigid, concentric, negatively charged shells of radius  $r$  about a central potential of positive charge,  $c$  is given by

$$c = (q/r_1 - q/r_2) / \epsilon_2 - \epsilon_1 \quad (3-6)$$

where  $q$  is the charge of an electron and  $r_1$  and  $r_2$  are the radii of shells 1 and 2 in the neutral atom.

The above considerations can be applied to neon as an example where  $E_1 = 21.6$  eV and  $E_2 = 48.3$  eV for the 2p and 2s orbitals,<sup>11</sup> respectively. By using the radii listed for the Hartree-Fock solutions of neon,<sup>58</sup> one obtains from equation (3-6) a value of 0.086 for  $c$ . In Table XXIII the energy values obtained from the simple model are compared with experiment, where the experimental values are the weighted average of the term values for the Auger transitions 1s-2p2p, 1s-2s2p and 1s-2s2s in neon.

TABLE XXIII

COMPARISON OF DIFFERENCE IN AUGER ELECTRON ENERGIES BETWEEN  
REGIONS B AND C AND BETWEEN B AND D FOR NEON

Region <sup>a</sup>	Theory <sup>b</sup> (eV)	Experiment <sup>c</sup> (eV)
$E_1 - E_2$	26.7	27.5
$E_1 - E_3$	55.7	56.1

<sup>a</sup>The highest kinetic energy Auger process that appears in region B is represented by  $E_1$ .  $E_2$  and  $E_3$  represent the kinetic energy of Auger processes that are present in regions C and D, respectively.

<sup>b</sup>These values were calculated by using equations (3-4) and (3-5). A value for  $c$  of 0.086 was used in the calculations.

<sup>c</sup>The experimentally determined values were ascertained from the neon K-LL Auger spectrum by using intensity-weighted term values for  $E_1$ ,  $E_2$  and  $E_3$ .

For the molecular studies,  $c$  is arbitrarily chosen to be 0.1 in the calculations, which is consistent with what one would expect for the removal of electrons from orbitals made up of atomic outer-shell  $s$  and  $p$  electrons. Examining the case of molecular nitrogen by assuming shell 1 to be the weighted sum of the least bound,  $2p\sigma_g$ ,  $2p\pi_u$  and  $2s\sigma_u$ , molecular orbitals and shell 2 the  $2s\sigma_g$  orbital, the binding energies of 17.1 and 37.3 eV, respectively, were found. By using equations (3-4) and (3-5),  $E_1 - E_2$  and  $E_1 - E_3$  are calculated to be 21 and 40 eV. Table XXIV lists the energies where regions C and D (relative to region B) would appear for the other studied diatomic molecules.

In the nitrogen K-LL Auger spectrum, the center of the main structure of region B appears at 362 eV; thus, one would expect  $ls$ - $ws$  (region C) and  $ls$ - $ss$  (region D) processes to appear at 342 and 320 eV, respectively. In Figure 13, page 37, bands C-1 through C-4 and D-1 do appear in the regions C and D. The assignment of the bands as to diagram or satellite lines is difficult. Most likely C-1 arises from  $ls$ - $2s\sigma_g 2p\sigma_g$  or  $ls$ - $2s\sigma_g 2p\pi_u$  processes and D-1 is probably due to  $ls$ - $2s\sigma_g 2s\sigma_g (^1\Sigma_g^+)$  process. The electronic states of  $N_2^{+2}$  that arise from  $sw$  and  $ss$  configurations are listed below: for region C,

$$\begin{aligned} (2s\sigma_g)^{-1}(2p\sigma_g)^{-1} &- \quad {}^1\Sigma_g^+, \quad {}^3\Sigma_g^+ \\ (2s\sigma_g)^{-1}(2p\pi_u)^{-1} &- \quad {}^1\Pi_u, \quad {}^3\Pi_u \\ (2s\sigma_g)^{-1}(2s\sigma_u)^{-1} &- \quad {}^1\Sigma_u^+, \quad {}^3\Sigma_u^+ \end{aligned}$$

for region D,

$$(2s\sigma_g)^{-1}(2s\sigma_g)^{-1} - \quad {}^1\Sigma_g^+$$

TABLE XXIV

LOCATION OF REGIONS C AND D RELATIVE TO REGION B IN THE  
K-LL AUGER SPECTRA OF N<sub>2</sub>, O<sub>2</sub>, CO AND NO

Spectra <sup>a</sup>	Energy Shell 1 <sup>b</sup> (eV)	Energy Shell 2 <sup>c</sup> (eV)	E <sub>1</sub> - E <sub>2</sub> <sup>d</sup> (eV)	E <sub>1</sub> - E <sub>3</sub> <sup>e</sup> (eV)
N <sub>2</sub>	17.1	38.3	21.2	40.3
O <sub>2</sub>	18.8	40.6	21.8	41.4
Carbon of CO	17.3	38.3	21.0	39.9
Oxygen of CO	17.3	38.3	21.0	39.9
Nitrogen of NO	17.1	42.0	24.9	47.3
Oxygen of NO	17.1	42.0	24.9	47.3

<sup>a</sup>The K-LL Auger spectra of N<sub>2</sub>, O<sub>2</sub>, CO and NO are illustrated in Figures 13-18, pages 37-42.

<sup>b</sup>The molecular orbitals used in computing the energy of shell 1 for the different molecules are as follows: for N<sub>2</sub>, 2pσ<sub>g</sub>, 2pπ<sub>u</sub> and 2sσ<sub>u</sub>; for O<sub>2</sub>, 2pπ<sub>g</sub>, 2pπ<sub>u</sub>, 2pσ<sub>g</sub> and 2sσ<sub>u</sub>; for CO, 2pσ<sup>b</sup>, 2pπ<sup>b</sup> and 2sσ<sup>\*</sup>; and for NO, 2pπ<sup>\*</sup>, 2pπ<sup>b</sup>, 2pσ<sup>b</sup> and 2sσ<sup>\*</sup>. Figures 19, 25, 28 and 32, pages 51, 63, 70 and 79, give the values of the different molecular orbitals. The energy given for shell 1 is computed from the weighted sum of the electrons in the different orbitals.

<sup>c</sup>The molecular orbitals used for computing the energy of shell 2 for the different molecules are as follows: for N<sub>2</sub>, 2sσ<sub>g</sub>; for O<sub>2</sub>, 2sσ<sub>g</sub>; for CO, 2sσ<sup>b</sup>; for NO, 2sσ<sup>b</sup>.

<sup>d</sup>E<sub>1</sub> - E<sub>2</sub> values were calculated from equation (3-4), page 88.

<sup>e</sup>E<sub>1</sub> - E<sub>3</sub> values were calculated from equation (3-5), page 88.

If the analysis of D-1 in the nitrogen spectrum to the process is correct, an estimate for the second ionization energy of the orbital can be made. In calculating the second ionization energy,  $I(X)^{-2}$ , for a given orbital X, equation (3-7) is used:

$$I(X)^{-2} = E_{1s}(X_2) - E_A(P) - I(X)^{-1} \quad (3-7)$$

where  $E_{1s}(X_2)$  is the binding energy of the 1s electron for a molecule  $X_2$ ,  $E_A(P)$  is the Auger electron energy for a given peak P, and  $I(X)^{-1}$  is the first ionization energy for the orbital X. For  $P = D-1$ ,  $E_A(D-1) = 315.0$  eV; for  $X = 2s\sigma_g$  orbital,  $I(2s\sigma_g)^{-1} = 37.3$  eV; and for  $X_2 = N_2$ ,  $E_{1s}(N_2) = 409.9$  eV. Substitution of the above energies into equation (3-7),  $I(2s\sigma_g)^{-2}$  was calculated to be 57.6 eV.

By substitution of  $E_A(B-1)$  into equation (3-3), page 83, one is allowed to estimate the minimum energy required to remove the two least bound electrons from a neutral nitrogen molecule  $E_{N_2+2}(\text{min})$ . This value was calculated to be 43.4 eV. Dorman and Morrison<sup>55</sup> have measured two final electronic states of  $N_2^{+2}$  of  $42.7 \pm 0.1$  eV and  $43.8 \pm 0.1$  eV by electron impact studies. Perhaps a better value for comparison with 42.7 eV would be the onset of the highest normal Auger peak B-1. This is labeled B-1' in Figure 13, page 37, and has an Auger electron energy of 367.0 eV. Substitution of this value into equation (3-3) gives an estimate of 42.9 eV for  $E_{N_2+2}(\text{min})$ .

b. Oxygen. The diagram line region of the molecular oxygen K-LL Auger (Figure 14, page 38) lies between 442 and 508 eV. The two possible initial states of  $O_2^{K+}$ ,  $4\Sigma^-$  and  $2\Sigma^-$  are separated by 1.2 eV and are formed in an approximate two to one intensity ratio. A few of the final electronic states for  $O_2^{+2}$  have been calculated by Hurley.<sup>22</sup> Since the

splitting of some of the final  $O_2^{+2}$  electronic states have approximately the same energy separations as the initial two states, the explanation of the K-LL Auger spectrum of molecular oxygen is more difficult than in the analysis of nitrogen. The energy spacings between B-1 and B-2, B-4 and B-5, B-8 and B-9, B-10 and B-11 are approximately the splitting of the 1s level in oxygen; and, each set is approximately in a two to one intensity ratio. Therefore, these peak combinations have been assigned to the decay of the  $^4\Sigma^-$  and  $^2\Sigma^-$  of  $O_2^{K+}$ , respectively.

Using the observed Auger data from Table VIII, page 44, and equation (3-3), page 83, energies for the electronic states of  $O_2^{+2}$ ,  $E_{O_2^{+2}}$ , can be computed.  $E_{O_2^{+2}}$  values are listed in Table XXV, and assignments are made and compared with the theoretical calculations of Hurley<sup>22</sup> and the experimental results of Mehlhorn.<sup>28</sup>

Experimentally, four bands (C-1 through C-4) are observed in region C. Characterization of these bands is difficult. C-1 is probably due to a  $1s-2s\sigma_g 2p\pi_u$  process although a  $1s-2s\sigma_u 2s\sigma_u$  transition might also arise in this region. The  $1s-2s\sigma_g 2s\sigma_g$  process apparently is not seen in our molecular oxygen spectrum either because of its low probability of occurrence or because of the large span of the peaks observed in region C. The arrow at 445 eV in Figure 14 indicates approximately where the  $1s-2s\sigma_g 2s\sigma_g$  process would be expected to appear.

If the assignment of B-1 and B-2 is correct, then the second ionization energy of the  $2p\pi_g$  orbital can be computed. By substituting  $E_{1s}(O_2) = 543.1$  eV and  $E_A(B-2) = 504.0$  eV and  $I(2p\pi_g)^{-1} = 13.1$  eV into equation (3-7), page 92,  $I(2p\pi_g)^{-2}$  was calculated to be 26.0 eV. The value obtained by substitution of B-1 into equation (3-7) is 25.2 eV; therefore,

TABLE XXV

ASSIGNMENTS OF THE PEAKS IN THE DIAGRAM LINE REGION OF THE  
MOLECULAR OXYGEN K-LL AUGER SPECTRUM

Peak <sup>a</sup>	Probable Initial State <sup>b</sup>	Possible Final Electronic State <sup>c</sup>	$E_{O_2+2d}$ (eV)	Results of Mehlhorn <sup>28</sup> (eV)	Calculations <sup>e</sup> (eV)
B-1			37.4 < 36.5 >		
B-1	$O_2^{K+} (4\Sigma^-)$	$X^1\Sigma_g^+$	38.3	}	35.48 (0.0)
B-2	$O_2^{K+} (2\Sigma^-)$	$X^1\Sigma_g^+$	39.1		
B-3					
B-4	$O_2^{K+} (4\Sigma^-)$	$A^3\Sigma_u^+$	42.8	}	(4.3)
B-5	$O_2^{K+} (2\Sigma^-)$	$A^3\Sigma_u^+$	42.8		
B-6	$O_2^{K+} (4\Sigma^-)$		43.4 (4.7)		(4.5)
B-7					
B-8	$O_2^{K+} (4\Sigma^-)$		48.6	}	(9.5)
B-9	$O_2^{K+} (2\Sigma^-)$		48.5		
B-10	$O_2^{K+} (4\Sigma^-)$	$C^3\Pi_u$	52.5	}	(12.5)
B-11	$O_2^{K+} (2\Sigma^-)$	$C^3\Pi_u$	52.4		
B-12					(13.0)

TABLE XXV (continued)

Peak <sup>a</sup>	Probable Initial State <sup>b</sup>	Possible Final Electronic State <sup>c</sup>	$E_{O_2^{+2}}$ <sup>d</sup> (eV)	Results of Mahlhorn <sup>28</sup> (eV)	Calculations <sup>e</sup> (eV)
B-13					
B-14					
C-1	$O_2^{K+} ({}^4\Sigma^-)$				
C-2					
C-3					
C-4					

<sup>a</sup>The electron energies of these peaks are listed in Table VIII, page 44. B-1' is the onset of the normal Auger line B-1.

<sup>b</sup> $O_2^{K+} ({}^4\Sigma^-)$  and  $O_2^{K+} ({}^2\Sigma^-)$  are the initial states and denote an oxygen molecular ion with a hole in the 1s-level. Peaks B-12 through B-14 and C-2 through C-4 probably arise from the decay of  $O_2^{KL++}$  initial states, although they could arise from decay of  $O_2^{K*}$ ,  $O_2^{K+*}$  or excitations caused by the Auger electrons.

<sup>c</sup>These are the final electronic states of the doubly charged oxygen molecular ion.

<sup>d</sup> $E_{O_2^{+2}}$  are the energies of the electronic states of  $O_2^{+2}$  relative to the ground electronic state of neutral oxygen, as determined from equation (3-3), page 83. The values given in parentheses are related to the B-1 line. The value of 37.4 eV represents the minimum energy required for double electron removal from the ground state of a neutral oxygen molecule. The value listed in brackets, 36.5, was obtained by Dormann and Morrison, reference 60, for the appearance potential of the doubly charged ion of molecular oxygen.

<sup>e</sup>These values were obtained from reference 22.

an average value of 25.6 eV can be estimated for the second ionization energy of the  $2p\pi_g$  orbital. The beginning of B-1, B-1', appears at 506.8 eV in the Auger spectrum. By using the value of B-1' and  $E_{1s}(O_2)$  in equation (3-3), page 83,  $E_{O_2}^{+2}(\text{min})$  was computed to be 37.4 eV.

c. Carbon monoxide. In Figure 35, the carbon and oxygen K-LL Auger spectra of carbon monoxide are compared in the regions where the diagram lines ought to appear. The two spectra are compared such that their energy scales differ by the 1s-binding energy of the carbon and oxygen in CO.<sup>11</sup> This difference in energy should correspond to the difference in energy between the initial states  $C^{K+}O$  (a carbon atom with a hole in the 1s-level) and  $CO^{K+}$  (an oxygen atom with a hole in the 1s-level) involved in the Auger transitions. The final electronic states of  $CO^{+2}$  expected for the different regions B, C and D are listed below: for region B,

$$\begin{aligned} &(2p\sigma^b)^{-1}(2p\sigma^b)^{-1} - 1\Sigma^+ \\ &(2p\sigma^b)^{-1}(2p\pi^b)^{-1} - 3\Pi, 1\Pi \\ &(2p\pi^b)^{-1}(2p\pi^b)^{-1} - 1\Delta, 3\Sigma^-, 1\Sigma^+ \\ &(2s\sigma^*)^{-1}(2p\sigma^b)^{-1} - 3\Sigma^+, 1\Sigma^+ \\ &(2s\sigma^*)^{-1}(2p\pi^b)^{-1} - 3\Pi, 1\Pi \\ &(2s\sigma^*)^{-1}(2s\sigma^*)^{-1} - 1\Sigma^+ \end{aligned}$$

for region C,

$$\begin{aligned} &(2p\sigma^b)^{-1}(2s\sigma^b)^{-1} - 3\Sigma^+, 1\Sigma^+ \\ &(2p\pi^b)^{-1}(2s\sigma^b)^{-1} - 3\Pi, 1\Pi \\ &(2s\sigma^*)^{-1}(2s\sigma^b)^{-1} - 3\Sigma^+, 1\Sigma^+ \end{aligned}$$

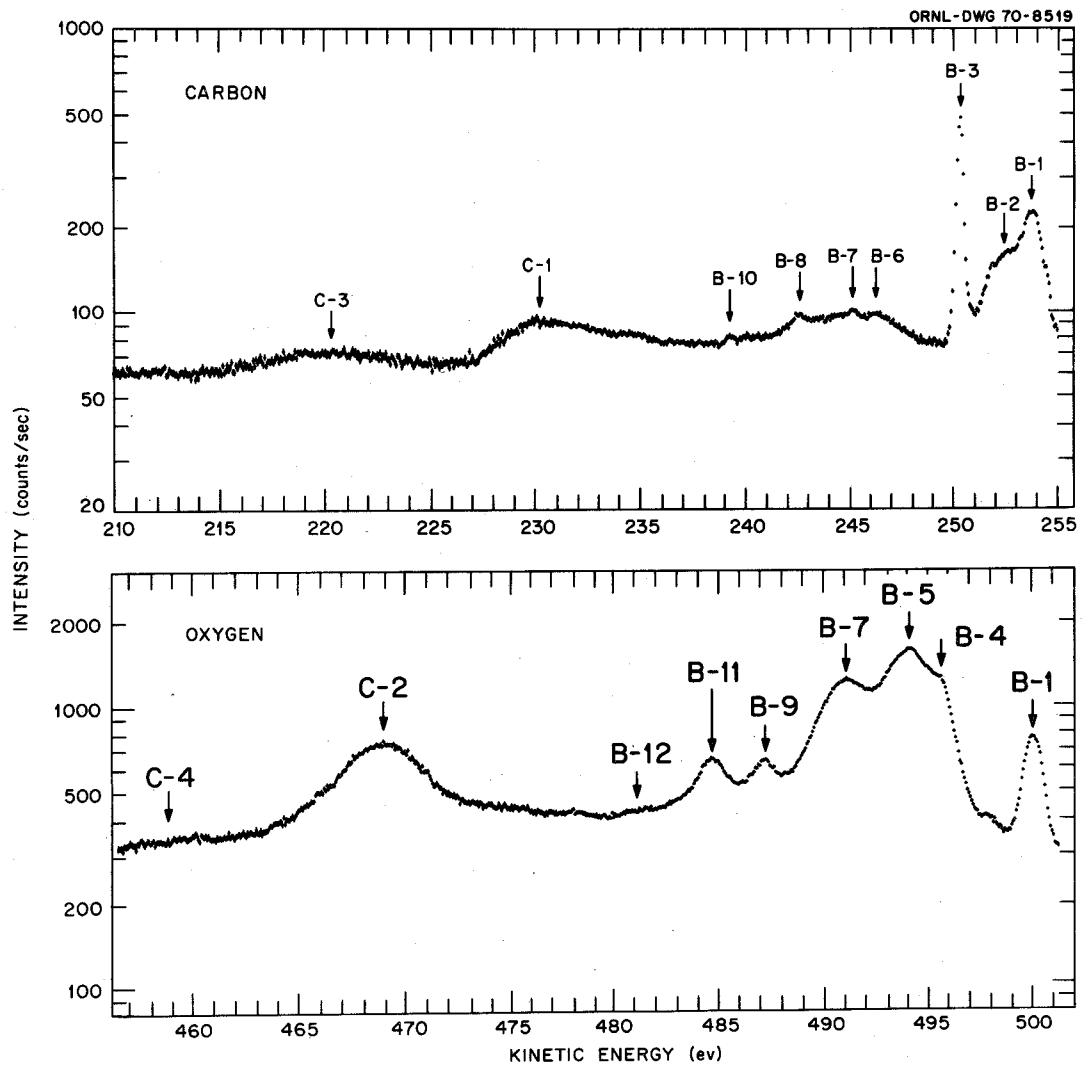


Figure 35. Diagram line regions of the carbon and oxygen K-LL Auger electron spectra of carbon monoxide excited by electron impact.

for region D,

$$(2s\sigma^b)^{-1}(2s\sigma^b)^{-1} - 1\Sigma^+$$

Since the final electronic states of  $CO^{+2}$  for Auger transitions are the same regardless of whether the initial state was  $C^{K+}O$  or  $CO^{K+}$ , one might expect some similar calculated  $E_{CO+2}$  values to result from both the carbon and oxygen spectra. The  $E_{CO+2}$  values can be computed by using the observed Auger data in Tables IX and X, pages 45 and 46, and equation (3-3), page 83. The binding energies of the 1s level were taken from Siegbahn's results.<sup>11</sup> The calculated  $E_{CO+2}$  values are listed in Table XXVI. Since only a few peaks match in the carbon and oxygen Auger spectra, the probability of filling a 1s vacancy in carbon with a given Auger transition to a particular final electronic state of  $CO^{+2}$  is different than for the filling of a 1s-vacancy in oxygen by the same process.

Another explanation of why only a few peaks are coincident in the comparison of the carbon and oxygen spectra can be formulated by considering the atomic populations of the molecular orbitals in neutral CO. Neumann and Moskowitz<sup>59</sup> have calculated the percentage character of the valence molecular orbitals in CO and have found the percent carbon character in each orbital to be as follows:  $2p\sigma^b$  - 92,  $2p\pi^b$  - 33,  $2s\sigma^*$  - 20 and  $2s\sigma^b$  - 33. Auger transitions involving the least bound  $2p\sigma^b$  molecular orbital might result in a large transition moment for a readjustment to a carbon 1s-vacancy. The first three peaks, B-1, B-2 and B-3, in region B of the carbon spectra are strong in intensity, and the remaining lines B-5 through B-8 are correspondingly weak. Therefore, B-1, B-2 and B-3 probably involve the  $2p\sigma^b$  electrons in the Auger process. In the K-LL oxygen spectrum of CO the strongest peaks occur between B-5 through B-7

TABLE XXVI

## ENERGIES OF THE FINAL ELECTRONIC STATES FOR THE DOUBLY CHARGED CARBON MONOXIDE MOLECULAR ION

Peak <sup>a</sup>	$E_{CO^{+2}}$ (Carbon Data) <sup>b</sup> eV	$E_{CO^{+2}}$ (Oxygen Data) <sup>c</sup> eV	Assignment
B-1'	39.9	40.2 < 41.8 >	
B-1	41.9	41.7	1s-2p $\sigma^b$ 2p $\pi^b$
B-2	43.4		1s-2p $\sigma^b$ w
B-3	45.5		1s-2p $\sigma^b$ w
B-4		46.0	1s-ww
B-5		47.6	1s-ww
B-7	50.6	50.6	1s-ww
B-9		54.5	1s-ww
B-11		57.0	1s-ww
C-1	65.6		1s-2s $\sigma^b$ w
C-2		72.7	1s-2s $\sigma^b$ w
D-1		94.9	1s-2s $\sigma^b$ 2s $\sigma^b$

<sup>a</sup>Peaks were observed in Figure 35. B-1' is the onset of the normal Auger line B-1.

<sup>b</sup> $E_{CO^{+2}}$  values are the energies of the final electronic states of the doubly charged carbon monoxide molecular ion. These values were calculated by using the carbon Auger data of Table IX, page 45, and equation (3-3), page 83.

<sup>c</sup>These values were calculated by using the oxygen Auger data of Table X, page 46, and equation (3-3). The value given in brackets, 41.8 eV, was obtained by Dorman and Morrison, reference 60, for the appearance potential of  $CO^{+2}$ .

and apparently involve the  $2p\pi^b$ ,  $2s\sigma^*$  and  $2s\sigma^b$  molecular orbitals. The intensity of the first peak, B-1, in both the carbon and oxygen spectra of CO is strong, suggesting that this peak arises from a  $1s-2p\pi^b 2p\sigma^b$  transition. Also consistent with the atomic population of the  $2p\sigma^b$  orbital is the assignment of peak D-1 to the  $1s-2s\sigma^b 2s\sigma^b$  processes. This process is present in the oxygen but absent in the carbon spectrum of CO.

If one assumes the assignment of D-1 to be correct, the second ionization energy of the  $2s\sigma^b$  orbital can be calculated similarly to that described for nitrogen on page 92.  $I(2s\sigma^b)^{-2}$  was ascertained to be 56.6 eV. The onset of B-1, B-1', can be used with equation (3-3) to calculate a value of 40.1 eV for  $E_{CO^{+2}}(\text{min})$ . This value was calculated to be 39.9 eV from the carbon data and 40.2 eV from the oxygen data, for an average value of 40.1 eV. Dorman and Morrison<sup>60</sup> have measured the appearance potential of 41.8 eV for  $CO^{+2}$ .

d. Nitric oxide. Figure 36 compares the nitrogen and oxygen K-LL Auger spectra in the diagram line region. The two spectra are related to each other by the energy difference between the initial  $^3\Pi$  states of nitrogen and oxygen in NO. From the Auger data that were given in Tables XI and XII, pages 47 and 48, and equation (3-3), energies for the different final electronic states of  $NO^{+2}$  were ascertained. These energy values are listed in Table XXVII and compared to the electronic states that have been calculated by Hurley.<sup>22</sup> Also, the assignments for  $NO^{+2}$  are given in Table XXVII.

A double hole vacancy in nitric oxide of  $2p\pi^* 2p\sigma^b$  gives rise to a  $X^2\Sigma^+$  final electronic state, and a  $2p\pi^* 2p\pi^b$  combination forms a  $A^2\Pi$  state.

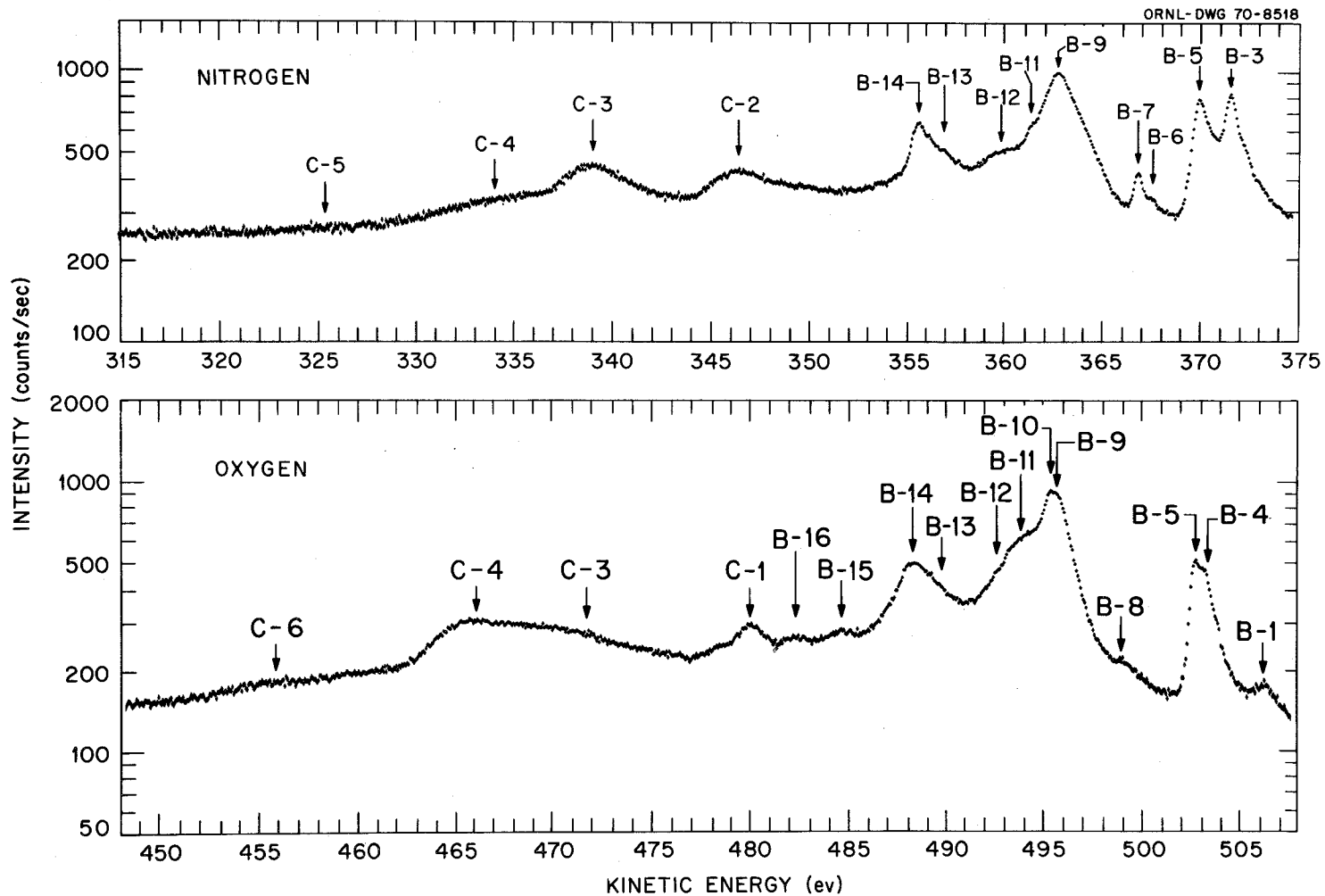


Figure 36. Diagram line regions of the nitrogen and oxygen K-LL Auger electron spectra of nitric oxide excited by electron impact.

TABLE XXVII

ENERGIES OF THE FINAL ELECTRONIC STATES FOR THE DOUBLY  
CHARGED NITRIC OXIDE MOLECULAR ION

Peak <sup>a</sup>	Initial State <sup>b</sup>	Final Electronic State <sup>c</sup>	$E_{\text{NO}^{+2}\text{d}}$ Nitrogen Data (eV)	$E_{\text{NO}^{+2}\text{d}}$ Oxygen Data (eV)	Calculations <sup>e</sup> (eV)
B-1'			35.7 < 39.8 >	35.1	
B-1	$1_{\text{II}}$	$X^2\Sigma^+$	37.0	36.1	38.10
B-2	$3_{\text{II}}$	$X^2\Sigma^+$	37.2		
B-3	$3_{\text{II}}$	$A^2\Pi$	38.6		38.72
B-4	$1_{\text{II}}$	$B^2\Sigma^+$		40.0	42.87
B-5	$3_{\text{II}}$	$B^2\Sigma^+$	40.3	40.4	42.87
B-7	$3_{\text{II}}$		43.4		
B-8	$3_{\text{II}}$			44.1	
B-9	$1_{\text{II}}$			47.3	
B-10	$3_{\text{II}}$		47.6	47.8	
B-14	$3_{\text{II}}$		54.5		
C-2			63.7		
C-3			71.2	71.8	
C-4			76.1	77.2	
D-1				98.8	

<sup>a</sup>Energies of the peaks were obtained from Figures 33, page 80, and 36, page 101. B-1' is the onset of peak B-1.

<sup>b</sup> $3_{\text{II}}$  and  $1_{\text{II}}$  are the initial states for  $\text{N}^{\text{K}^+}\text{O}$  (an NO molecule with a 1s vacancy in the nitrogen atom) and for  $\text{NO}^{\text{K}^+}$  (an NO molecule with a 1s vacancy in the oxygen atom). For  $\text{N}^{\text{K}^+}\text{O}$  the initial singlet and triplet states are separated by 1.5 eV. For  $\text{NO}^{\text{K}^+}$  the initial singlet and triplet states are separated by 0.7 eV.

<sup>c</sup>These are the final electronic states of  $\text{NO}^{+2}$ .

<sup>d</sup> $E_{\text{NO}^{+2}}$  are the energies of the electronic states of  $\text{NO}^{+2}$  relative to the ground electronic state of neutral NO. These values were calculated by using the Auger data in Tables XI and XII, pages 47 and 48, and equation (3-3), page 83. The values of 35.7 and 33.9 eV are the calculated values from the nitrogen and oxygen Auger data for the minimum energy required for double energy of NO ( $E_{\text{NO}^{+2}(\text{min})}$ ). The value listed in brackets, 39.8, was obtained by Dorman and Morrison, reference 60, for the appearance potential of  $\text{NO}^{+2}$ .

<sup>e</sup>These values were obtained from reference 22.

Atomic populations of the different molecular orbitals for neutral NO have been theoretically obtained by Brion et al.<sup>52</sup> They arrived at the following percentages of nitrogen character:  $2p\pi^*$  - 64,  $2p\pi^b$  - 33,  $2p\sigma^b$  - 60 and  $2s\sigma^*$  - 50. From the above percentages, one might expect (1) the  $1s-2p\pi^*2p\sigma^b(X^2\Sigma^+)$  transition to have a large intensity in the nitrogen spectrum and a smaller one in the oxygen spectrum and (2) a transition to the  $A^2\Pi$  electronic state of  $NO^{+2}$  to appear with equal probability in both spectra. Peak B-3 in the nitrogen spectrum does not have a counterpart in the oxygen spectrum, suggesting that B-3 could have originated from a  $1s-2p\pi^*2p\sigma^b(X^2\Sigma^+)$  transition. Likewise, the large intensity of B-5 in both spectra suggests that B-5 resulted from a  $1s-2p\pi^*2p\pi^b(A^2\Pi)$  transition. These latter assignments are possible with the observed Auger data from two additional considerations: (1) there is some doubt about the origin of B-1 and B-2 -- they have not been conclusively shown to have formed from normal Auger processes (these low intensity peaks could have formed from the decay of monopole excited states - see page 82) and (2) the experimentally determined value for  $E_{NO^{+2}}(\min)$ , the minimum energy for double electron removal from neutral NO, from the Auger data would be closer to the appearance potential measured from electron impact studies (39.8 eV).<sup>60</sup> By using the energy of B-1' and equation (3-3), an average value of  $E_{\min}(NO)^{+2}$  was calculated to be 35.4 eV.

In addition to the  $3\Pi$  initial states of  $N^{K+}O$  and  $NO^{K+}$  (as mentioned in the first paragraph of this section), there exists a singlet initial state,  $1\Pi$ , for each  $N^{K+}O$  and  $NO^{K+}$ . As shown by Siegbahn et al.,<sup>11</sup> the triplet and singlet states are separated by 1.5 eV for nitrogen and 0.7 eV in oxygen. The relative population of the triplet to singlet states is

three to one. Some evidence for the splitting of the initial state is seen in both the oxygen and nitrogen spectra. In the nitrogen spectrum B-1 and B-2 are separated by 1.7 eV in approximately a three to one ratio; and, in the oxygen spectrum splittings of 0.4 eV between B-4 and B-5 and of 0.5 eV between B-9 and B-10 are seen.

## B. Triatomic Molecules

### 1. Water

The electron configuration of water is  $1s_o 1a_1^2 1b_2^2 2a_1^2 1b_1^2$ . The molecular orbital diagram of water, accompanied with the orbital energies, is presented in Figure 37. The K-LL Auger spectrum of water is shown in Figure 38. Compared to other oxygen spectra, such as molecular oxygen and nitric oxide (Figures 14 and 18, pages 38 and 42, respectively), the water spectrum is exceedingly simple. Of the eight bands visible in the water spectrum, the four lying in region B involve  $w$  orbitals ( $w = 1b_1, 2a_1$  and  $1b_2$ ) in the Auger process, the two lying in region C involve  $w$  and  $s$  electrons ( $s = 1a_1$ ), and the remaining two appearing in region D probably involve  $s$  electrons. Four of the bands, B-1, B-2, C-1 and D-1, probably arise from normal Auger transitions, and the remaining four from low energy satellite processes.

Since the  $1b_1$  orbital of water has the lowest binding energy, one might expect the first normal Auger line, B-1, to have resulted from a  $1s-1b_1 1b_1$  process. From calculations,<sup>61</sup> the  $1b_1$  orbital can be simply written as the  $2p_x$  atomic orbital of oxygen, indicating that the  $1b_1$  orbital is 100 percent localized on the oxygen atom in the water molecule. It also seems reasonable to assign the most intense Auger line, B-1, to a

ORNL-DWG. 70-700

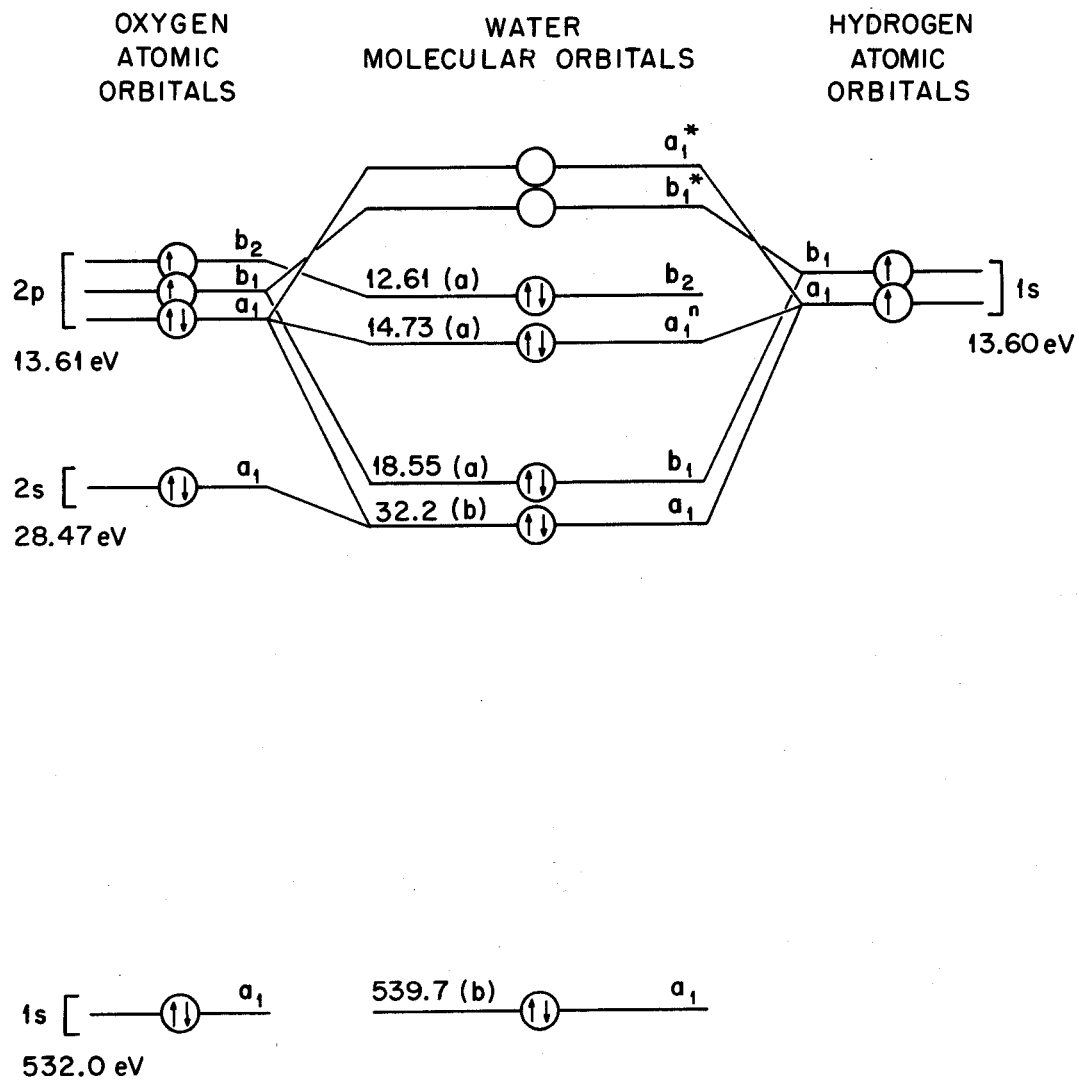


Figure 37. Molecular orbital diagram for water.

(a), obtained from reference 62; (b), obtained from reference 11.

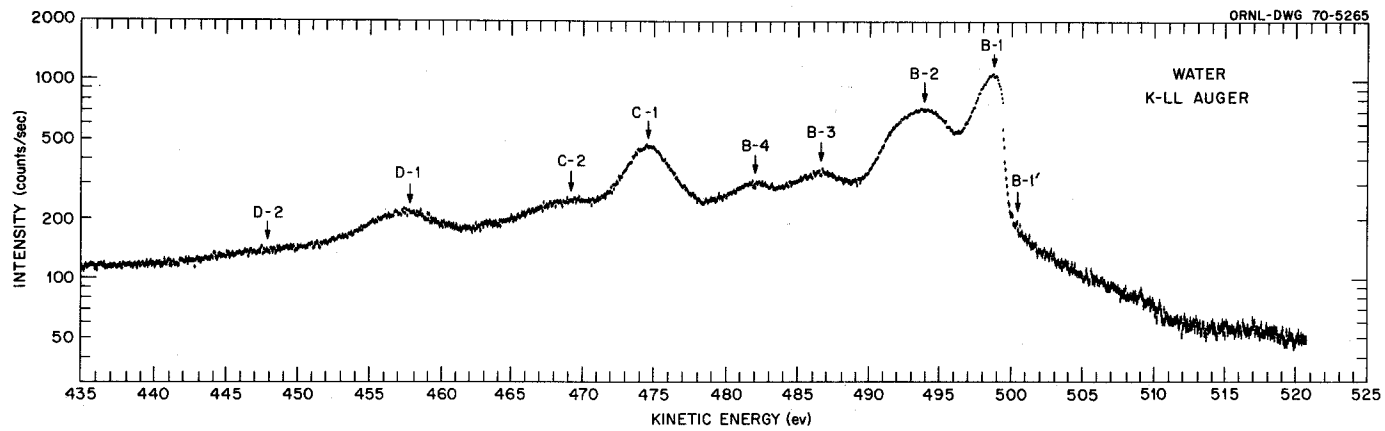


Figure 38. K-LL Auger electron spectra of water excited by electron impact.

transition involving the maximum use of this orbital, i.e., the  $1s-1b_1 1b_1$  transition. The energies of the different peaks and their assignments are given in Table XXVIII.

If the assignments of B-1 at  $498.6 \pm 0.3$  eV and D-1 at  $457.4 \pm 0.6$  eV are correct, the second ionization energy of the  $1b_1$  and  $1a_1$  orbitals can be ascertained by using equation (3-7), page 92.  $I(1b_1)^{-2}$  and  $I(1a_1)^{-2}$  were calculated to be 28.5 and 50.1 eV, respectively. By using equation (3-3), page 83, and the onset of B-1, B-1', an estimate of 39.2 eV is made for  $E_{H_2O}+2(\text{min})$ , the minimum energy required for removing the two least tightly bound electrons from an unexcited water molecule.

## 2. Carbon Dioxide

Carbon dioxide has a  $1s_o^2 1s_c^2 (1\sigma_g^+)^2 (1\sigma_u^+)^2 (2\sigma_g^+)^2 (2\sigma_u^+)^2 1\pi_u^4 1\pi_g^4$  electron configuration. Figure 39 shows the molecular orbital diagram of  $CO_2$ . The carbon and oxygen K-LL Auger spectra of carbon dioxide are shown in Figures 40 and 41, respectively. Each spectrum is divided into regions A, B, C and D. The Auger electron energies for the observed peaks in each spectrum are given in Table XXIX.

The relative positions of the Auger lines in the carbon and oxygen spectra are compared in Figure 42 as to the difference in the two  $1s$  binding energies of carbon and oxygen in  $CO_2$  (for a similar comparison see CO and NO, pages 96 and 100). The peaks in region A have been attributed to high energy satellite lines. Six peaks in region B have been assigned to normal Auger lines. Energies of six possible final states of  $CO_2^{+2}$  can be calculated by using equation (3-3) and the corresponding energy for each of the identified normal lines. By using

TABLE XXVIII  
 ASSIGNMENTS AND ELECTRON PEAK ENERGIES  
 IN WATER K-LL AUGER SPECTRUM

Peak	Absolute Energy (eV) <sup>a</sup>	$E_{H_2O^{+2}}$ (eV) <sup>b</sup>	Assignment <sup>c</sup>
B-1'	500.5 ± 1	39.2	
B-1	498.6 ± 0.3	41.1	$1s_o - 1b_1 1b_1$
B-2	493.8 ± 0.4	45.8	$1s_o - ww$
B-3	486.8 ± 0.4		satellite <sup>c,d</sup>
B-4	482.2 ± 0.4		satellite <sup>c</sup>
C-1	474.6 ± 0.4	63.1	$1s_o - 1a_1 w$
C-2(sh)	469.2 ± 0.6		satellite <sup>c</sup>
D-1	457.4 ± 0.6	82.3	$1s_o - 1a_1 1a_1$
D-2(sh)	447.6 ± 1.0		satellite <sup>c</sup>

<sup>a</sup>The absolute energy of the peaks listed in column 1 were obtained from Figure 38, page 106.

<sup>b</sup> $E_{H_2O^{+2}}$  is energy of the different electronic states of the doubly charged water ion. The  $E_{H_2O^{+2}}$  values were calculated from equation (3-3), page 83.

<sup>c</sup>Refers to a low energy satellite line.

<sup>d</sup>B-3 could also result from a  $1s_o - 1b_2 1b_2$  transition.

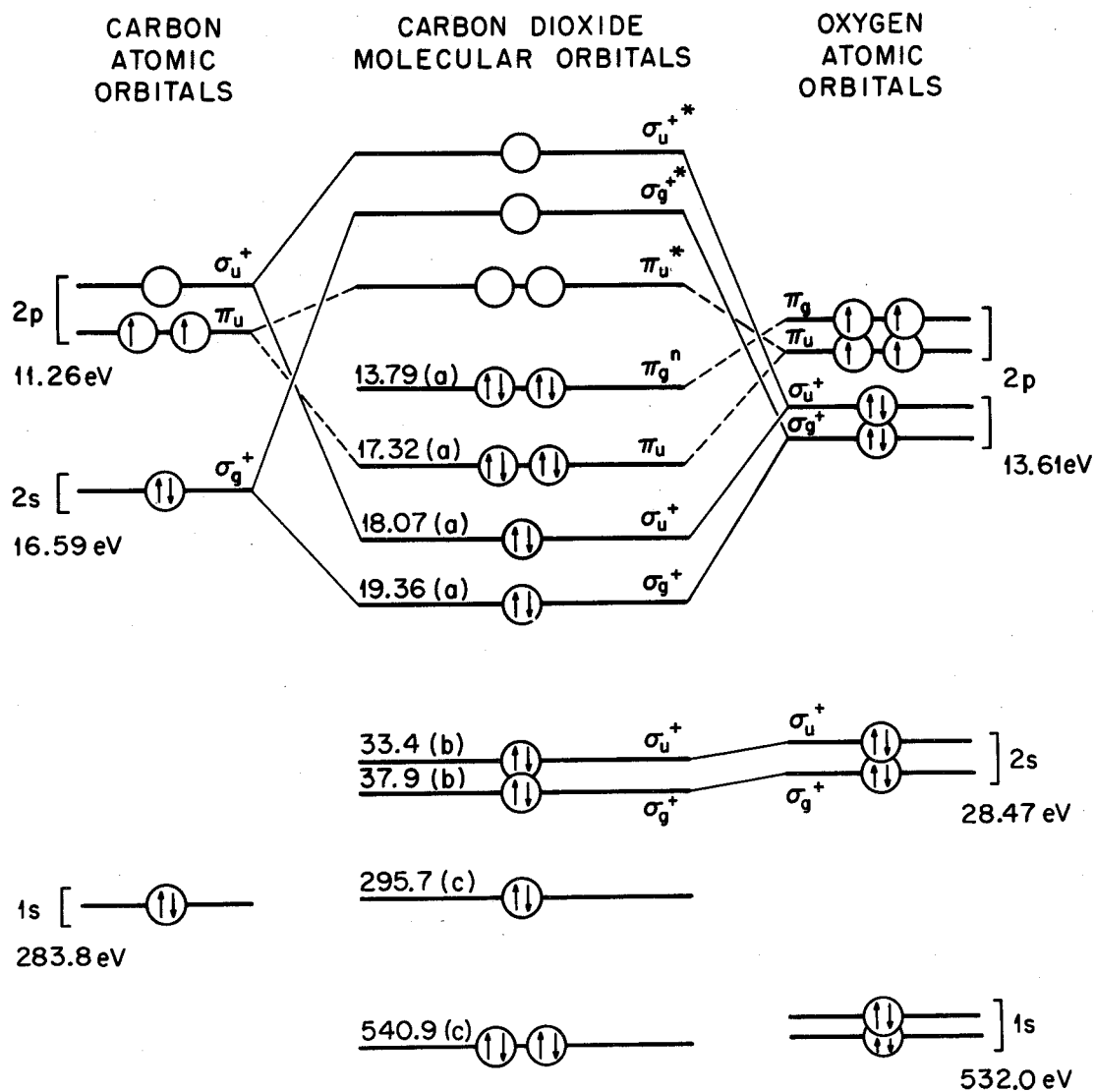


Figure 39. Molecular orbital diagram for carbon dioxide.

(a), obtained from reference 63; (b), obtained from reference 64;  
 (c), obtained from reference 11.

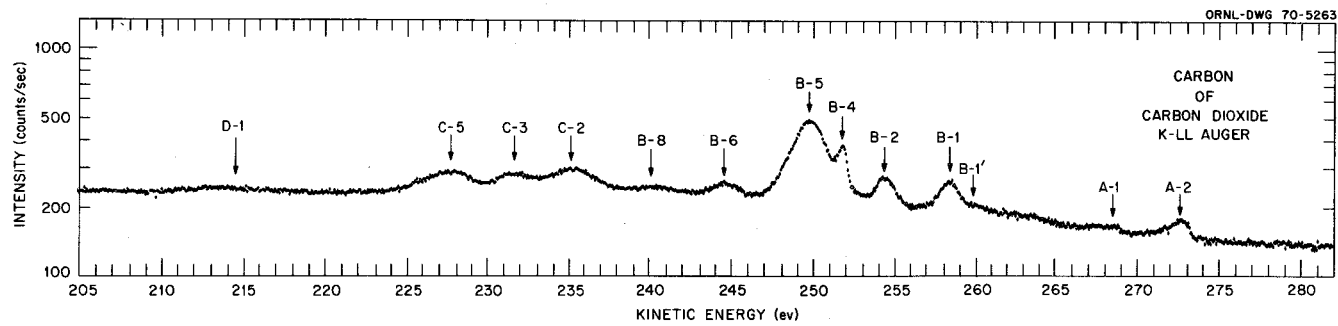


Figure 40. Carbon K-LL Auger electron spectrum of carbon dioxide excited by electron impact.

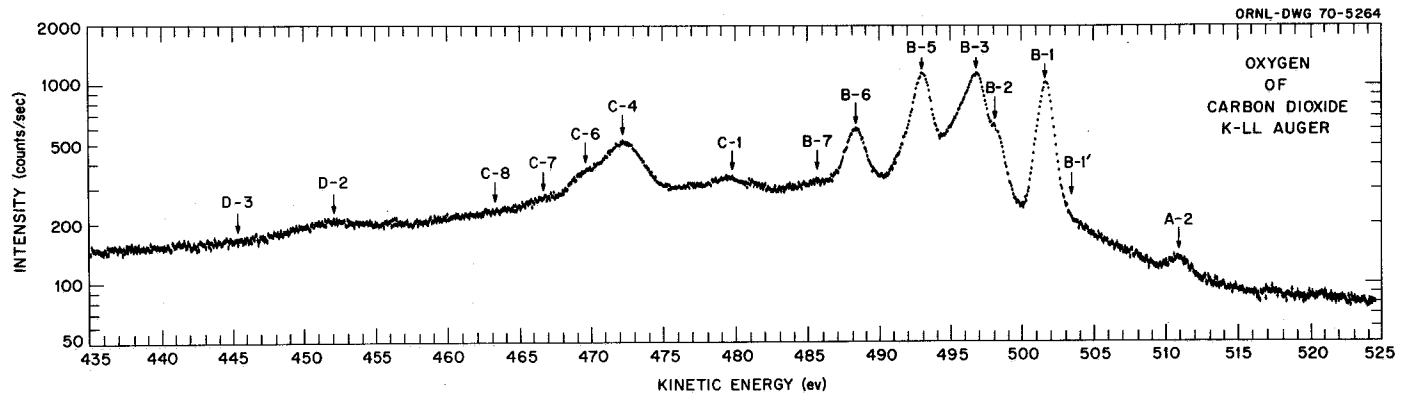


Figure 41. Oxygen K-LL Auger electron spectrum of carbon dioxide excited by electron impact.

TABLE XXIX

ELECTRON PEAK ENERGIES IN THE CARBON AND OXYGEN  
K-LL AUGER SPECTRA OF CARBON DIOXIDE

Peak <sup>a</sup>	$E_A(\text{C} - \text{CO}_2)$ (eV) <sup>b</sup>	$E_A(\text{O} - \text{CO}_2)$ (eV) <sup>c</sup>
A-1	272.6 ± 0.5	
A-2	268.2 ± 0.5	511.3 ± 0.3
B-1'	259.7	503.4
B-1	258.3 ± 0.2	501.9 ± 0.3
B-2	254.2 ± 0.4	498.3 ± 0.5
B-3		497.0 ± 0.3
B-4	251.7 ± 0.2	
B-5	249.6 ± 0.3	493.3 ± 0.3
B-6	244.1 ± 0.5	488.6 ± 0.4
B-7		485.6 ± 0.5
B-8	240.2 ± 0.6	
C-1		479.7 ± 0.5
C-2	235.2 ± 0.5	
C-3	231.5 ± 0.5	
C-4		472.6 ± 0.5
C-5	228.4 ± 0.6	
C-6		469.8 ± 0.8
C-7		466.6 ± 1.0
C-8		463.4 ± 1.2
D-1	214.1 ± 0.7	
D-2		450.8 ± 0.8
D-3		445.1 ± 1.0

<sup>a</sup>The onset of a given peak is indicated by a primed number.

<sup>b</sup> $E_A(\text{C} - \text{CO}_2)$  represents the electron energies of the different Auger lines measured in the carbon K-LL Auger spectrum of  $\text{CO}_2$  (Figure 40).

<sup>c</sup> $E_A(\text{O} - \text{CO}_2)$  represents the electron energies of the different Auger lines measured in the oxygen K-LL Auger spectrum of  $\text{CO}_2$  (Figure 41).

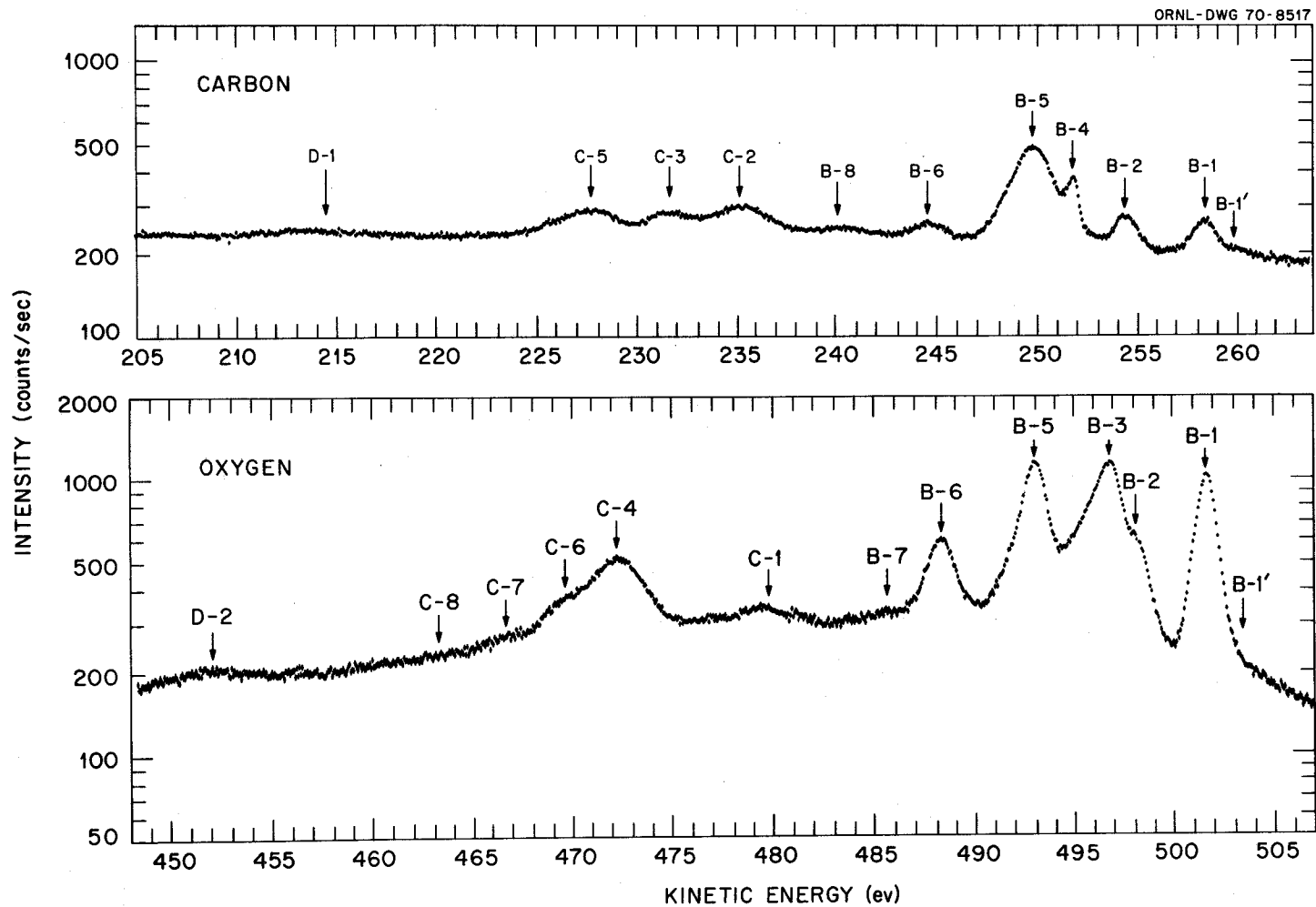


Figure 42. Diagram line regions of the carbon and oxygen K-LL Auger electron spectra of carbon dioxide excited by electron impact.

the value for  $B-1'$  and equation (3-3), the minimum ionization energy required to remove the two least bound electrons of  $\text{CO}_2$  was estimated to be 37.6 eV. Table XXX summarizes the above results.

### C. Polyatomic Molecules

#### 1. Methane and the Fluoromethanes

The K-LL Auger spectra of the carbon and fluorine elements in  $\text{CH}_4$ ,  $\text{CH}_3\text{F}$ ,  $\text{CH}_2\text{F}_2$ ,  $\text{CHF}_3$  and  $\text{CF}_4$  are shown in Figures 43-51; and, Tables XXXI-XXXIX give the peak energies indicated by the arrows in each of the figures. Figure 52 gives an orbital energy diagram for the above listed compounds.

a. The carbon spectra. A composite of all the carbon spectra of the fluoromethane series is illustrated in Figure 53. This figure indicates an increase in the complexity of the spectra from  $\text{CH}_4$  and  $\text{CH}_2\text{F}_2$  and then a leveling-off to  $\text{CF}_4$ . This observation of the increasing complexity parallels the number of non-degenerate molecular orbitals available to form different electronic states of the final doubly charged ion. As the number of molecular orbitals increases, the number of possible double hole combinations also may be expected to increase, thereby enlarging the complexity of the resulting Auger spectra.

In the methane spectrum a broad maximum occurs at 250.0 eV. This can be assigned to transitions involving  $t_2$  electrons, i.e.,  $1s-t_2t_2$  process. In photoelectron spectroscopy<sup>37</sup> the appearance of a broad band has been attributed to (1) transitions to several unresolved vibrational states of a stable electronic state, (2) transitions to unstable electronic states,

TABLE XXX

ASSIGNMENTS AND ENERGIES OF THE FINAL ELECTRONIC STATES FOR  
THE DOUBLY CHARGED CARBON DIOXIDE MOLECULAR ION

Peak <sup>a</sup>	$E_{\text{CO}_2^{+2}}$ (Carbon Data) eV	$E_{\text{CO}_2^{+2}}$ (Oxygen Data) eV	Assignment <sup>c</sup>
B-1'	37.8	37.5 < 36.4 >	1s-ww
B-1	39.2	39.0	1s-ww
B-2	43.3	42.6	1s-ww
B-3		43.9	1s-ww
B-4	45.8		1s-ww
B-5	47.9	47.6	1s-ww
B-6	53.4	52.3	1s-ww
C-2	60.5		1s-ws
C-3	67.3		1s-ws
C-4		68.3	1s-ws
D-1	81.6		1s-ss
D-2		90.1	1s-ss

<sup>a</sup>Peaks were observed in Figure 42.

<sup>b</sup> $E_{\text{CO}_2^{+2}}$  values are the energies of the final electronic states of the doubly charged carbon dioxide molecular ion. These values were calculated by using the carbon Auger data of Table XXIX and equation (3-3), page 83.

<sup>c</sup>These values were calculated by using the oxygen data in Table XXIX. The value given in brackets, 36.4 eV, was obtained by Dorman and Morrison, reference 60, for the appearance potential of  $\text{CO}_2^{+2}$ .

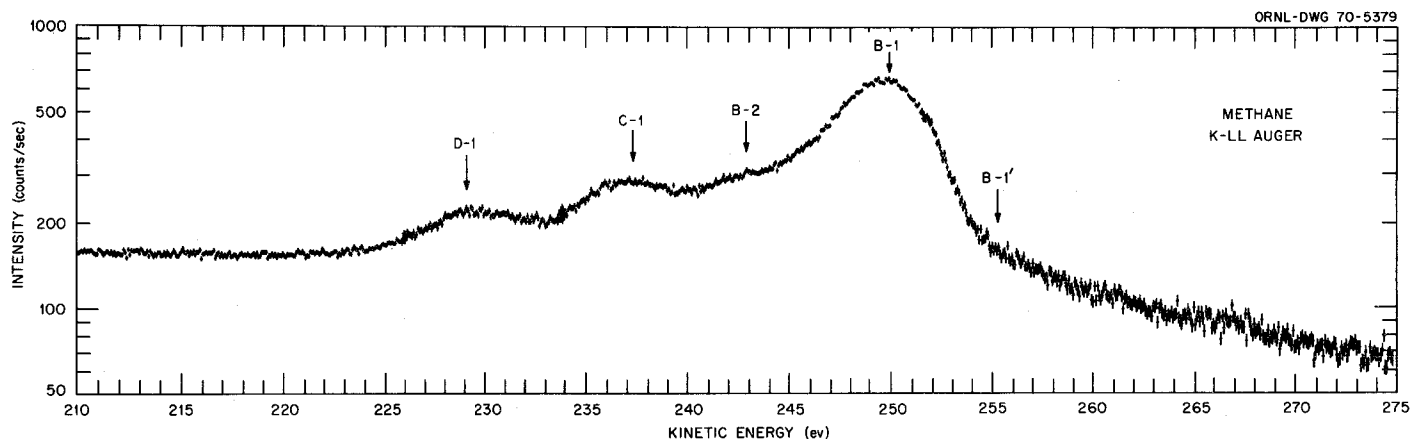


Figure 43. K-LL Auger electron spectrum of methane excited by electron impact.

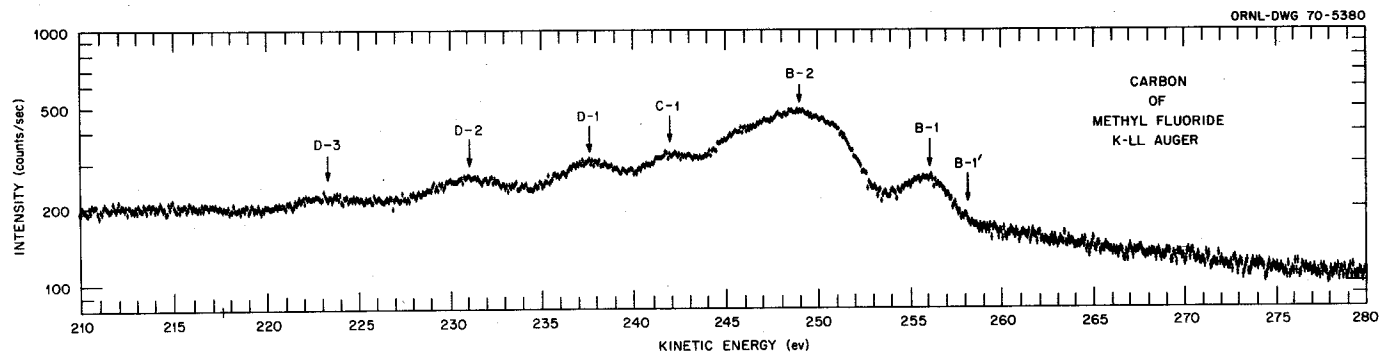


Figure 44. Carbon K-LL Auger electron spectrum of methyl fluoride excited by electron impact.

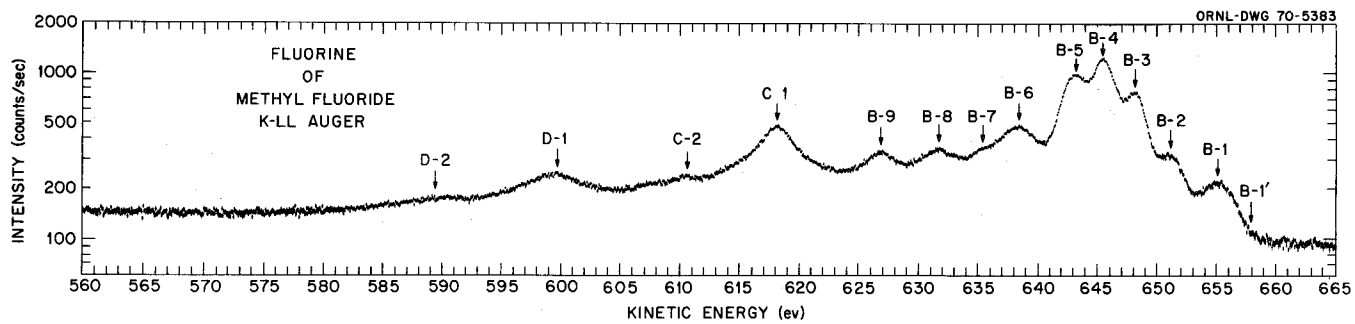


Figure 45. Fluorine K-LL Auger electron spectrum of methyl fluoride excited by electron impact.

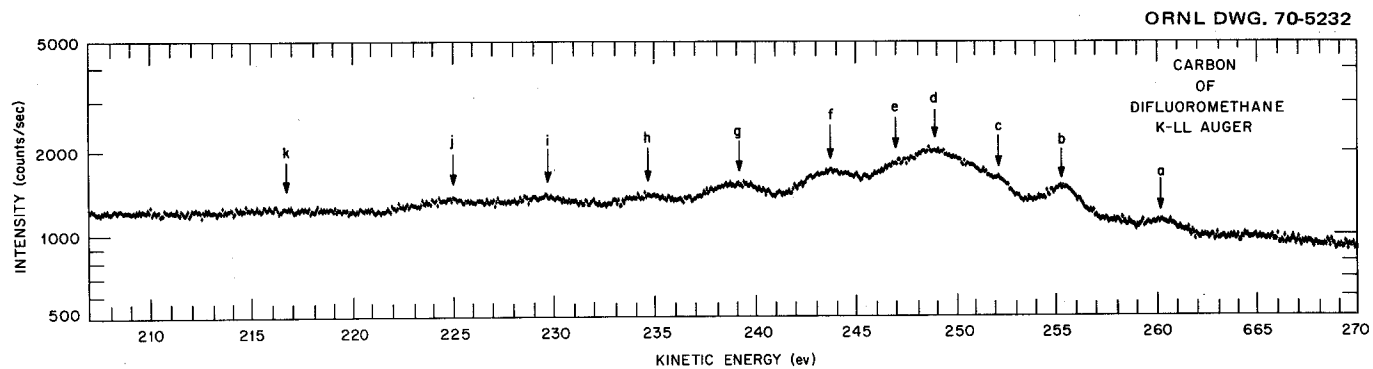


Figure 46. Carbon K-LL Auger electron spectrum of difluoromethane excited by electron impact.

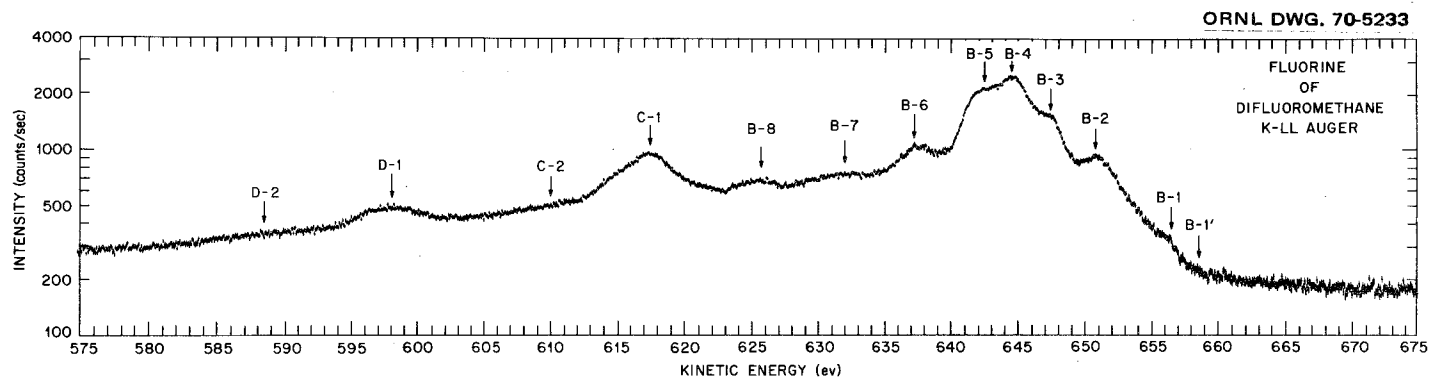


Figure 47. Fluorine K-LL Auger electron spectrum of difluoromethane excited by electron impact.

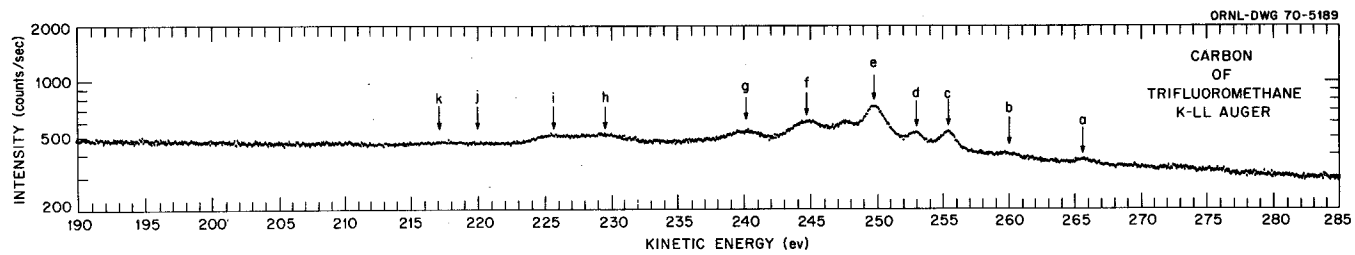


Figure 48. Carbon K-LL Auger electron spectrum of trifluoromethane excited by electron impact.

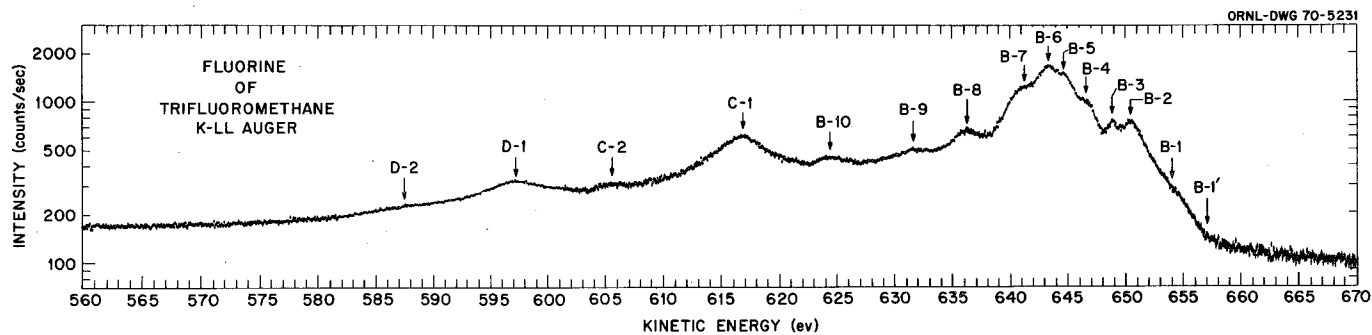


Figure 49. Fluorine K-LL Auger electron spectrum of trifluoromethane excited by electron impact.

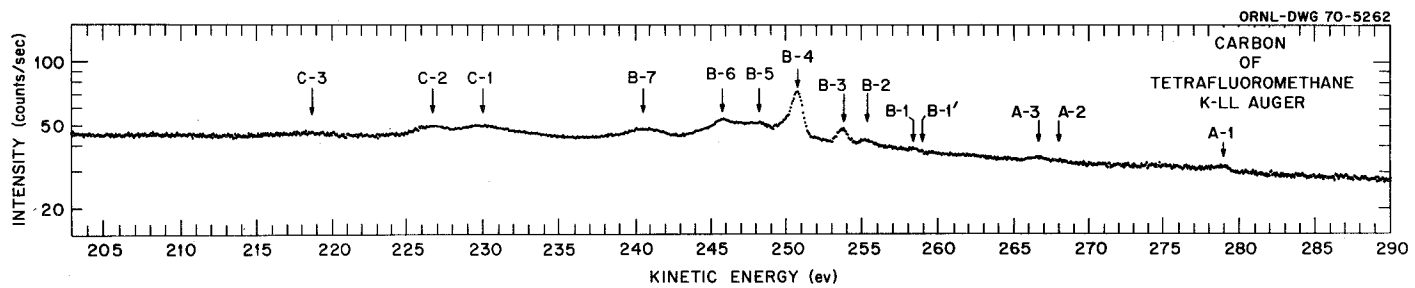


Figure 50. Carbon K-LL Auger electron spectrum of tetrafluoromethane excited by electron impact.

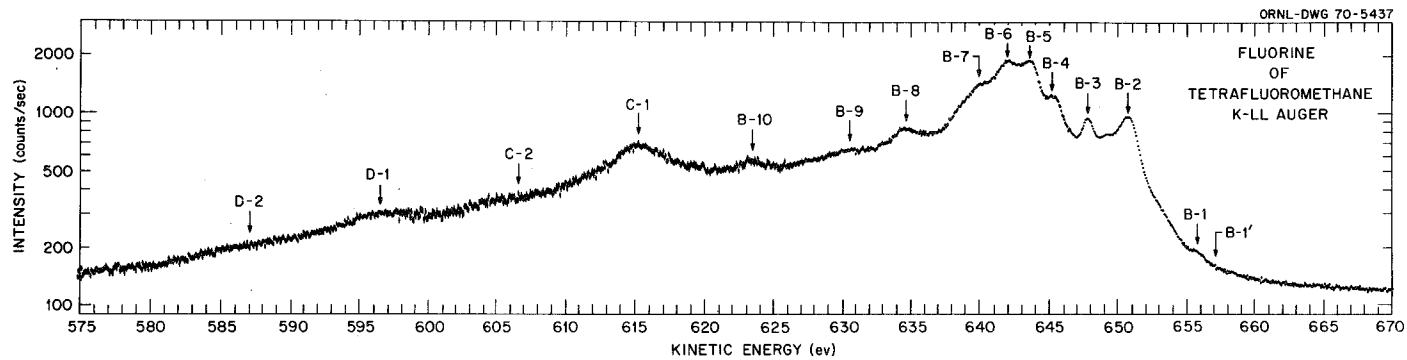


Figure 51. Fluorine K-LL Auger electron spectrum of tetrafluoromethane excited by electron impact.

TABLE XXXI  
ELECTRON PEAK ENERGIES IN THE K-LL  
AUGER SPECTRUM OF METHANE

Peak <sup>a</sup>	Absolute Energy (eV)
B-1'	255.5
B-1	250.0 ± 0.5
B-2	243.3 ± 1.1
C-1	237.3 ± 0.8
D-1	229.6 ± 0.7

<sup>a</sup>Peaks were observed in Figure 43.

TABLE XXXII  
ELECTRON PEAK ENERGIES IN THE CARBON K-LL AUGER  
SPECTRUM OF METHYL FLUORIDE

Peak <sup>a</sup>	Absolute Energy (eV)
B-1'	258.3
B-1	256.1 ± 0.4
B-2	247.2 ± 0.8
C-1	242.3 ± 0.5
C-2	238.1 ± 0.5
D-1	231.5 ± 0.4
D-2	223.2 ± 1.0
D-3	217.1 ± 1.2

<sup>a</sup> Peaks were observed in Figure 44.

TABLE XXXIII

ELECTRON PEAK ENERGIES IN THE FLUORINE K-LL AUGER  
SPECTRUM OF METHYL FLUORIDE

Peak <sup>a</sup>	Absolute Energy (eV)
B-1	657.8
B-1	655.1 ± 0.4
B-2	651.0 ± 0.5
B-3	648.1 ± 0.4
B-4	645.4 ± 0.4
B-5	643.0 ± 0.5
B-6	638.4 ± 0.8
B-7	635.3 ± 1.0
B-8	631.6 ± 0.8
B-9	626.8 ± 0.7
C-1	618.1 ± 0.6
C-2	610.6 ± 1.0
D-1	599.6 ± 0.7
D-2	589.7 ± 1.2

<sup>a</sup>Peaks were observed in Figure 45.

TABLE XXXIV

ELECTRON PEAK ENERGIES IN THE CARBON K-LL AUGER  
SPECTRUM OF DIFLUJROMETHANE

Peak <sup>a</sup>	Absolute Energy (eV)
a	260.2 ± 0.7
b	255.2 ± 0.5
c	252.2 ± 0.7
d	248.9 ± 0.6
e	246.9 ± 0.7
f	243.9 ± 0.6
g	239.2 ± 0.7
h	234.7 ± 0.8
i	229.8 ± 1.0
j	225.0 ± 1.0
k	216.6 ± 1.2

<sup>a</sup>Peaks were observed in Figure 46.

TABLE XXXV  
ELECTRON PEAK ENERGIES IN FLUORINE K-LL AUGER  
SPECTRUM OF DIFLUOROMETHANE

Peak <sup>a</sup>	Absolute Energy (eV)
B-1'	658.8
B-1	656.4 ± 0.7
B-2	651.2 ± 0.5
B-3	647.4 ± 0.6
B-4	644.7 ± 0.5
B-5	642.4 ± 0.5
B-6	637.6 ± 0.5
B-7	631.8 ± 0.9
B-8	625.6 ± 0.9
C-1	618.1 ± 0.5
C-2	611.3 ± 1.2
D-1	598.0 ± 1.0
D-2	588.7 ± 1.2

<sup>a</sup>Peaks were observed in Figure 47.

TABLE XXXVI

ELECTRON PEAK ENERGIES IN THE CARBON K-LL AUGER  
SPECTRUM OF TRIFLUOROMETHANE

Peak <sup>a</sup>	Absolute Energy (eV)
a	265.8 ± 0.5
b	260.0 ± 0.7
c	255.5 ± 0.4
d	253.0 ± 0.5
e	249.8 ± 0.4
f	247.6 ± 0.4
g	245.0 ± 0.5
h	240.3 ± 0.6
i	229.5 ± 1.1
j	225.9 ± 1.1
k	217.7 ± 1.5

<sup>a</sup>Peaks were observed in Figure 48.

TABLE XXXVII

ELECTRON PEAK ENERGIES IN THE FLUORINE K-LL AUGER  
SPECTRUM OF TRIFLUOROMETHANE

Peak <sup>a</sup>	Absolute Energy (eV)
B-1	657.5
B-1	654.0 ± 2.3
B-2	650.4 ± 0.4
B-3	648.9 ± 0.4
B-4	646.8 ± 0.6
B-5	644.6 ± 0.4
B-6	643.4 ± 0.5
B-7	641.2 ± 0.6
B-8	636.2 ± 0.6
B-9	631.6 ± 0.8
B-10	624.4 ± 0.7
C-1	617.0 ± 0.6
C-2	605.6 ± 0.9
D-1	597.4 ± 1.7
D-2	587.8 ± 2.3

<sup>a</sup>Peaks were observed in Figure 49.

TABLE XXXVIII  
ELECTRON PEAK ENERGIES IN THE CARBON K-LL AUGER  
SPECTRUM OF TETRAFLUOROMETHANE

Peak <sup>a</sup>	Absolute Energy (eV)
A-1	278.9 ± 0.5
A-2	268.1 ± 0.5
A-3	266.7 ± 0.5
B-1'	259.0
B-1	258.5 ± 0.5
B-2	255.2 ± 0.5
B-3	253.8 ± 0.4
B-4	250.8 ± 0.3
B-5	248.2 ± 0.7
B-6	245.9 ± 0.5
B-7	240.9 ± 0.7
C-1	230.2 ± 0.8
C-2	227.1 ± 0.7
C-3	218.5 ± 1.1

<sup>a</sup>Peaks were observed in Figure 50.

TABLE XXXIX

ELECTRON PEAK ENERGIES IN THE FLUORINE K-LL AUGER  
SPECTRUM OF TETRAFLUOROMETHANE

Peak <sup>a</sup>	Absolute Energy (eV)
B-1'	657.5
B-1	655.9 ± 0.8
B-2	651.0 ± 0.4
B-3	648.0 ± 0.4
B-4	645.5 ± 0.5
B-5	643.9 ± 0.5
B-6	642.3 ± 0.4
B-7	640.3 ± 0.6
B-8	634.8 ± 0.6
B-9	631.0 ± 0.9
B-10	623.8 ± 0.6
C-1	615.7 ± 0.6
C-2	604.3 ± 1.0
D-1	596.8 ± 1.3
D-2	587.1 ± 2.0

<sup>a</sup>Peaks were observed in Figure 51.

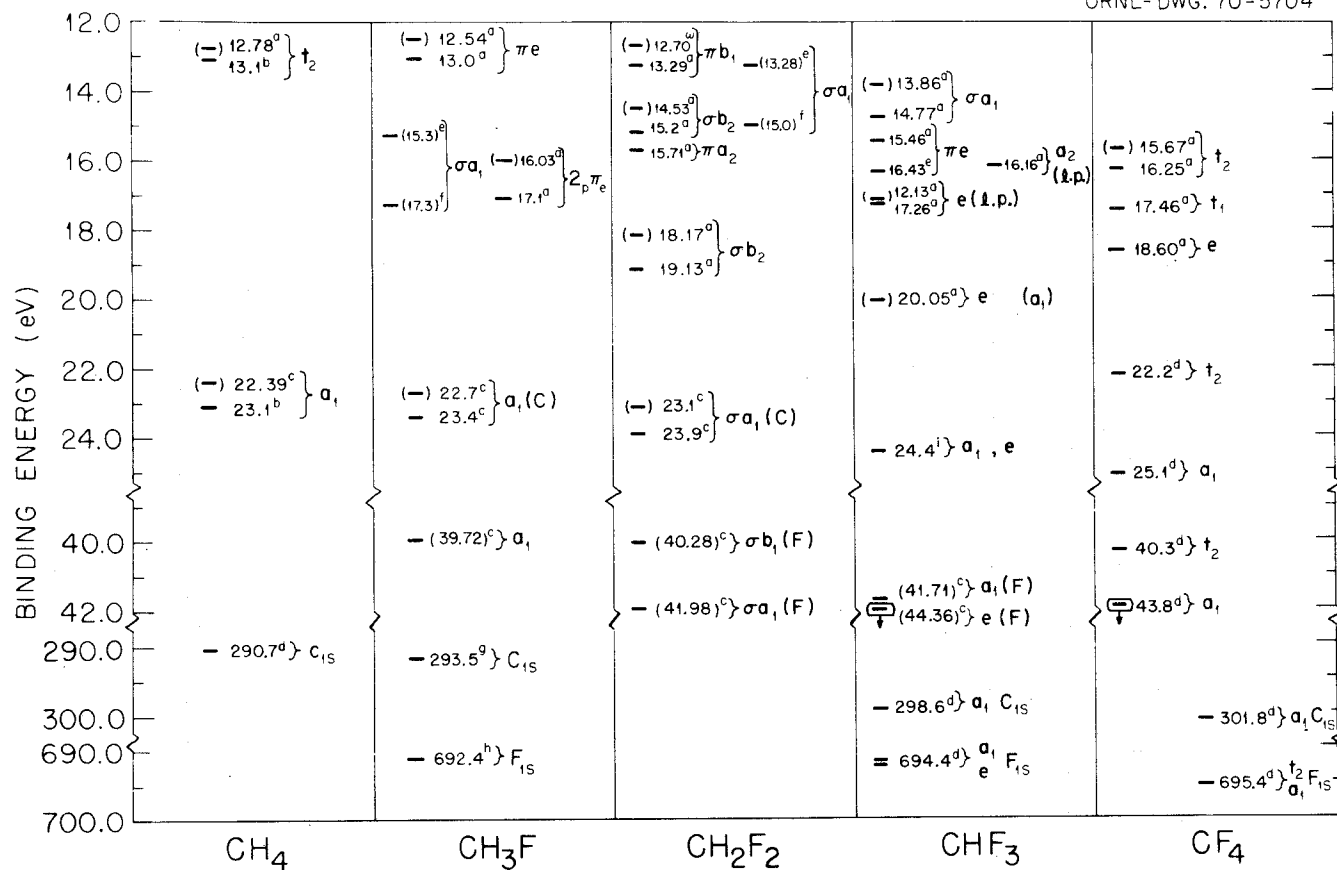


Figure 52. Orbital energies of CH<sub>4</sub>, CH<sub>3</sub>F, CH<sub>2</sub>F<sub>2</sub>, CHF<sub>3</sub> and CF<sub>4</sub>.

-, represent vertical ionization energies; (-), represent adiabatic ionization energies; ( ), represent calculated orbital energies; a, obtained from reference 37; b, obtained from reference 65; c, obtained from reference 66; d, obtained from reference 11; e, obtained from reference 67, f, obtained from reference 68, g, obtained from reference 69, h, interpreted from references 69 and 11; i, obtained from reference 70.

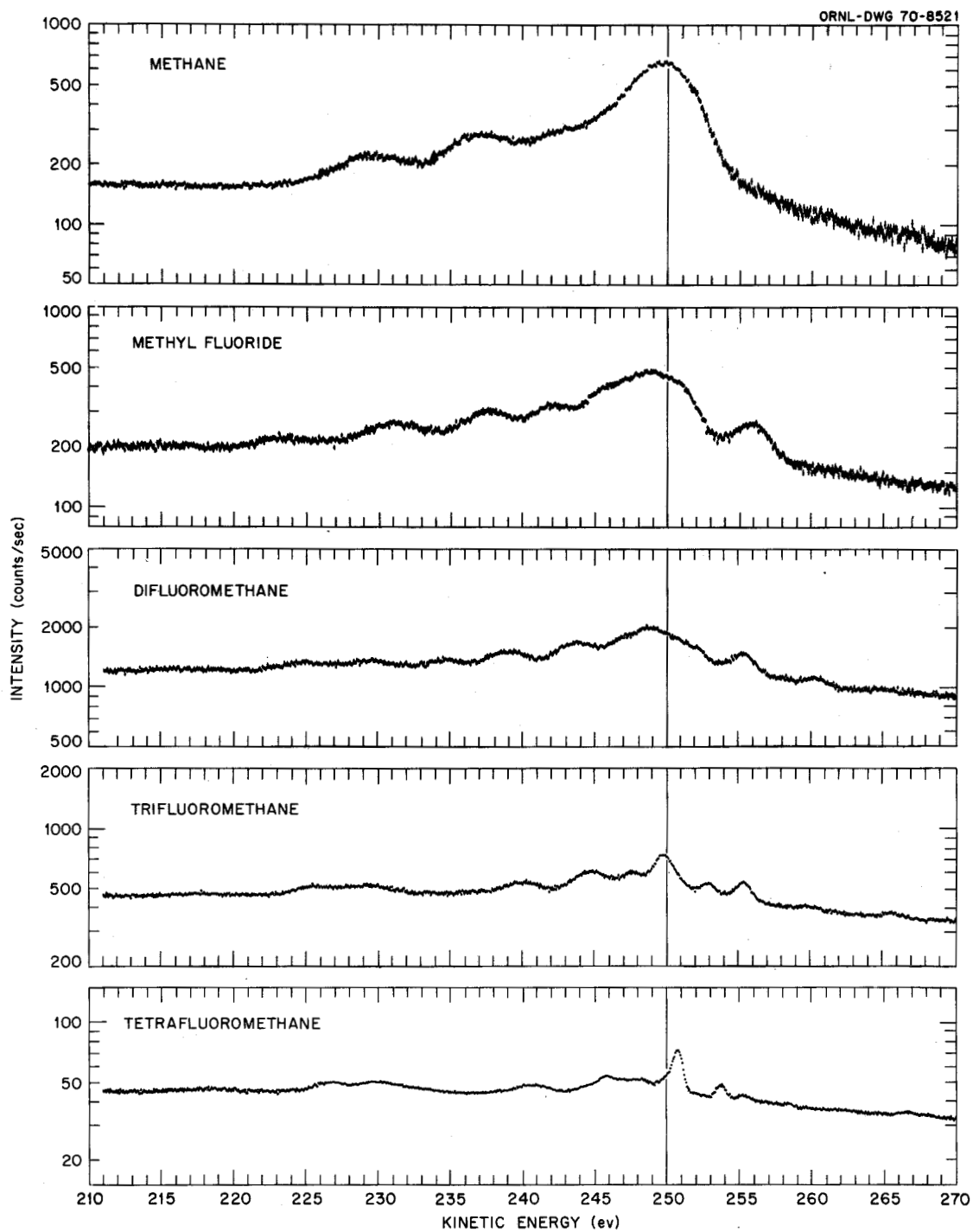


Figure 53. Composite of the carbon K-LL Auger electron spectra for the fluoromethane series.

or (3) transitions which involve pre-dissociation. Siegbahn et al<sup>11</sup> have suggested that the broad band in methane results from the rapid pre-dissociation of  $\text{CH}_4^{+2}$ . To support their suggestion they measured the dissociation energy of  $\text{CH}_4^{+2}$  (-13 eV), or  $\text{C}_2\text{H}_6^{+2}$  (-8 eV), and of  $\text{C}_6\text{H}_6^{+2}$  (+1.3 eV); and, they relate the observation of the sharp peaks in the benzene Auger spectrum to the stability of  $\text{C}_6\text{H}_6^{+2}$ . However, the  $t_2^4$  electronic configuration of  $\text{CH}_4^{+2}$  would exhibit Jahn-Teller distortion. The degeneracy of the  $t_2$  state would be expected to be split and, consequently, Auger transitions to these different states might also be the reason for the observed broad band. Thus far, no calculations on the electronic states of  $\text{CH}_4^{+2}$  have been attempted. If Jahn-Teller distorted final states are the cause of the observed broad band for the  $1s-t_2t_2$  process in the methane spectrum, one might expect a decrease in the FWHM (full width at half maximum) of the peak attributed to this process, as one proceeds from  $\text{CH}_4$  to  $\text{SiH}_4$  to  $\text{CF}_4$  where the amount of splitting of the electronic states is known to decrease. This supposition is made by analogy to the band widths observed upon the removal of a  $t_2$  electron in the photoelectron spectrum of  $\text{CH}_4$ ,  $\text{SiH}_4$  and  $\text{CF}_4$ . The FWHM of the peak in the Auger spectrum resulting from the  $1s-t_2t_2$  process does, indeed, decrease in this series.

The strongest peak appears at 249.2 eV for  $\text{CH}_3\text{F}$ , 248.9 eV for  $\text{CH}_2\text{F}_2$ , 249.8 eV for  $\text{CHF}_3$ , and 250.8 eV for  $\text{CF}_4$ ; and, the FWHM decreases from a broad band of 6.7 eV for  $\text{CH}_4$  to a sharp peak of 0.8 eV for  $\text{CF}_4$ . This reduction in FWHM suggests a decreasing trend toward pre-dissociation or Jahn-Teller distortion and an increasing trend toward stability of the final doubly charged ion.

As pointed out previously with the diatomic molecules (Section A of Chapter III), analyses of the peaks in a K-LL Auger spectrum are assisted by the division of the spectrum into different regions. For example, in the methane spectrum (Figure 42, page 113) peaks B-1 and B-2 most likely involve the  $t_2$  electrons in the Auger process, C-1 most likely originates from  $1s-a_1t_2$  processes, and D-1 from a  $1s-a_1a_1$  process.

The carbon Auger spectrum of tetrafluoromethane (Figure 50, page 123) is also divided into different regions according to the electrons involved in the Auger process. From the division, the  $1s_C$ - $ww$  process ( $w = 3t_2, 1t_1, 1e$ ) involves essentially all fluorine-like electrons. These transitions appear low in intensity compared to the  $1s_F$ - $ww$  processes in the fluorine spectrum (see Figure 51, page 124). In Figure 50, the strongest peak at 250.8 eV possibly results from a  $1s_C$ - $2t_23t_2$  process, and the peak at 230.2 eV originates from a  $1s_C$ - $1t_23t_2$  process. This assignment is formulated from the large 2p-carbon character in the  $1t_2$  and  $2t_2$  orbitals.<sup>11</sup> Peaks A-1, A-2 and A-3 are probably due to autoionization.

Division of the carbon spectra of mono-, di- and tri-fluoromethane into different regions is difficult because there are many electrons with different energies available to fill the  $1s$  carbon vacancy. However, some tentative assignments are given to the methyl fluoride spectrum (see Table XL).

If we assume that the first peak in each spectrum results from a  $1s_C$ - $ww$  process to lowest energy electronic state of the doubly charged ion, then estimates of  $E_{CH_xF_y}^{+2}(\min)$ , the minimum energy required to remove the two least bound electrons from a neutral molecule, can be made.

$E_{CH_xF_y}^{+2}(\min)$  values of 35.2, 35.2, 36.9 and 40.3 were ascertained by

TABLE XL

SUMMARY OF THE RESULTS OBTAINED FROM THE K-LL AUGER SPECTRA  
OF METHANE AND THE FLUOROMETHANES

Compound	Spectrum <sup>a</sup>	Process	$E(\text{CH}_x\text{F}_y)^{+2b}$	$I(X)^{-1c}$	$I(X)^{-2d}$
CH <sub>4</sub>	C	1s-t <sub>2</sub> t <sub>2</sub>	(35.2)	12.8	22.4
	C	1s-a <sub>1</sub> t <sub>2</sub>	53.4		
	C	1s-a <sub>1</sub> a <sub>1</sub>	(61.1)	23.1	38.0
CH <sub>3</sub> F	C	1s-π <sub>e</sub> π <sub>e</sub>	(35.2)	12.5	22.7
	C	1s-a <sub>1</sub> a <sub>1</sub>	62.0	23.4	38.6
	C	1s-a <sub>1</sub> a <sub>1</sub> (F)	70.3		
CH <sub>3</sub> F	F	1s-a <sub>1</sub> (F)a <sub>1</sub> (F)	92.8	39.7	53.1
CHF <sub>3</sub>	F		(36.9)		
CF <sub>4</sub>	C	1s-3t <sub>2</sub> 3t <sub>2</sub>	(42.8)	16.2	26.6
	C	1s-2t <sub>2</sub> 3t <sub>2</sub>	51.0		
	C	1s-1t <sub>2</sub> 3t <sub>2</sub>	71.6		
CF <sub>4</sub>	F		(37.9)		

<sup>a</sup>C and F represent the carbon and fluorine K-LL Auger spectra, respectively, of the compound listed in column 1.

<sup>b</sup> $E(\text{CH}_x\text{F}_y)^{+2}$  represents the energy of the final doubly charged ion of  $\text{CH}_x\text{F}_y^{+2}$ . x and y can vary from 0 to 4, such that  $x + y = 4$ . The values listed in parentheses represent the minimum energy required for the process listed in column 3.

<sup>c</sup> $I(X)^{-1}$  is the first ionization energy for a given orbital X.

<sup>d</sup> $I(X)^{-2}$  is the second ionization energy for a given orbital X.

using: the onset of the first peak,  $B-1'$ ; the  $1s$  binding energies of carbon in  $CH_4$ ,  $CH_3F$ ,  $CHF_3$  and  $CF_4$ ; and equation (3-3), page 83. These, along with some additional calculations from the observed carbon and fluorine data, are summarized in Table XL.

b. The fluorine spectra. Figure 54 shows a composite of all the fluorine K-LL Auger spectra of the fluoromethane series. The main peaks in each spectrum appear at approximately the same energy; however, small differences in structure appear in the processes that reflect differences in the chemical bonding, i.e., the  $1s_F$ -ww processes. If the first peak is due to the removal of the two least bound electrons, then  $E_{CH_xF_y} + 2(\text{min})$  can be estimated (see Table XL).

## 2. Silane and Silicon Tetrafluoride

Thus far, we have discussed the Auger spectra of molecules with only the K and L shells occupied. The inclusion of silicon-containing compounds in the list of materials studied allows for the study of Auger processes involving the M shell. Also the two silicon compounds allowed one to study Auger processes of molecules occurring beneath the valence level.

a. The silicon L-MM spectra. Figures 55 and 56 illustrate the silicon L-MM Auger spectra of  $SiH_4$  and  $SiF_4$ , and Tables XLI and XLIII list the energies of the observed structure. In the silane spectrum, Figure 55, there exists a broad maximum at 73.7 eV of approximately 2.7 eV FWHM. Also, some sharp peaks are observed at 77.7, 77.0 and 76.4 eV. In the silicon tetrafluoride spectrum, Figure 56, there exists little structure superimposed on a high background. The main band appears at 66.3 eV of approximately 3.0 eV FWHM.

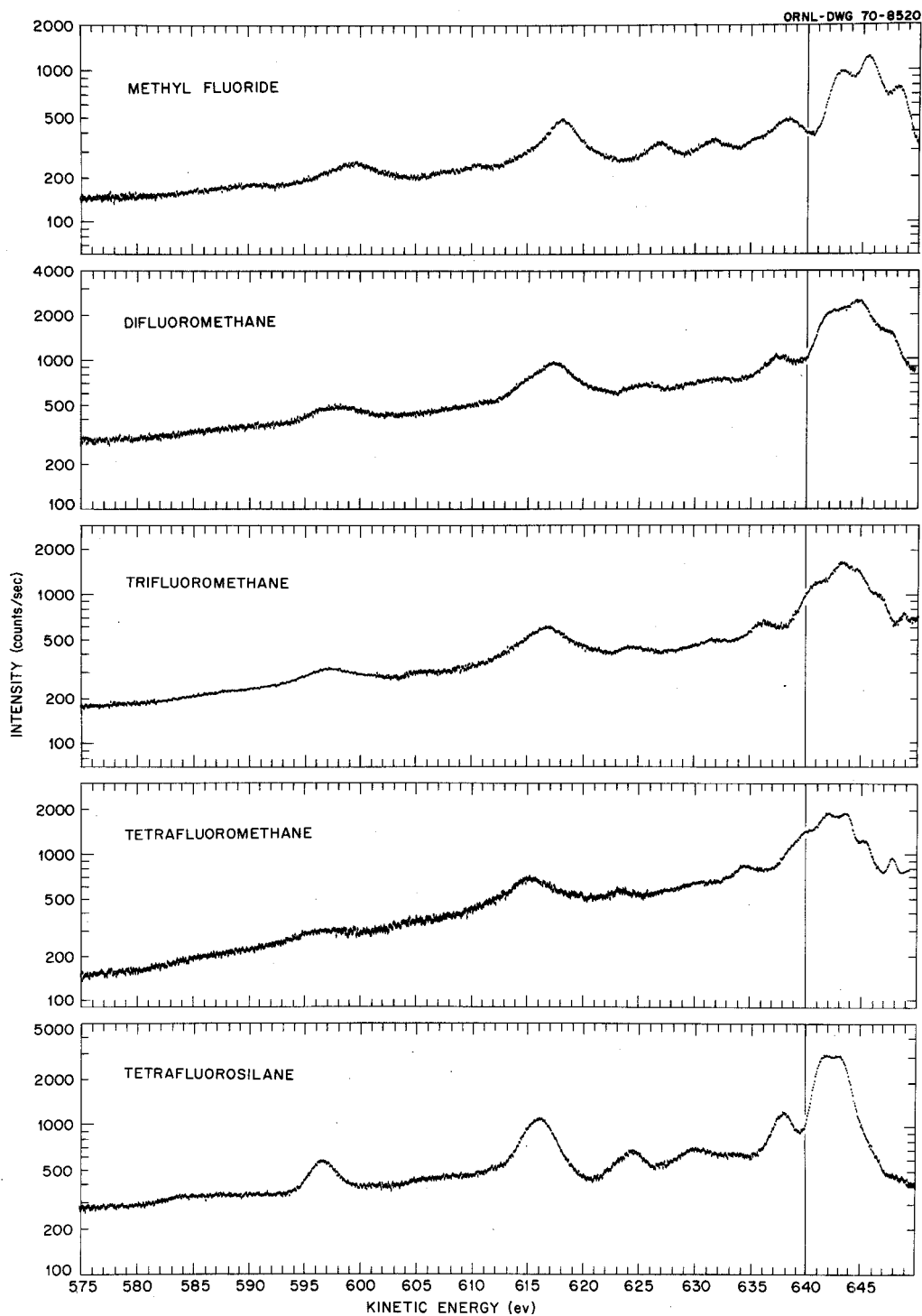


Figure 54. Composite of the fluorine K-LL Auger electron spectra for the fluoromethane series.

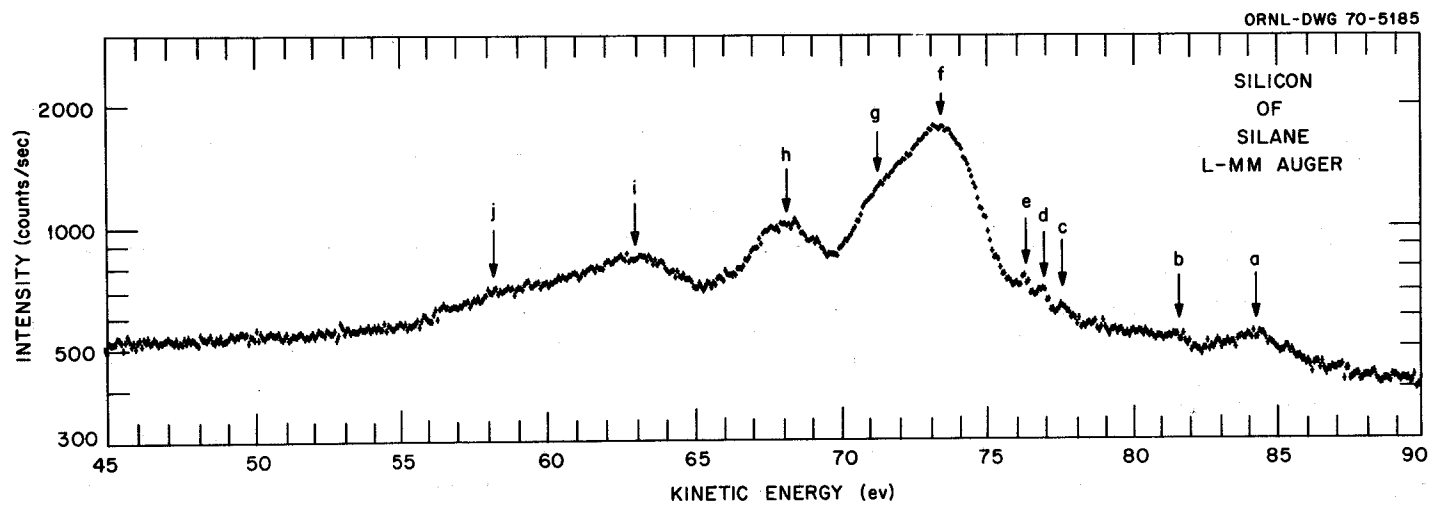


Figure 55. Silicon L-MM Auger electron spectrum of silane excited by electron impact.

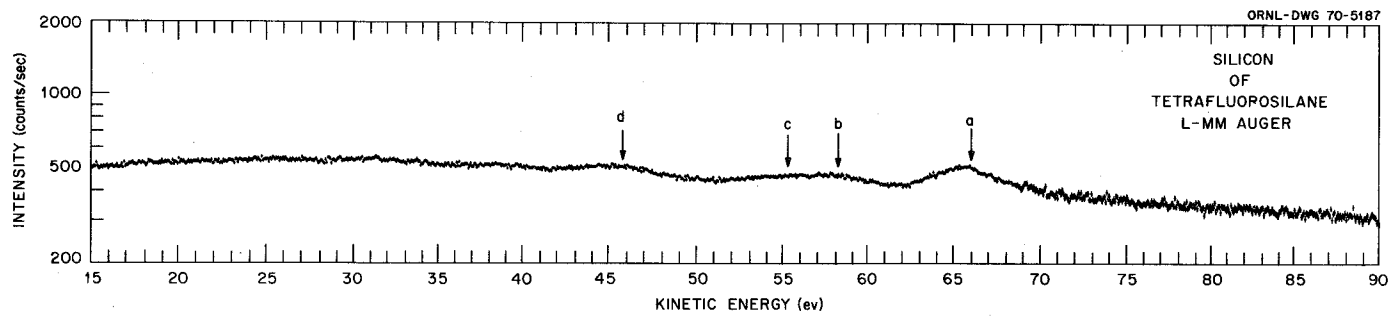


Figure 56. Silicon L-MM Auger electron spectrum of tetrafluorosilane excited by electron impact.

TABLE XLI

ELECTRON PEAK ENERGIES IN THE SILICON  
L-MM AUGER SPECTRUM OF SILANE

Peak <sup>a</sup>	Absolute Energy (eV)
a	84.4 ± .5
b	81.8 ± .5
c	77.7 ± .4
d	77.0 ± .3
e	76.4 ± .3
f	73.7 ± .6
g	71.0 ± .8
h	68.0 ± .6
i	63.3 ± .8
j	58.5 ± 1.0

<sup>a</sup>Peaks were observed in Figure 55.

TABLE XLII

ELECTRON PEAK ENERGIES IN THE SILICON L-MM  
AUGER SPECTRUM OF TETRAFLUROSILANE

Peak <sup>a</sup>	Absolute Energy (eV)
a	66.3 ± 1.1
b	58.5 ± 1.1
c	55.7 ± 1.4
d	46.0 ± 1.6

<sup>a</sup>Peaks were observed in Figure 56.

Comparison of  $\text{SiH}_4$  with  $\text{CH}_4$  Auger spectra (Figure 55, page 141, and Figure 43, page 116) presents a narrower main peak in the case of  $\text{SiH}_4$ , suggesting (1) a greater stability of  $\text{SiH}_4^{+2}$  compared to  $\text{CH}_4^{+2}$ , or (2) a smaller splitting of Jahn-Teller distorted electronic states with  $\text{SiH}_4^{+2}$ . This latter comparison was discussed in section C.1.a., page 136.

b. The silicon K-LL spectra. Silicon K-LL Auger processes take place beneath the valence M level. The K- and L-shell electrons are localized on the silicon atom, thus changes in the K-LL Auger line energies result mainly from a change in electron density surrounding the silicon, such as may occur with changes in the oxidation state. These changes or chemical shifts have been thoroughly exploited in the case of photoionization and have proved to be a powerful tool for chemical analysis. A chemical shift of  $5.5 \pm 0.7$  eV was witnessed in measuring the K-LL Auger spectra of  $\text{SiH}_4$  and  $\text{SiF}_4$  (Figures 57 and 58). Tables XLIII and XLIV give the energies of the lines observed in the  $\text{SiH}_4$  and  $\text{SiF}_4$  spectra.

c. The fluorine spectrum of tetrafluorosilane. The fluorine K-LL Auger spectrum of  $\text{SiF}_4$  is similar in appearance and energy to that observed with fluorine spectra of the fluoromethanes and for this reason is included in Figure 54, page 140. Also, the spectrum is presented in Figure 59 and Table XLV lists the energies of the observed peaks.

#### D. Tabulation of Results

The identification of the normal lines in the Auger spectra allows for the calculation of (1) the minimum energy required for double electron removal from the ground electron state of a neutral molecule (Table XLVI) and (2) the second ionization energy for a given molecular orbital (Table XLVII).

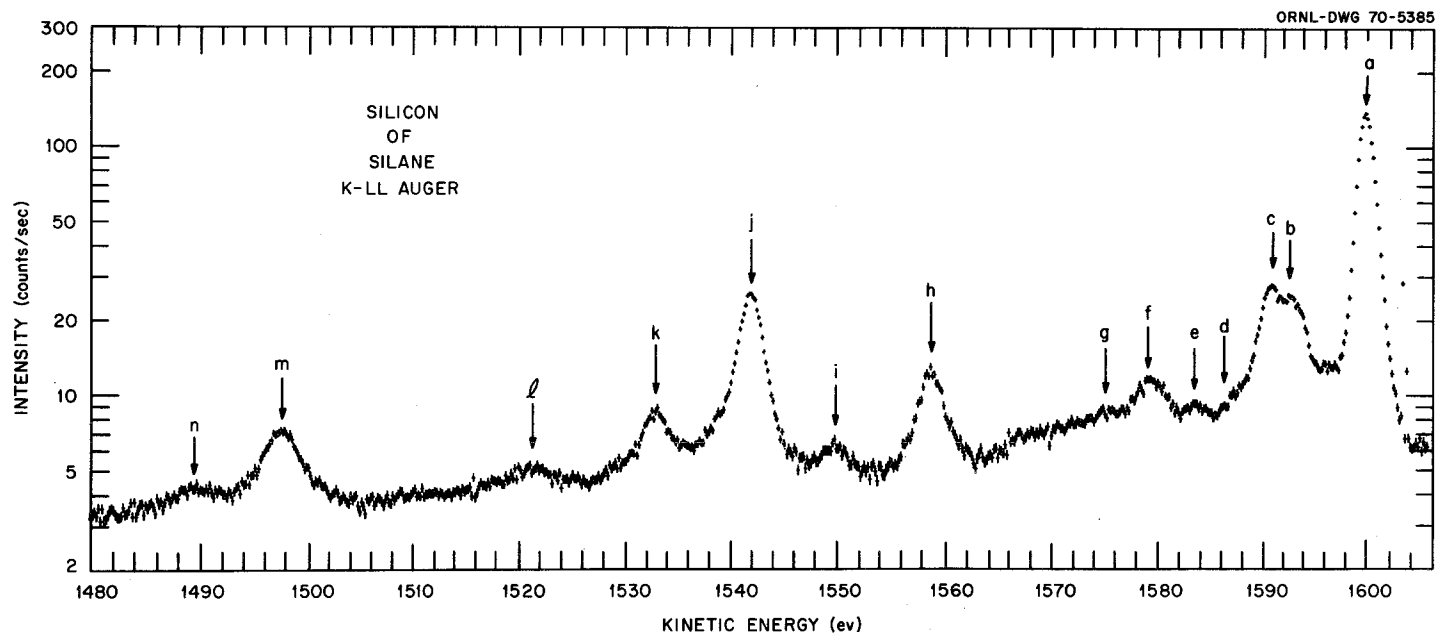


Figure 57. Silicon K-LL Auger electron spectrum of silane excited by electron impact.

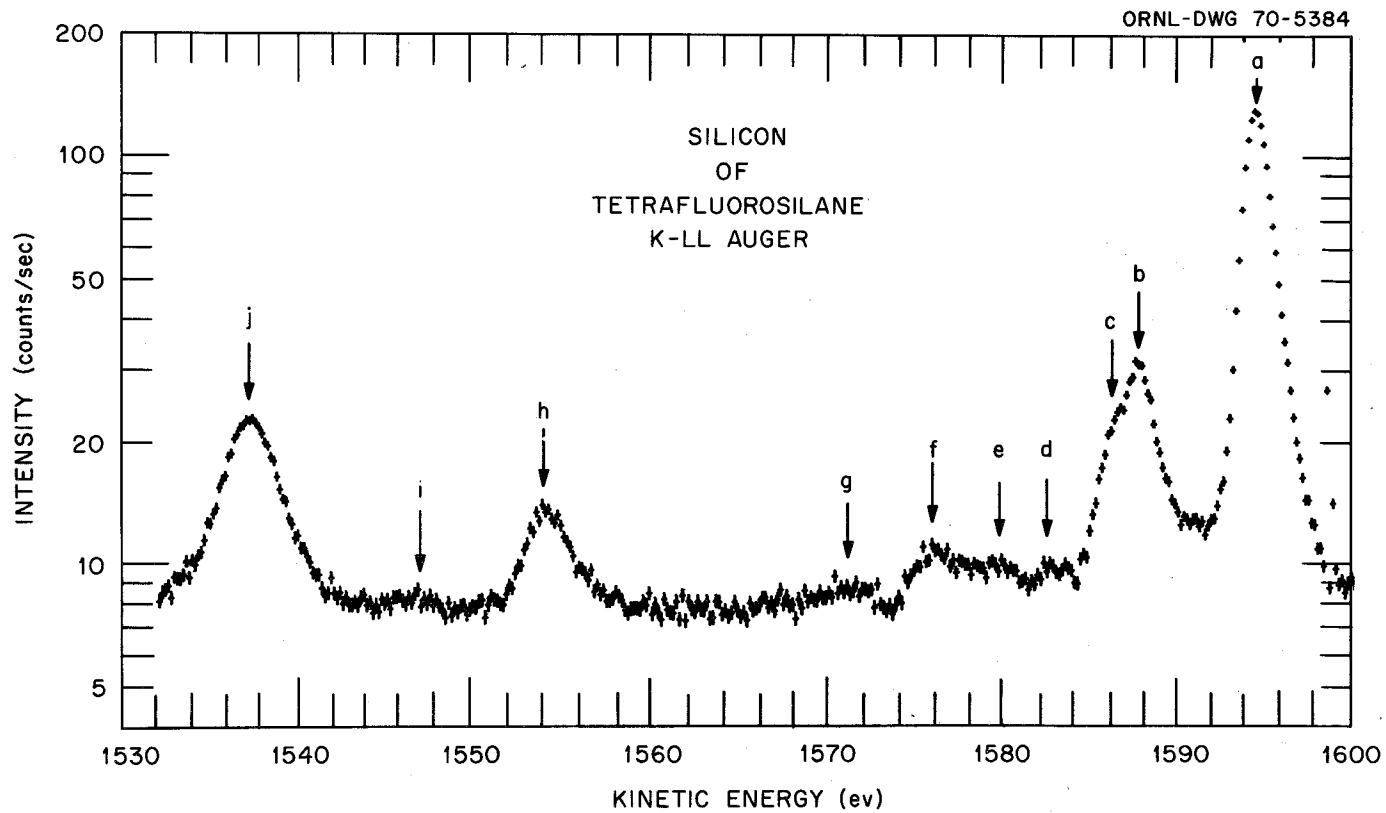


Figure 58. Silicon K-LL Auger electron spectrum of tetrafluorosilane excited by electron impact.

TABLE XLIII

ELECTRON PEAK ENERGIES IN THE SILICON  
K-LL AUGER SPECTRUM OF SILANE

Peak <sup>a</sup>	Absolute Energy (eV)
a	1599.8 ± .3
b	1592.7 ± .4
c	1591.0 ± .4
d	1586.5 ± .6
e	1583.8 ± .5
f	1579.2 ± .5
g	1571.8 ± .6
h	1558.8 ± .4
i	1549.7 ± .6
j	1542.0 ± .3
k	1533.0 ± .4
l	1521.4 ± .8
m	1497.7 ± .6
n	1489.6 ± .8

<sup>a</sup>Peaks were observed in Figure 57.

TABLE XLIV

ELECTRON PEAK ENERGIES IN THE SILICON K-LL  
AUGER SPECTRUM OF TETRAFLUOROSILANE

Peak <sup>a</sup>	Absolute Energy (eV)
a	1593.8 ± .3
b	1587.2 ± .4
c	1585.5 ± .4
d	1582.0 ± .4
e	1579.1 ± .6
f	1575.5 ± .5
g	1571.0 ± .8
h	1553.3 ± .4
i	1545.2 ± .8
j	1537.0 ± .4

<sup>a</sup>Peaks were observed in Figure 58.

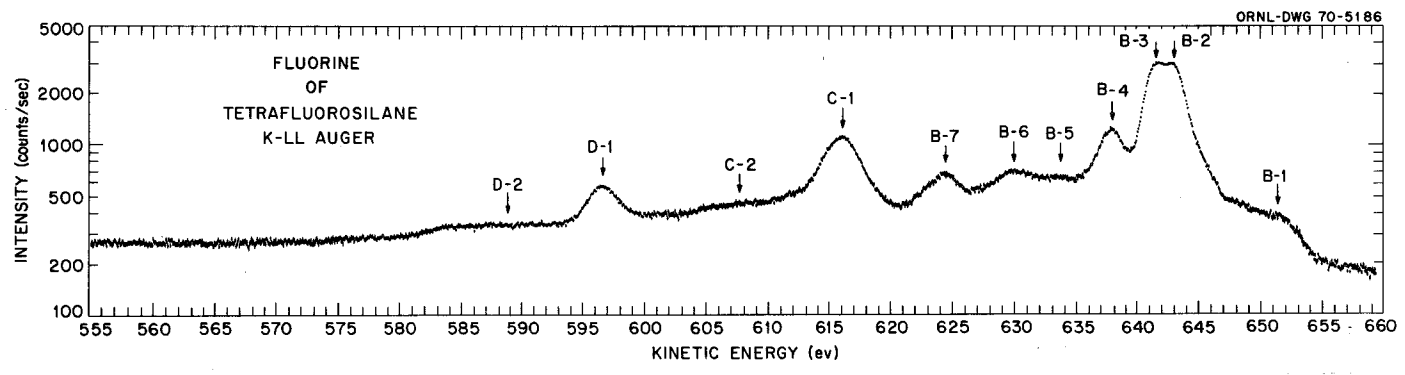


Figure 59. Fluorine K-LL Auger electron spectrum of tetrafluorosilane excited by electron impact.

TABLE XLV  
ELECTRON PEAK ENERGIES IN THE FLUORINE K-LL  
SPECTRUM OF TETRAFLUROSILANE

Peak <sup>a</sup>	Absolute Energy (eV)
B-1	651.6 ± 1.0
B-2	643.2 ± 0.4
B-3	641.8 ± 0.4
B-4	637.9 ± 0.4
B-5	633.6 ± 0.7
B-6	630.2 ± 0.4
B-7	624.5 ± 0.4
C-1	615.9 ± 0.4
C-2	608.1 ± 1.5
D-1	596.3 ± 0.5
D-2	589.0 ± 1.5

<sup>a</sup>Peaks were observed in Figure 59.

TABLE XLVI

MINIMUM ENERGY REQUIRED FOR DOUBLE ELECTRON REMOVAL  
FOR A NUMBER OF SIMPLE MOLECULES AS MEASURED  
BY AUGER SPECTROSCOPY

Molecule	$E_{X+2}(\text{min})^a$ (eV)
N <sub>2</sub>	42.9
O <sub>2</sub>	37.4
CO	40.2
NO	35.4
H <sub>2</sub> O	39.2
CO <sub>2</sub>	37.6
CH <sub>4</sub>	35.0
CH <sub>3</sub> F	35.0
CHF <sub>3</sub>	36.9
CF <sub>4</sub>	40.4

<sup>a</sup> $E_{X+2}(\text{min})$  is the minimum energy required to remove the two least bound electrons from the ground state of a neutral molecule, as determined from the onset of the normal Auger lines.

TABLE XIVII

SECOND IONIZATION ENERGY OF A MOLECULAR ORBITAL FOR  
SOME SIMPLE GASEOUS MOLECULES AS MEASURED  
BY AUGER SPECTROSCOPY

Molecule	Process (1s-xx)	$I(X)^{-2}$ eV <sup>a</sup>
N <sub>2</sub>	1s-2s <sub>g</sub> 2s <sub>g</sub>	57.6
O <sub>2</sub>	1s-2p <sub>g</sub> 2p <sub>g</sub>	25.3
CO	1s <sub>o</sub> -2s <sub>o</sub> <sup>b</sup> 2s <sub>o</sub> <sup>b</sup>	56.6
H <sub>2</sub> O	1s <sub>o</sub> -1b <sub>1</sub> 1b <sub>1</sub>	26.6
CH <sub>4</sub>	1s-t <sub>2</sub> t <sub>2</sub>	22.4
	1s-a <sub>1</sub> a <sub>1</sub>	37.8
CH <sub>3</sub> F	1s <sub>c</sub> -π <sub>e</sub> π <sub>e</sub>	22.7
CH <sub>3</sub> F	1s <sub>F</sub> -a <sub>1</sub> (F)a <sub>1</sub> (F)	53.1
CF <sub>4</sub>	1s <sub>c</sub> -3t <sub>2</sub> 3t <sub>2</sub>	26.6

<sup>a</sup> $I(X)^{-2}$  is the second ionization energy for a given orbital X that is involved in the transition 1s-xx in column 2.

## CHAPTER IV

## SUMMARY

Auger electron emissions have been examined from some simple gaseous molecules ( $N_2$ ,  $O_2$ ,  $CO$ ,  $NO$ ,  $H_2O$ ,  $CO_2$ ,  $CH_4$ ,  $CH_3F$ ,  $CH_2F_2$ ,  $CHF_3$ ,  $CF_4$ ,  $SiH_4$  and  $SiF_4$ ). An attempt has been made to separate each spectrum into regions so as to distinguish the normal Auger processes from the satellite processes. After analyzing the Auger spectrum for high energy satellite contributions a simplified shell model (ignoring any coupling schemes) was used in determining for some of the molecules the molecular orbital occupancy and the final electronic states of the doubly charged ion involved in the Auger transition. Besides obtaining information about doubly charged ions, high resolution Auger spectroscopy affords one a tool for molecular identification; and, it reflects information concerning initial excitation processes that can occur in molecules.

BIBLIOGRAPHY

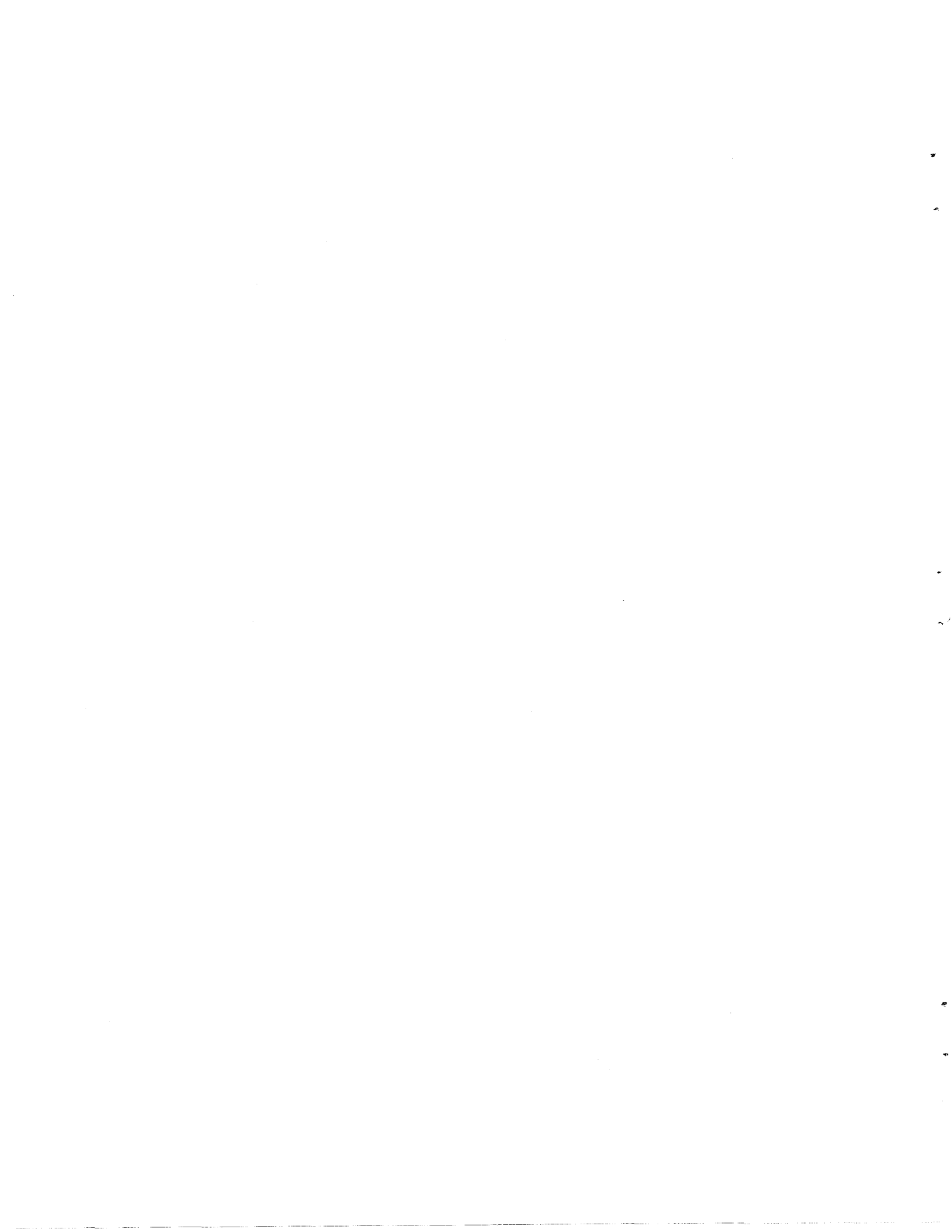
## BIBLIOGRAPHY

1. H. S. Massey and E. H. S. Burhop, "Electronics and Ionic Impact Phenomena, Clarendon Press, Oxford, England, 1969.
2. R. Stephen Berry, "Electronic Spectroscopy by Electron Spectroscopy," in Annual Review of Physical Chemistry, Vol. 20, 1969.
3. V. Cermak, J. Chem. Phys., 44, 3781 (1966).
4. K. Siegbahn, C. Nordling, A. Fahlman, R. Nordberg, K. Hamrin, J. Hedman, G. Johansson, T. Bergmark, S. Karlsson, I. Lindgren, B. Lindberg, "ESCA: Atomic, Molecular and Solid State Structure Studied by Means of Electron Spectroscopy," (Almqvist and Wiksells Boktryckeri AB, Upsala, 1967).
5. David M. Hercules, Anal. Chem., 42, 20A (1970).
6. D. Betteridge and A. D. Baker, Anal. Chem., 42, 43A (1970).
7. L. A. Harris, Anal. Chem., 40, 25A (1968).
8. D. Stahlherm, B. Cleff, H. Hillig and W. Mehlhorn, Z. Naturforsch., 24a, 1729 (1969).
9. T. A. Carlson, W. E. Moddeman, B. P. Pullen and M. O. Krause, (in press).
10. W. E. Moddeman, T. A. Carlson, B. P. Pullen, M. O. Krause, G. K. Schweitzer, F. A. Grimm and W. E. Bull, (to be published). See also T. A. Carlson, M. O. Krause, W. E. Moddeman, B. P. Pullen and F. H. Ward, Oak Ridge National Laboratory Report ORNL-4395, p. 87 (1969).
11. K. Siegbahn, C. Nordling, G. Johansson, J. Hedman, P. F. Heden, K. Hamrin, V. Gelius, T. Bergmark, L. O. Werme, R. Manne and Y. Baer, "ESCA: Applied to Free Molecules," (North-Holland Publishing Company, 1969).
12. P. Auger, J. Phys. Radium, 6, 205 (1925).
13. R. A. Rubenstein, "Theoretical Study of the Auger Effect in the Light to Medium Range of Atomic Number," Ph.D. Dissertation, University of Illinois, Urbana, 1955.
14. M. O. Krause, M. L. Vestal, W. H. Johnston and T. A. Carlson, Phys. Rev., 133, A385 (1964).
15. M. O. Krause, F. A. Stevie, L. J. Lewis, T. A. Carlson and W. E. Moddeman, Phys. Lett., 31A, 81 (1970).
16. M. Wolfsberg and M. L. Perlman, Phys. Rev., 99, 1833 (1955).

17. T. A. Carlson and M. O. Krause, Phys. Rev., 137, A1655 (1965).
18. T. A. Carlson and M. O. Krause, Phys. Rev. Lett., 14, 390 (1966).
19. E. H. S. Burhop, "The Auger Effect and Other Radiationless Transitions," University Press, Cambridge, England, 1952.
20. M. O. Krause and T. A. Carlson (to be published).
21. A. C. Hurley and V. W. Maslen, J. Chem. Phys., 34, 1919 (1961).
22. A. C. Hurley, J. Mol. Spectr., 9, 18 (1962).
23. H. Korber and W. Mehlhorn, Z. Physik, 191, 217 (1966).
24. W. Mehlhorn and W. N. Asaad, Z. Physik, 191, 231 (1966).
25. W. N. Asaad, Nuclear Phys., 66, 494 (1965).
26. E. J. Callen, T. K. Krueger and W. L. McDavid, Bull. Am. Phys. Soc., 14, 830 (1969).
27. W. Mehlhorn and D. Stalherm, Z. Physik, 217, 294 (1968).
28. W. Mehlhorn, private communication.
29. A. Fahlman, R. Nordberg, C. Nordling and K. Siegbahn, Z. Physik, 192, 476 (1966).
30. A. Fahlman and C. Nordling, Arkiv Fysik, 26, 248 (1964).
31. E. Sokolowski and C. Nordling, Arkiv Fysik, 14, 557 (1959).
32. C. Nordling, E. Sokolowski and K. Siegbahn, Arkiv Fysik, 13, 282 (1958).
33. E. Nordling, E. Sokolowski and K. Siegbahn, Arkiv Fysik, 13, 483 (1958).
34. A. Fahlman, K. Hamrin, G. Axelson, C. Nordling and K. Siegbahn, Z. Physik, 192, 484 (1966).
35. A. Fahlman, K. Hamrin, R. Nordberg, C. Nordling and K. Siegbahn, Phys. Lett., 20, 159 (1966).
36. R. G. Albridge, K. Hamrin, G. Johansson and A. Fahlman, Z. Physik, 209, 419 (1968).
37. Bailey P. Pullen, "The Construction and Use of a High Resolution Photoelectron Spectrometer," Doctoral Dissertation, The University of Tennessee, Knoxville, 1970. Also see B. P. Pullen, T. A. Carlson, W. E. Moddeman, G. K. Schweitzer, W. E. Bull and F. A. Grimm, J. Chem. Phys., (in press).

38. J. R. Pierce, "Theory and Design of Electron Beams, D. Van Nostrand Company, Inc., New York, 1949, p. 186.
39. J. A. Bearden, Rev. Mod. Phys., 39, 78 (1967).
40. D. W. Fischer and W. L. Bamm, Spectrochim. Acta, 21, 443 (1965).
41. M. Nakamura, M. Sasanuma, S. Sato, M. Watanabe, H. Yamashita, Y. Iguchi, A. Ejiri, S. Nakai, S. Yamaguchi, T. Sagawa, Y. Nakai and T. Oshio, Phys. Rev., 178, 80 (1969).
42. A. Lofthus, "The Molecular Spectrum of Nitrogen," Spectroscopic Report No. 2, University of Oslo, Blindern, Norway (1960).
43. G. L. Weissler, J. A. R. Samson, M. Ogawa and G. R. Cook, J. Opt. Soc. Am., 49, 338 (1959).
44. F. R. Gilmore, J. Quant. Spectrosc. Radiat. Transfer, 5, 369 (1965).
45. T. Namioka, K. Yoshino and Y. Tanaka, J. Chem. Phys., 39, 2629 (1963).
46. E. N. Lassettre, A. Skerbele, M. A. Dillon and K. J. Ross, J. Chem. Phys., 48, 5066 (1968).
47. D. W. Turner and D. P. May, J. Chem. Phys., 45, 471 (1966).
48. J. T. Vanderslice, E. A. Mason and W. G. Maish, J. Chem. Phys., 32, 515 (1960).
49. C. E. Moore, "Atomic Energy Levels," National Bureau of Standards Circular No. 467, Vol. 1, United States Government Printing Office, Washington, D. C., 1958.
50. Paul H. Krupenie, "The Band Spectrum of Carbon Monoxide," NSRDS-NBS 5, United States Government Printing Office, Washington, D. C., 1966.
51. G. Herzberg, "Spectra of Diatomic Molecules," 2nd Ed., Van Nostrand, Princeton, N. J., 1950.
52. H. Brion, C. Moser, M. Yamazaki, J. Chem. Phys., 30, 673 (1959).
53. J. Hedman, P. F. Heden, C. Nording and K. Siegbahn, Phys. Lett., 29A, 178 (1969).
54. J. E. Collin and P. Natalis, Chem. Phys. Lett., 2, 194 (1968).
55. F. H. Dorman and J. D. Morrison, J. Chem. Phys., 39, 1906 (1963).
56. T. A. Carlson, W. E. Moddeman and M. O. Krause, Phys. Rev., A1, 1406 (1970).

57. M. O. Krause, Oak Ridge National Laboratory, Oak Ridge, Tennessee, (personal communication).
58. C. W. Nestor, T. C. Tucker, T. A. Carlson, L. D. Roberts, F. B. Malik and C. Froese, "Relativistic and Non-Relativistic SCF Wave Functions for Atoms and Ions from  $Z = 2$  to 80, Together with Calculations of Binding Energies, Mean Radii, Screening Constants, Charge Distributions and Electron Shake-off Probabilities," Oak Ridge National Laboratory Report No. 4027, United States Department of Commerce, Springfield, Virginia, 1966.
59. D. B. Neumann and J. W. Moskowitz, J. Chem. Phys., 50, 2216 (1969).
60. F. H. Dorman and J. D. Morrison, J. Chem. Phys., 35 575 (1961).
61. F. Fiquet-Fayard, Israel J. Chem., 1, 275 (1969).
62. C. R. Brundle and D. W. Turner, Proc. Roy. Soc., A307, 27 (1968).
63. D. W. Turner and D. P. May, J. Chem. Phys., 46, 1156 (1967).
64. W. E. Moddeman, T. A. Carlson, W. E. Bull and G. K. Schweitzer, (unpublished results).
65. K. Hamrin, G. Johannson, V. Gelius, A. Fahlman, C. Nordling and K. Siegbahn, Chem. Phys. Lett., 1, 613 (1968).
66. C. R. Brundle, M. B. Robin and H. Basch (submitted to J. Chem. Phys.).
67. S. Stokes and A. B. F. Duncan, J. Am. Chem. Soc., 80, 6177 (1958).
68. D. W. Davis, Chem. Phys. Lett., 2, 173 (1968).
69. D. W. Davis, J. M. Hollander, D. A. Shirley and T. D. Thomas, J. Chem. Phys., 52, 3295 (1970).
70. H. J. Lempka, O. G. Streets, A. W. Potts and W. C. Price, Proc. Roy. Soc., (to be published).



## DISTRIBUTION

- 1-200. T. A. Carlson
- 201. M. O. Krause
- 202-203. J. L. Fowler
- 204. E. H. Taylor
- 205. J. A. Fahey
- 206. L. D. Hulett
- 207. G. E. Boyd
- 208. A. E. Jonas
- 209. R. J. Herdklotz
- 210. K. L. Cheng
- 211-260. W. E. Moddeman
- 261-262. Central Research Library
- 263-272. Laboratory Records Department
- 273. Document Reference Section
- 274. Laboratory Records, ORNL R.C.
- 275. ORNL Patent Office
- 276-290. Division of Technical Information  
Extension
- 291. Laboratory and University Division, ORO

## EXTERNAL DISTRIBUTION

- 292-321. G. K. Schweitzer, University of Tennessee, Knoxville,  
Tennessee 37916
- 322. B. P. Pullen, Department of Physical Science, Southeastern  
Louisiana State College, Hammond, Louisiana 70401
- 323. D. A. Zatko, P. O. Box H, University of Alabama, University,  
Alabama 35486
- 324. H. B. Hupf, University of Miami, Coral Gables, Florida 33124
- 325. R. Brundle, Bell Laboratories, Murray Hill, New Jersey 07971
- 326. W. A. Chupka, Argonne National Laboratory, Argonne, Ill. 60439
- 327. W. S. Koski, Johns Hopkins University, Baltimore, Md. 21218
- 328. R. G. Albridge, Physics Department, Vanderbilt University,  
Nashville, Tennessee 37203
- 329. F. Grimm, Dept. of Chemistry, University of Tennessee,  
Knoxville, Tennessee 37916
- 330. J. F. Redina, McPherson Instruments Corp., Acton, Mass.
- 331. R. Nordberg, Klinisk-Kemiska Institutionen, Sahlgrenska  
Sjukhuset S-413 45 Goteborg, Sweden
- 332. T. M. King, Monsanto Inorganic Chemicals Division,  
800 N. Lindbergh Blvd., St. Louis, Missouri 63166
- 333. R. R. Slater, Gulf Research and Development Company,  
P. O. Box 2038, Pittsburgh, Pennsylvania 15230
- 334. S. D. Worley, Manned Spaceflight Center, Space Physics Div.,  
TG-1, Houston, Texas 77058
- 335. L. H. Toburen, Battelle Memorial Institute, Pacific Northwest  
Laboratory, P. O. Box 999, Richland, Washington 99352
- 336. W. L. Baun, Air Force Materials Laboratory, Materials Physics  
Div., Analytical Branch, Wright Patterson AFB, Ohio 45433

337. R. P. Buch, Dept. of Chemistry, University of North Carolina, Chapel Hill, North Carolina 27514
338. R. Hudson, Ethyl Corporation, Baton Rouge, Louisiana 70800
339. L. Broussard, Esso Research Laboratories, P. O. Box 2226, Baton Rouge, Louisiana 70821
340. T. C. Herndon, 217 Ridgeway Drive., Richmond, Kentucky
341. M. Nakamura, INS-SOR Group, Institute for Nuclear Study, University of Tokyo, Tanashi, Tokyo, Japan
342. C. E. Johnson, Monsanto Company, 800 N. Lindbergh Boulevard, St. Louis, Missouri 63166
343. A. Mabis, Miami Valley Laboratory, Ross, Ohio
344. N. Jonathan, Dept. of Chemistry, The University, Southampton SO9 5NH, England
345. D. W. Turner, Physical Chemical Laboratory, South Parks Road, Oxford, England
346. T. W. Couch, Iowa State University, Ames, Iowa
347. K. D. Sevier, Post Office Box 127, Eureka, California 95501
348. V. R. Johnson, Physics Department, University of Tulsa, Tulsa, Oklahoma
349. W. C. Jones, Concord College, Athens, West Virginia 24740